PRE-CLINICAL EVALUATION OF EARLY OSTEOARTHRITIS VIA BIOMECHANICAL PROPERTIES DERIVED FROM LOW-FIELD MAGNETIC RESONANCE IMAGING

HASHEMI BIN HASHIM

Master of Science in Manufacturing Engineering

2025

Faculty of Industrial and Manufacturing Technology and Engineering

PRE-CLINICAL EVALUATION OF EARLY OSTEOARTHRITIS VIA BIOMECHANICAL PROPERTIES DERIVED FROM LOW-FIELD MAGNETIC RESONANCE IMAGING

Hashemi Bin Hashim

Master of Science in Manufacturing Engineering

2025

PRE-CLINICAL EVALUATION OF EARLY OSTEOARTHRITIS VIA BIOMECHANICAL PROPERTIES DERIVED FROM LOW-FIELD MAGNETIC RESONANCE IMAGING

HASHEMI BIN HASHIM

A thesis submitted
in fulfilment of the requirements for the degree of
Master of Science in Manufacturing Engineering

Faculty of Industrial and Manufacturing Technology and Engineering

UNIVERSITI TEKNIKAL MALAYSIA MELAKA

2025

DECLARATION

I declare that this thesis entitled “Pre-Clinical Evaluation of Early Osteoarthritis via Biomechanical Properties Derived from Low-Field Magnetic Resonance Imaging” is the result of my own research except as cited in the references. The thesis has not been accepted for any degree and is not concurrently submitted in candidature of any other degree.

Signature :

Name :HASHEMI BIN HASHIM

Date :23rd April 2025

APPROVAL

I hereby declare that I have read this thesis, and, in my opinion, this thesis is sufficient in terms of scope and quality for the award of Master of Science in Manufacturing Engineering.

Signature :

.....

Supervisor Name :PROFESSOR IR. DR. HAMBALI BIN AREP

Date :23rd April 2025

DEDICATION

I dedicate this thesis to my parents,

And

To my life partner, Nur Ain Qistina

You have successfully made me the person I am today

You will always be remembered.

ABSTRACT

Osteoarthritis is a degenerative disease which is associated with the articular cartilage in the synovial joint. As the disease progresses, it changes the macromolecular structure inside the cartilage tissue and alters the biomechanical properties. Hence, the ability to detect the disease at its earliest grade is crucial for early intervention of the disease. The osteoarthritis is clinically diagnosed using Magnetic Resonance Imaging (MRI) by examining the morphology of the articular cartilage and the geometrical data of the synovial joint. However, most of the diagnoses were performed when this disease is already progressed into advanced grade. At early grade of osteoarthritis, the biomechanical properties start to show noticeable change. Although studies were conducted to correlate the biomechanical properties of cartilage with MRI image, high-field MRI was utilized to produce the cartilage image. Therefore, this study aimed to investigate the potential use of low-field MRI to monitor the biomechanical properties of articular cartilage. This includes to determine the greyscale of low-field MRI image, characterize the biomechanical properties of articular cartilage and finally to observe the correlation between the greyscale and biomechanical properties of articular cartilage from fibrillated cartilage sample. Cartilages from hip joints of bovine were scanned using 0.18 T MRI. The images of cartilage were characterized based on the intensity of the greyscale. Creep indentation test was then conducted on the cartilage specimens and subsequently the indentation test was simulated using finite element method. The biomechanical properties of Elastic Modulus and Permeability of cartilage were characterized by incorporating the experimental data from the indentation test with the computational finite element model. The mean Elastic Modulus was found to be 0.26 ± 0.07 while the Permeability was $5.26 \pm 1.72 \times 10^{-15}$ m^4/Ns. Further correlation analyses were performed to examine the relationship between the greyscale of MRI image and biomechanical properties of Elastic Modulus and Permeability of the cartilage. Good correlation was found between the cartilage greyscale and cartilage biphasic Elastic Modulus ($r= 0.74$) and a strong correlation with negative value was observed between the cartilage greyscale and cartilage Permeability ($r= -0.86$). Hence, present results indicate that the low-field MRI has potential for non-invasive assessment of the condition of articular cartilage. It could be further developed to serve as an early intervention of osteoarthritis disease. However further validation using human samples is necessary before clinical application.

PENILAIAN PRA-KLINIKAL OSTEOARTRITIS PERINGKAT AWAL MELALUI SIFAT BIOMEKANIKAL YANG DIPEROLEHI DARIPADA PENGIMEJAN MAGNETIK RESONANS MEDAN RENDAH

ABSTRAK

Osteoartritis adalah salah satu penyakit degenerasi yang berkait rapat dengan rawan artikular pada sendi sinovia. Penyakit ini akan mengubah struktur makromolekul di dalam tisu rawan dan ciri-ciri biomekaniknya. Oleh itu, keupayaan untuk mengesan penyakit ini pada peringkat awal adalah penting sebagai intervensi awal bagi rawatan penyakit ini. Secara klinikal, osteoartritis didiagnosis menggunakan pengimbas pengimejan resonans magnetik untuk memeriksa morfologi rawan artikular dan data geometri pada sendisinovia. Walau bagaimanapun, diagnosis bagi penyakit ini biasanya dijalankan apabila penyakit ini sudah di peringkat akhir. Walaupun kajian telah dijalankan untuk mendapatkan korelasi antara ciri-ciri biomekanikal rawan artikular dengan imej dari medan pengimejan resonans magnetik, medan pengimejan resonans magnetik berkekuatan tinggi telah digunakan untuk menghasilkan imej rawan artikular tersebut. Oleh hal yang demikian, kajianini bertujuan untuk mengkaji potensi pengimejan resonans magnetik berkekuatan rendah dalam pemantauan ciri-ciri biomekanikal rawan artikular. Ini termasuk, untuk menentukan skala kelabu imej dari medan pengimejan resonans magnetik berkekuatan rendah, untuk mencirikan sifat biomekanikal rawan artikular dan akhirnya untuk memerhati korelasi antara skala kelabu dengan sifat biomekanika fibrilasi rawan artikular. Rawan dari sendi pinggul utuh lembu telah digunakan untuk pengimejan dengan mengaplikasikan medan pengimejan resonans magnetik yang berkekuatan serendah 0.18 T. Imej rawan artikular ini kemudian dicirikan mengikut keamatan skala kelabu. Ujian lekukan dijalankan ke atas specimen rawan artikular dan seterusnya data eksperimen daripada ujian lekukan telah disimulasikan dengan menggunakan kaedah unsur tidak terhingga. Kajian mengkaji ciri-ciri biomekanikal rawan artikular dilakukan dengan menggabungkan data eksperimen dari ujian lekukan dengan model unsur tidak terhingga. Nilai purata Modulus Elastik rawan artikular yang didapati adalah 0.26 ± 0.07 MPa manakala purata untukkebolehtelapan adalah 5.26 ± 1.72×10⁻¹⁵ m⁴/Ns. Selanjutnya, analisis korelasi telah dilakukan untuk mengenalpasti hubungan antara skala kelabu dan sifat biomekanikalModulus Elastik dan kebolehtelapan rawan artikular. Berdasarkan hasil kajian, skala kelabu rawan artikular menunjukkan hubungan yang sangat baik dengan Modulus Elastik rawan artikular (r=0.74) dan hubungan yang sangat baik dengan nilai negatif diperhatikan diantara skala kelabu rawan artikular dan kebolehtelapan rawan artikular (r=-0.86). Oleh itu, hasil dari kajian ini menunjukkan pengimejan resonans magnetik yang berkekuatan rendah berpontensi untuk menghasilkan data yang boleh dipercayai untuk menentukan keadaan rawan artikular. Pendekatan ini boleh dikembangkan lebih lanjut sebagai panduan kepada intervensi awal penyakit osteoartritis.Walau bagaimanapun, pengesahan lanjut menggunakan sampel manusia adalah diperlukan sebelum aplikasi klinikal.

ACKNOWLEDGEMENTS

First, I express my gratitude to Allah Almighty for granting me the health, patience, and resilience needed to complete this thesis. This endeavor marks the most challenging period of my life. Throughout this journey, your constant presence has been my solace.

The successful culmination of my master journey, encompassing both triumphs and tribulations, owes much to the unwavering support of Supervisor Professor. IR. Dr. Hambali Bin Arep. His ex-emplary supervision and academic guidance have left me deeply indebted. Also, his profound knowledge, invaluable experiences, insightful feedback, and constructive critiques were instrumental in navigating the challenges of my master degree.

I extend heartfelt thanks to my co supervisor Associate Professor. Dr. Mohd Juzaila Bin Abd Latif and Madam Ruzy Haryati Binti Hambali, whose continuous support and vast knowledge played a crucial role in shaping my research. Working with you over the past two years has been a genuine pleasure.

I owe immense gratitude to my family, who allowed me to pursue this path and endure the pain of separation. To my parents, the seeds you planted with nurturing hands have now flourished into fruition. May you both live long to savour the fruits of your efforts.

Appreciation is also extended to my friends and fellow master research at the university, who made this journey joyful and pleasant. The beautiful moments we shared will forever reside in my heart. Special thanks are reserved for the faculty members and administration staff for their unwavering guidance and support throughout my study, always ready to assist with academic and personal matters.

TABLE OF CONTENTS

PAGES

DECLARATION

DEDICATION

ABSTRACT **i**

ABSTRAK **ii**

ACKNOWLEDGEMENT **iii**

TABLE OF CONTENTS **iv**

LIST OF TABLES **vii**

LIST OF FIGURES **viii**

LIST OF SYMBOLS AND ABBREVIATIONS **x**

LIST OF APPENDICES **xii**

LIST OF PUBLICATIONS **xiii**

CHAPTER 1 INTRODUCTION **1**

1.1 Research Background 1
1.2 Problem Statements 4
1.3 Research Objectives 6
1.4 Research Scopes 6
1.5 Hypotheses 7
1.6 Research Questions 7
1.7 Significance of Study 8
1.8 Outline of Thesis 8

CHAPTER 2 LITERATURE REVIEW **10**

2.1 Introduction 10
2.2 Osteoarthritis 11
2.3 Synovial Joints 13
2.3.1 Anatomy of synovial joints 13
2.3.2 Types of synovial joints 14
2.4 Articular Cartilage 15
2.4.1 Composition 16
2.4.2 Structure 19

2.4.3 Alteration in osteoarthritis 21
2.4.4 Thickness 22
2.5 Preparation of osteoarthritic cartilage 23
2.5.1 In vivo degradation method 24
2.5.2 In vitro degradation method 26
2.5.2.1 Enzyme Degradation 27
2.5.3 Animal models 32
2.6 Magnetic Resonance Imaging 35
2.6.1 Studies of articular cartilage 36
2.6.2 Low-field magnetic resonance imaging 38
2.7 Biomechanical properties of articular cartilage 39
2.7.1 Mechanical testing 39
2.7.2 Theoretical modelling 43
2.8 Summary 44

CHAPTER 3 METHODOLOGY 46
3.1 Introduction 46
3.2 Material Preparation 48
3.2.1 Phosphate-buffered saline 48
3.2.2 Trypsin Solution 48
3.2.3 Collagenase Type II 49
3.2.4 Hank's Balanced Salt Solution 50
3.3 Sample Preparation 51
3.3.1 Grade II Cartilage 52
3.4 Microscopic Assessment of Fibrillated Cartilage 53
3.5 Measurement of Water Content 56
3.6 Magnetic Resonance Imaging Image Analysis 57
3.7 Experimental Methods 59
3.7.1 Indentation Test Apparatus 60
3.7.2 Calibration Procedure 61
3.7.3 Creep Indentation Test 62
3.7.4 Cartilage Thickness Measurement 63
3.8 Computational Methods 64
3.8.1 Modelling of Contact-Dependent Flow 64
3.8.2 Finite Element Model 66
3.9 Characterization of Biomechanical Properties of Articular Cartilage 66
3.10 Summary 68

CHAPTER 4 RESULT AND DISCUSSION 69
4.1 Introduction 69
4.2 Fibrillation Assessment of OA Cartilage 69
4.3 Measurement of Cartilage Water Content 74
4.4 Evaluation of Low-field MRI Grayscale 76
4.5 Biomechanical Properties of Articular Cartilage 79

4.6 Correlation of Cartilage Greyscale and Biomechanical Properties 83
4.7 Summary 85

CHAPTER 5 CONCLUSION 87
5.1 Introduction 87
5.2 Research Summary 87
5.3 Research Contributions 88
5.4 Limitations of the Present Study 89
5.5 Future Works 91

REFERENCES 93

APPENDICES 124

LIST OF TABLES

TABLE	TITLE	PAGE
Table 2.1	OA cartilage grade assessment (Waldstein et al., 2016)	12
Table 2.2	Comparative overview of enzymatic cartilage digestion	28
Table 2.3	Comparisons of cartilage fibrillation in different type of enzyme	30
Table 2.4	Comparisons of cartilage fibrillation in different animal models	34
Table 2.5	Cartilage studies using low-field MRI	37
Table 2.6	Comparison of biphasic biomechanical properties in human synovial joints	43
Table 3.1	Imaging parameter of pulse sequence in low-field MRI (Zhang et al., 2023)	58
Table 3.2	Material properties of articular cartilage (Lian et al., 2015)	65

LIST OF FIGURES

FIGURE	TITLE	PAGE
Figure 1.1	Image of knee joint using high-field MRI (Hani et al., 2015)	3
Figure 1.2	Comparison MRI for assessment of knee osteoarthritis. a) Standard high-field MRI shows small subchondral (SBMLs). b) At low-field MRI, SBMLs (arrows) are visualized diagnostic image quality (Pogarell et al. 2024).	4
Figure 2.1	(a) Normal and (b) Osteoarthritic joints (Antony et al., 2020)	12
Figure 2.2	Structure of synovial joint in knee (Usgu and Usgu, 2023)	13
Figure 2.3	Types of synovial joints (Siddaiah and Menezes, 2016)	14
Figure 2.4	Extracellular matrix of articular cartilage (Chen et al., 2006)	17
Figure 2.5	Diagram of PGs aggregate and aggrecan molecule (Pearle et al., 2005)	18
Figure 2.6	The zonal architecture and cells arrangement of articular cartilage (Schmidt, 2021)	19
Figure 2.7	MRI images of cartilage (a) 1.5 T MRI and (b) 0.2 T (Wansin et al., 2017; Biggi and Dyson, 2018)	36
Figure 2.8	Esaote C-scanner (Ghazinoor and Crues, 2006)	38
Figure 2.9	Mechanical testing configurations (a) Unconfined compression (b) Confined compression (c) Indentation (DiSilvestro and Suh, 2001)	41
Figure 3.1	Methodology flow chart	47
Figure 3.2	100 ml PBS tablet (Bio Basic Inc.)	48
Figure 3.3	0.05% Trypsin (Gibco)	49
Figure 3.4	0.2% Collagenase Type II (STEMCELL Technologies.)	50
Figure 3.5	HBSS (Thermo Fisher Scientific)	51
Figure 3.6	(a) before drilling and (b) after drilling; (c) drilled sample with intact subchondral bone (d) Used 8 mm bore diameter hollow diamond drill bit	52
Figure 3.7	A trimmed cartilage had been observed under microscope	54
Figure 3.8	Reference area for the microscope image	55
Figure 3.9	(a) Image of the cartilage that had been captured through microscope (b) Converted image into grayscale (c) ROI of cartilage from the grayscale image in (b)	56
Figure 3.10	(a) C-scan MRI system (b) Cartilage sample set-up at receiving coil	58
Figure 3.11	MRI image of the cartilage sample at the sagittal view through GE sequence	59

Figure 3.12	Indentation test apparatus	60
Figure 3.13	(a) Calibration test set-up (b) Different heights of gauge blocks	61
Figure 3.14	Graph represents the measurement taken in the load calibration	62
Figure 3.15	Creep indentation test set-up	62
Figure 3.16	Apparatus for indentation thickness test (a) Close-view on the thickness test (b) Needle indenter	63
Figure 3.17	Cartilage thickness measurement based on load and displacement data	64
Figure 3.18	Axisymmetric FE model of a cartilage	65
Figure 3.19	Axisymmetric FE model of a cartilage	66
Figure 3.20	Cartilage deformation curve (a) before matching and (b) after matching	67
Figure 4.1	Mean cartilage thicknesses of bovine femoral head with different interval time	70
Figure 4.2	Area changes in fibrillation of progressive cartilage	72
Figure 4.3	Superficial zone of articular cartilage decrease (a) Grade I (b) Grade II after fibrillated 120 mins.	72
Figure 4.4	Mean water content for control, degraded and fibrillated samples	75
Figure 4.5	Mean greyscale intensity for control, degraded and fibrillated samples.	77
Figure 4.6	Correlation between greyscale and water content	79
Figure 4.7	Biomechanical properties of progressive OA cartilage (a) Elastic Modulus, (b) Permeability	81
Figure 4.8	Linear Pearson correlations between greyscale intensity and (a) Elastic Modulus, and (b) Permeability of cartilage	84

LIST OF SYMBOLS AND ABBREVIATIONS

E	-	Elastic Modulus
k	-	Permeability
υ	-	Poisson's ratio
e	-	Void ratio
T	-	Tesla
r	-	Correlation coefficient
°C	-	Celsius
mm	-	millimetres
µm	-	micrometres
CDU	-	Cellulase Degrading Units
mg	-	milligram
ml	-	milliliter
mins	-	minutes
3D	-	Three-dimensional
CAX4P	-	Four-node bilinear displacement and pore pressure
CNR	-	Contrast-to-noise ratio
COMP	-	Cartilage oligomeric matrix protein
DAQ	-	Data acquisition
DICOM	-	Digital Imaging and Communication in Medicine
ECM	-	Extracellular Matrix
EDTA	-	Ethylenediaminetetraacetic acid
FCD	-	Fixed charge density

FE	-	Finite Element
FEA	-	Finite Element Analysis
FOV	-	Field of view
GAG	-	Glycosaminoglycan
GE	-	Gradient echo
HA	-	Hyaluronic acid
HBSS	-	Hank's Balanced Salt Solution
kDa	-	kilodalton
LVDT	-	Linear variable differential transformer
MIA	-	Monosodium iodoacetate
MRI	-	Magnetic Resonance Imaging
MMP	-	Matrix Metalloproteinases
OA	-	Osteoarthritis
OARSI	-	Osteoarthritis Research Society International
PBS	-	Phosphate Buffered Saline
PGs	-	Proteoglycans
pH	-	power of hydrogen
RF	-	Radio Frequency
ROI	-	Region of interest
SBMLs	-	Subchondral bone marrow lesions
SNR	-	Signal-to-noise ratio
TE	-	Echo time
TR	-	Repetition time
YLD	-	Years lived with disability

LIST OF APPENDICES

APPENDIX	TITLE	PAGE
APPENDIX A	MATLAB script	124
APPENDIX B	MATLAB script	126

LIST OF PUBLICATIONS

The following is the list of publications related to the work of this thesis:

Hashim, H., Abd Latif, M. J., Zakaria, M. S., Hambali, R. H., Arep, H., Harun, M. N., Sha'ban, M.,(2024). Effect of Storage Temperature of Articular Cartilage on Magnetic Resonance Imaging Greyscale and Biomechanical Properties. Journal of Advanced Research in Applied Mechanics, 128(1), pp.40–49

Hashim, H., Latif, M.J.A., Ibramsa, R.S., Zakaria, M.S., Hambali, R.H., Arep, H. and Harun, M.N., 2023, September. Effects of Storage Temperature on Biomechanical Properties of Articular Cartilage. In *International Conference and Exhibition on Sustainable Energy and Advanced Materials* pp. 169-173. Singapore: Springer Nature Singapore.

CHAPTER 1

INTRODUCTION

1.1 Research Background

Osteoarthritis (OA), one of the most common degenerative joint diseases, burdens more than 7% of the worldwide population, around 528 million people (Cui et al., 2020; Leifer et al., 2022). It was especially prevalent in countries with advanced market economies and in regions with aging populations where it was reached 14% (Leifer et al., 2022). OA was reported to be the 15th leading contributor of years lived with disability (YLD) globally, contributing to 2.2% of all YLD worldwide in 2019 (Kuş et al., 2023). Whereas knee, hand and hip joints were the main targets of the disease, knee OA alone accounted for 365 million cases worldwide (Steinmetz et al., 2023).

Economically, OA is a heavy categorical cost on the Malaysia's healthcare systems and society (Abd Rahim et al., 2020). Although comprehensive national estimates are scarce, the financial toll of OA is significant, with direct health care costs and indirect costs such as lost productivity. As an example, knee replacement surgery in Malaysia costs around USD 7,500 per patient, significantly cheaper compared to countries such as the United States where such procedures can cost USD 15,000-35,000 (Foo et al., 2017). These economic burdens highlight the importance of effective prevention and management strategies to reduce the impact on individuals and the domestic economy (French and Vigne, 2019).

OA was classified into primary and secondary clinically. Primary OA was caused by idiopathic degeneration of the joint, related to aging and genetic predisposition, while secondary OA was associated with identifiable factors, including traumatic joint injury,

congenital abnormalities, or inflammatory diseases (Yang et al., 2020; Coaccioli et al., 2022). Post-traumatic OA, a type of secondary OA, generally occurs because of joint injuries from motor vehicle accidents, falls, and sports-related injuries (Wang et al., 2020). Such injuries compromised joint structural integrity, resulting in cartilage destruction and eventual OA development over a period of months to years. The use of human cartilage is constrained by moral considerations and availability issues. Therefore, bovine femoral head cartilage has become a widely accepted model for osteoarthritis research.

The pathophysiology of OA is characterized by a gradual loss of the articular cartilage tissue mainly attributed to chondrocyte apoptosis, compositional changes in the biochemistry of the ECM and a reduction in the biomechanical properties of articular cartilage, principally, compressive stiffness (He et al., 2020; Kosonen et al., 2023). A transition to osteochondritis and degenerative conditions manifested as joint pain, stiffness, and limited mobility, severely limiting quality of life. Additionally, OA resulted in the deposition of more intramuscular fat, which further compromised muscle strength and joint stability.

The criteria for diagnosing OA went through a multi-faceted process including patient history, physical examinations, lab tests, and imaging modalities (Abramoff and Caldera, 2020). To note, early identification is particularly important because it allows for timely therapeutic intervention that could improve therapeutic outcomes and may even postpone the evolution of the disease. However, traditional diagnostic methods often identified OA at advanced grades, highlighting the necessity for advanced imaging technologies capable of detecting early disease markers and providing detailed insights into joint pathology (Chalian et al., 2023; Li et al., 2023; D'Agostino et al., 2024).

MRI has long been recognized as a non-invasive imaging diagnosis in which increased spatial resolution has given new windows into the anatomy, cell structure, and

histopathology of living tissues as shown in Figure 1.1. Generally, the field strength of MRI can be classified into low (<1.5 T), high (1.5-7.0 T), and ultra-high (>7.0 T). However, most of the studies were carried out using high-field MRI unit to examine articular cartilage properties since these MRI units were clinically used to diagnose patients (Namiranian et al. 2020; Hänninen et al. 2021; Emanuel et al. 2022). High-field MRI techniques have successfully been developed to provide measures of the macromolecular environment within cartilage tissue (Eck et al. 2023; Zibetti et al. 2023). This is possible via the interaction between interstitial water, probed by MRI, and the macromolecular constituents that affect the nuclear magnetic relaxation properties characterizing the spin energetics of the water proton system (Hani et al., 2015; Hänninen et al. 2021).

Figure 1.1: Image of knee joint using high-field MRI (Hani et al., 2015)

MRI has become essential diagnosis procedure to monitor the condition of articular cartilage since it was introduced to medical imaging in early 1930s (Winalski and Rajiah, 2011). However, imaging on low-field strength is recently being favored due to its smaller size, lower initial purchase price compared to high-field MRI, lower operational costs, lower energy deposition in tissues and availability of easily installed scanners (Ghazinoor and Crues, 2006; Arnold et al., 2023; Campbell-Washburn et al., 2024). Even with lower

image quality compared to high-field MRI, low-field MRI offers enough diagnostic capability to detect Grade I and II osteoarthritis. (Schmidt et al., 2023.; Pogarell et al., 2024). Figure 1.2 shows MR images obtained at high-field and low-field of small subchondral bone marrow lesions (SBMLs) which both images showed well the affected area.

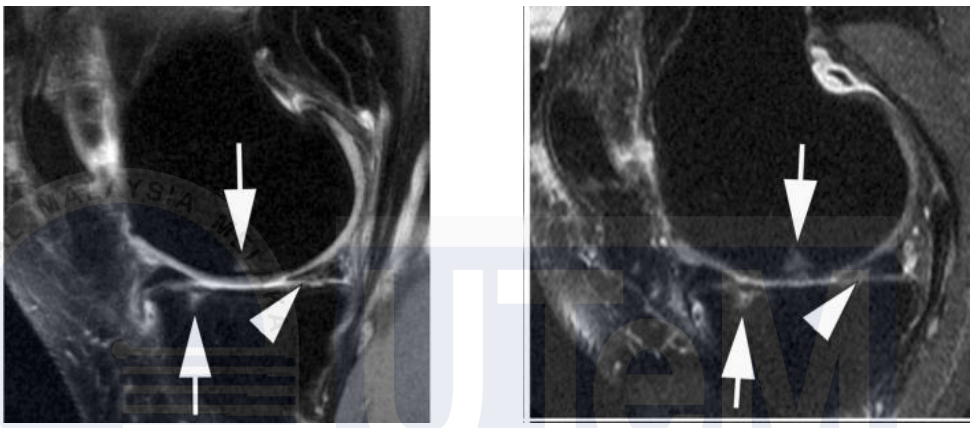

(a) (b)

Figure 1.2: Comparison MRI for assessment of knee osteoarthritis. a) Standard high-field MRI shows small subchondral (SBMLs). b) At low-field MRI, SBMLs (arrows) are visualized diagnostic image quality (Pogarell et al. 2024).

1.2 Problem Statements

OA is a slowly progressing joint disease that affects millions worldwide, mainly through the gradual breakdown of articular cartilage. OA remains one of the leading causes of disability worldwide, yet early diagnosis remains challenging due to the limitations of conventional imaging techniques. While MRI is widely used for cartilage assessment, most studies have focused on mid-field and high-field MRI systems, leaving a gap in research on the diagnostic potential of low-field MRI (Schmidt et al., 2023).

In previous quantitative MRI studies, cartilage was examined based on thickness, volume and cartilage loss (Hänninen et al., 2021; Zibetti et al., 2023). However, it has been reported that there is no significant differences of cartilage thickness at early grade of OA

(Edd et al., 2021). Although further quantitative MRI studies were carried out using high-field MRI to quantify the cartilage matrix composition particularly proteoglycans (PGs) and collagen content using contrast agents, the results described the biphasic behavior within the tissues.

While most research and clinical focus tend to be on advanced grades where cartilage becomes visibly thin or completely lost subtle but important changes actually begin much earlier. It was found that in the early grade of OA, the biomechanical properties of articular cartilage starts to change relatively which then lead to morphological alterations even before any thinning is noticeable (Chery et al., 2020; Linus et al., 2024). Unfortunately, these early signs often go unnoticed, and studies exploring this grade remain limited. Without a clear understanding of what's happening during the early phases, it's difficult to develop tools or treatments that could intervene before the damage becomes irreversible.

At the same time, there were still lacks of detailed knowledge about how cartilage changes across its depth as OA progresses through different grades (Szarek et al., 2020). In particular, the process of cartilage fibrillation where the surface becomes frayed and irregular was commonly seen in early OA but isn't fully understood. Clinically, it's known that this surface damage is linked to the breakdown of type II collagen, yet the biomechanical and structural reasons behind it are not well defined (Gao et al., 2023; Liphardt et al., 2024) . To truly understand how OA develops and to catch it earlier, we need a more thorough, layer-by-layer investigation of cartilage and how its properties change over time. Due to ethical and practical limitations in obtaining human cartilage, bovine femoral head cartilage was used as a model for OA progression.

Thus, there is a need to study on the potential application of the low-field MRI in order determine the biomechanical properties of the cartilage in order to detect early

changes in OA. The correlation of the quantitative low-field MRI image greyscale and cartilage biomechanical properties of Elastic Modulus and Permeability is yet to be fully explored. These findings could serve as the long-term goal to develop non-invasive technique for the early detection of the changes in biomechanical properties of articular to examine the condition of articular cartilage.

1.3 Research Objectives

This study aims to examine the correlation between biomechanical properties and image grayscale from low-field MRI in grade II OA articular cartilage. With the following specific objectives:

I. To assess the fibrillation and morphological changes of cartilage tissue during OA progression.

II. To characterize the biomechanical properties and low-field MRI grayscale features of bovine fibrillated cartilage using experimental and computational methods.

III. To establish correlations between MRI grayscale intensity, cartilage hydration, and biomechanical properties in grade II OA.

1.4 Research Scopes

This research was carried out to study the characterization of articular cartilage. Bovine femoral head cartilage samples were used as models for Grade I and Grade II OA progression. The cartilage samples were scanned using 0.18T Esaote C-scan MRI (Genova, Italy) to obtain grayscale images of fibrillated cartilage from the water content analysis. Only arthritic tissues were used in this study. Cartilage samples were examined under a low-power microscope with a 50x magnification to quantify the area. Observations were conducted at the enzymatic fibrillated process. The resulting data were analyzed using

MATLAB, which were used to identify the grayscale image and the black pixels within it. ImageJ software data were processed to quantify the changes observed before and after in the surface area of the articular cartilage. The biomechanical properties such as Elastic Modulus and Permeability of cartilage at OA were characterized through experimental and computational methods through the models that developed in ABAQUS 6.9 software (DS Simulia Corp., Providence, RI, USA), providing a correlation between mechanical study and low-field MRI.

1.5 Hypotheses

This study will lead to the following hypotheses:

I. OA cartilage could be prepared at different grades from early OA to progressive OA.

II. OA cartilage fibrillation affects both structural and biomechanical properties.

III. The morphology and biomechanical properties of articular cartilage can be represented at different OA grades.

IV. The correlation between cartilage morphology assessment and biomechanical properties could provide insights into OA grading.

1.6 Research Questions

This work will contribute to enhancing knowledge about examining the biomechanical properties of grade II OA articular cartilage using low-field MRI by imposing these main research questions:

I. **HOW** can the characteristics of grade I and grade II OA articular cartilage be prepared and determined?

II. **WHY** do cartilage component changes and surface area behaviors play an important role in determining the biomechanical properties of grade II OA cartilage?

III. **HOW** does the OA cartilage affect the biomechanical properties and MRI image grayscale at grade II?

IV. **HOW** does OA cartilage affect the correlation between the biomechanical properties and grayscale of low-field MRI images?

V. **HOW** can the correlation between the biomechanical properties and grayscale of low-field MRI images represent different OA grades?

1.7 Significance of Study

This study provided crucial insights into the correlation between biomechanical properties and grayscale intensities from low-field MRI in assessing OA cartilage. The findings could enhance progressive OA detection, facilitate preventive interventions, and improve clinical decision-making in OA management. Furthermore, the study supported the potential of low-field MRI as an accessible alternative for cartilage assessment, expanding its applications beyond traditional high-field MRI approaches.

1.8 Outline of Thesis

The thesis contains of six chapters as per following sequence:

Chapter 1: Introduction

This chapter briefly introduces about OA and the current MRI research background and problem statement in the study. There are objectives which need to be accomplished in the study.

Chapter 2: Literature Review

This chapter provides the information about the anatomy of human synovial joints, OA, and articular cartilage. This chapter also presents the typical application of MRI to assess the articular cartilage. It also briefly describes on the properties characterization of articular cartilage.

Chapter 3: Methodology

This chapter outlines the specimen preparation, equipment, imaging and experiment procedures, methods, computational modelling, and image processing methods in order to characterize the MRI image greyscale and biomechanical properties of the cartilage.

Chapter 4: Results and Discussion

This chapter presents the results and the analysis on both biomechanical properties and MRI image greyscale of articular cartilage. In the analysis, the biomechanical properties results obtained from grade I and grade II samples. The last section shows the correlation between the cartilage greyscale and biomechanical properties is discussed.

Chapter 5: Conclusion and Recommendation

This chapter summarizes the thesis with conclusion and recommendation, especially in characterizing the cartilage biomechanical properties using low-field MRI image.

CHAPTER 2

LITERATURE REVIEW

2.1 Introduction

This chapter begins by concise overview of OA and grading system. Then, outlining the anatomy and types of synovial joints to provide a foundational understanding of human joint architecture and its relevance to OA. The discussion shifts to in-depth examination of articular cartilage, including its composition describing its behavior, and physical organization, as well as alterations for cartilage tissue and thickness in experimental studies. Additionally, the preparation of in vivo and in vitro plays a crucial role in understanding cartilage degradation during OA, providing controlled conditions for studying tissue breakdown with animal models were provide valuable platforms for studying OA progression. Furthermore, aspects of cartilage degradation were explored, focusing on the types of collagenase used, their concentrations, and the time intervals for degradation. Besides that, a discussion on the capabilities of low-field MRI, along with computational techniques employed to improve greyscale image quality. This includes critical considerations such as the selection of magnetic field strength and pulse sequences to optimize imaging outcomes. The chapter concludes with methods for characterizing the biomechanical properties of fibrillated cartilage and previous developed finite element analysis models for articular cartilage characterization to enhance the understanding of its mechanical properties were also explored and reviewed.

2.2 Osteoarthritis

OA is the most common joint disease and a major cause of chronic disability, particularly among middle-aged and older adults. More than 30% of individuals over 45 years old have been diagnosed with OA (O'Neill et al., 2018). In Malaysia, projections estimate that 30.8% of the citizen aged 55 years and above will develop OA (Mat et al., 2019). With the aging population increasing globally, the prevalence of OA is expected to rise significantly from 2020 to 2050. OA most commonly develops without a known cause, a condition referred to as primary OA, which is rare in individuals under 40. However, secondary OA occurs due to joint degeneration from injuries, hereditary factors, inflammatory conditions, metabolic disorders, or neurologic diseases (Roškar and Hafner-Bratkovič, 2022).

While primary OA appears to develop spontaneously, many cases likely have underlying predisposing factors such as genetic susceptibility, prior joint injuries, or excessive mechanical stress as shown in Figure 2.1. Secondary OA, on the other hand, can result from specific conditions like joint infections, dysplasia, Legg–Perthes disease, avascular necrosis, and hemophilia (Driban et al., 2020). Regardless of the underlying cause, the progression of joint degeneration follows a similar pattern, involving the loss of articular cartilage, remodeling and sclerosis of subchondral bone, and the formation of subchondral bone cysts and osteophytes. Whether OA develops in young adults due to identifiable joint abnormalities or in older individuals without clear predisposing factors, the degenerative process remains fundamentally the same.

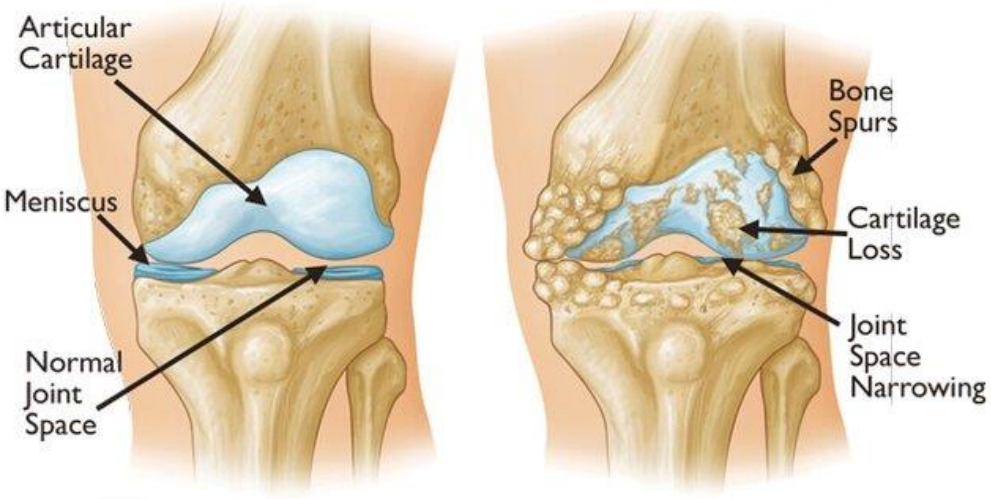

Figure 2.1: (a) Normal and (b) Osteoarthritic joints (Antony et al., 2020)

The Osteoarthritis Research Society International (OARSI) grading system is a widely used tool for assessing cartilage degeneration, ranging from grade 0 (intact cartilage) to grade 5 (severe cartilage erosion) as shown in Table 2.1. In early grade 0 indicates structurally cartilage with no damage, while grade 1 shows minimal degradation (<10%). As OA progresses, grade 2 presents superficial fibrillation (10–25%), and grade 3 reveals increasing deterioration, including fissures, irregularities, and notable cartilage thinning (25–50%). By grade 4, erosion extends to the subchondral bone (>50%), leading to severe tissue breakdown. Grade 5 represents the most advanced grade, with complete cartilage loss, exposed subchondral bone, and joint deformation. This system has been extensively validated and is crucial for diagnosing OA severity, tracking progression, and evaluating interventions as demonstrated by (Waldstein et al., 2016; Park et al., 2022)

Table 2.1: OA cartilage grade assessment (Waldstein et al., 2016)

Grade	Key Feature	% Involvement (Surface)
Grade 0	Cartilage intact	No OA activity seen
Grade 1	Cartilage degradation	<10%
Grade 2	Cartilage superficial fibrillation	10–25%
Grade 3	Cartilage vertical fissures	25–50%
Grade 4	Cartilage erosion	>50%
Grade 5	Complete cartilage loss	100%

2.3 Synovial Joints

This synovial joint, or arthrodial joint, possessed the greatest flexibility between bones (Popov et al., 2021). It allows the bones extensive motion for free movement and rotation of one another. The human body's synovial joints found most were the knees, hips, shoulders, wrists and ankles.

2.3.1 Anatomy of synovial joints

The synovial cavity, connective tissue, and articular cartilage make up the synovial joint. The gap between the bones was called the synovial cavity, and it was filled with lubricating synovial fluid (Pap et al., 2020). The synovial membrane was surrounded by a capsule made of thick connective tissue. The end of the articulating bone was covered in a bluish-white substance called articular cartilage. The synovial joint of the knee was seen in Figure 2.2.

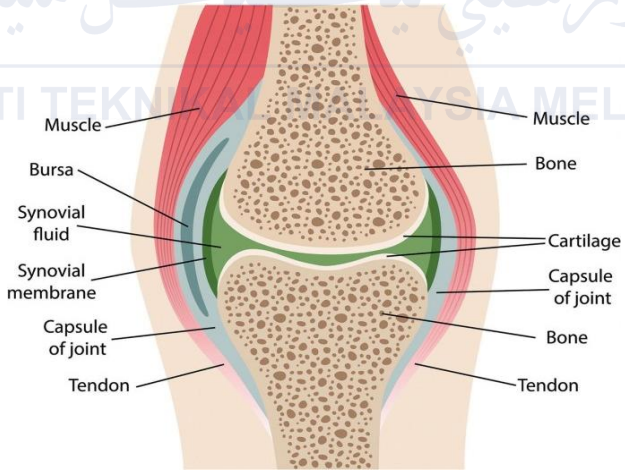

Figure 2.2: Structure of synovial joint in knee (Usgu and Usgu, 2023)

The purpose of the synovial joint was to reduce friction within the joint and shield the bone from impact stress (Lin and Klein, 2021). The synovial joint's articular cartilage works to keep the joint's bones from rubbing against one another. Nevertheless, the joint's thick connective tissue capsule acts as a seal to maintain the position of the lubricating synovial fluid and to provide stability by limiting joint movement (Redondo et al., 2019).

2.3.2 Types of synovial joints

The structure of synovial joints was present according to its position and function. Therefore, it can be classified into six different categories for the whole human body anatomy such as plane joint, hinge joint, pivot joint, condyloid joint, saddle joint and ball-and-socket joint (Siddaiah and Menezes, 2016). For instance, shoulder and hip joints were known as ball-and-socket joints which have different structures of synovial joint compared with knee joint as hinge joint. Figure 2.3 shows the types of synovial joints presented in human musculoskeletal system.

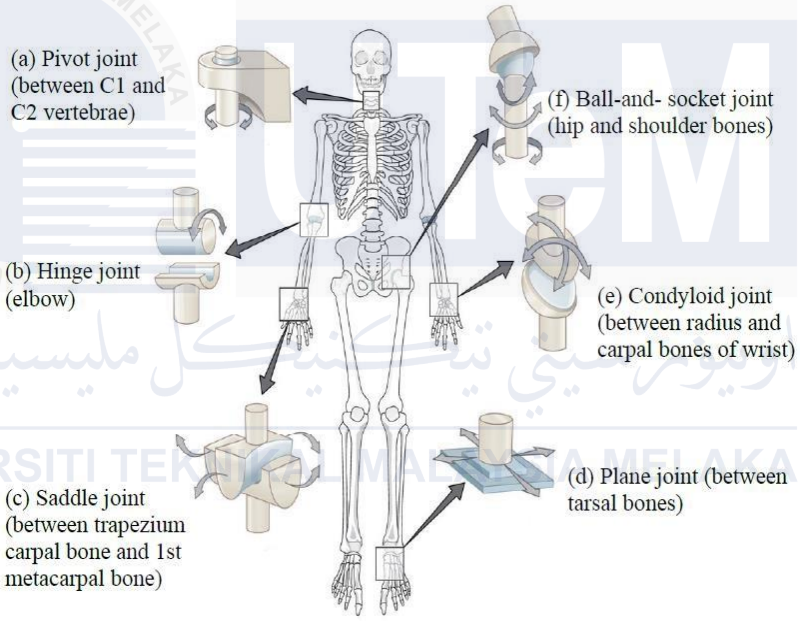

Figure 2.3: Types of synovial joints (Siddaiah and Menezes, 2016)

The pivot joints allow rotational movement because this type of synovial joint exist in rounded bone area where rounded end of one bone fits into a ring formed by the opposing bone. The articulation between the axis bones can be found in neck vertebrae and the wrist, which allow the head to turn back and forth and the palm of the hand can be turned up and down. In hinge joints, only slightly rounded end of one bone fits into the slightly hollow end of the other bone. Hinge joints were usually found between the upper and lower arm bones, such as elbow, ankles, fingers, toes, and knees. Hinge joints act like a door hinge that allow one bone to move while the other remain stationary. Saddle joints

allow angular movements with greater range of motion. Thumb joint was an example of saddle joint, which can move freely back and forth and up and down.

Plane joints allow gliding movements where the range of motion was limited, and no rotation was involved. Usually plane joints were found in hand carpal bones and foot tarsal bones. Condyloid joints allow angular movement along two axes such in the joints of the fingers (metacarpophalangeal joints). Condyloid joints composed of an oval- shaped end of one bone fitting into a similarly oval-shaped hollow of another bone. Whereas, in ball-and-socket joints ball-like end of one bone fits into a cup-like socket of opposing bone. Ball-and-socket joints allow greatest range of motion compared with other types of synovial joints, full-circle rotation was achievable and usually this type of joint was found in hip and shoulder joints.

2.4 Articular Cartilage

Consequently, articular cartilage was a type of hyaline cartilage with a thickness ranging from 2 to 4 mm (Sidharthan et al., 2021) . It was called hyaline cartilage as it does not contain blood vessels, nerves, or lymphatics. Articular cartilage was composed of a compact ECM that contains high cells called chondrocytes. The ECM primarily consists of water, collagen, PGs as well as other non-collagenous proteins and glycoproteins available in smaller quantities (Buckwalter and Mankin, 1997; Gahunia and Pritzker, 2020). These components help store the water within the ECM, as it was a crucial part of maintaining the unique mechanical properties of the cartilage. The principal function of articular cartilage was to give a smooth, lubricated, and low friction surface at the end of articulating bones (Belluzzi et al., 2023). Articular cartilage supports the joint and distributes the compressive, tensile, and shear forces in cyclic and repetitive task (Petitjean et al., 2023). It was responsible to minimize the peak pressures on the subchondral bone, perform as shock

absorber for loads, and provide a low friction on dynamic movement and gliding surface (Petitjean et al., 2023).These functions were achieved from the unique material properties possessed by the articular cartilage.

2.4.1 Composition

Articular cartilage was a unique tissue that shows biphasic behavior in which both the solid and fluid properties. Interstitial fluid of articular cartilage was made up of water and dissolved electrolytes which supports most of the joint contact load and provides nutrition and medium for lubrication in the corresponding synovial joint (Bhosale and Richardson, 2008; Kung et al., 2015). The articular cartilage tissue mainly consists 65% to 80% of water while the remainder of the tissue were composed primarily of solid sources of chondrocyte cells comprising 1% to 10% of the cartilage volume and an ECM rich in collagen particularly collagen type II which comprises 10% to 30% of its wet weight, PGs specifically aggrecan which comprises 5% to 15% of its wet weight, and other non-collagenous proteins, glycoproteins and lipids (Chen et al., 2006; Sophia Fox et al., 2009; Marks 2014; Fisher et al., 2019). The ECM was synthesized, organized, and maintained by chondrocytes which were the primary cellular component of the articular cartilage and liable for the integrity of the cartilage (Chen et al., 2006; Fisher et al., 2019; Hall 2019). Figure 2.4 shows components forming the ECM of articular cartilage.

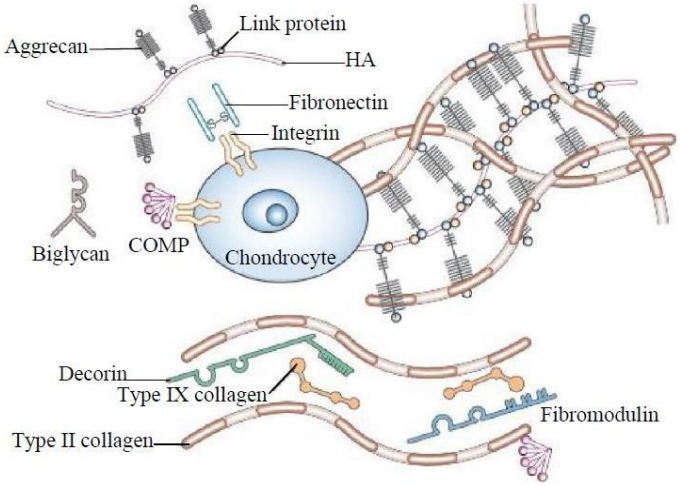

Figure 2.4: Extracellular matrix of articular cartilage (Chen et al., 2006)

Chondrocytes are protected from excessive joint forces and harmful chemical substrates by the pericellular matrix, as shown in Figure 2.4, which directly surrounds the cell, followed by the territorial and inter-territorial matrices as the more distant zones (Bhosale and Richardson, 2008; Marks, 2014; Takahata et al., 2020). As the central component of cartilage, chondrocytes are surrounded by three major protein classes: collagens (mainly type II), proteoglycans (PGs), and non-collagenous proteins such as link protein, fibronectin, cartilage oligomeric matrix protein (COMP), together with smaller PGs including biglycan, decorin, fibromodulin, and hyaluronic acid (HA). These macromolecules work collectively to maintain the flexibility and tensile strength of the extracellular matrix (ECM) throughout life. Collagens, the most abundant macromolecules in the body (Laronha and Caldeira, 2020), provide resistance to compressive forces while allowing diffusion of small molecules across the tissue matrix. At least 19 collagen types have been identified in the ECM, comprising no fewer than 33 polypeptide chains (Alcaide-Ruggiero et al., 2021). Cartilage itself contains at least five types of collagen, with type II accounting for 90–95% of the ECM framework (Hollander et al., 1994; Bhosale and Richardson, 2008; Alcaide-Ruggiero et al., 2021), while minor collagens contribute to the stabilization of type II fibril networks.

Proteoglycans represent the second largest group of ECM macromolecules, making up 10–15% of the wet weight. They consist of protein cores with sulfated glycosaminoglycans (GAGs), synthesized by chondrocytes, and composed of disaccharides of chondroitin sulphate and keratin sulphate. PGs are generally classified into large aggregating and small PGs, as shown in Figure 2.5. Their primary role is to regulate fluid and electrolyte balance, thereby providing compressive strength to the cartilage (Bhosale and Richardson, 2008). Alongside collagen degradation, the gradual loss of PGs significantly impairs cartilage function, particularly by altering permeability and equilibrium elastic modulus (Horkay et al., 2024).

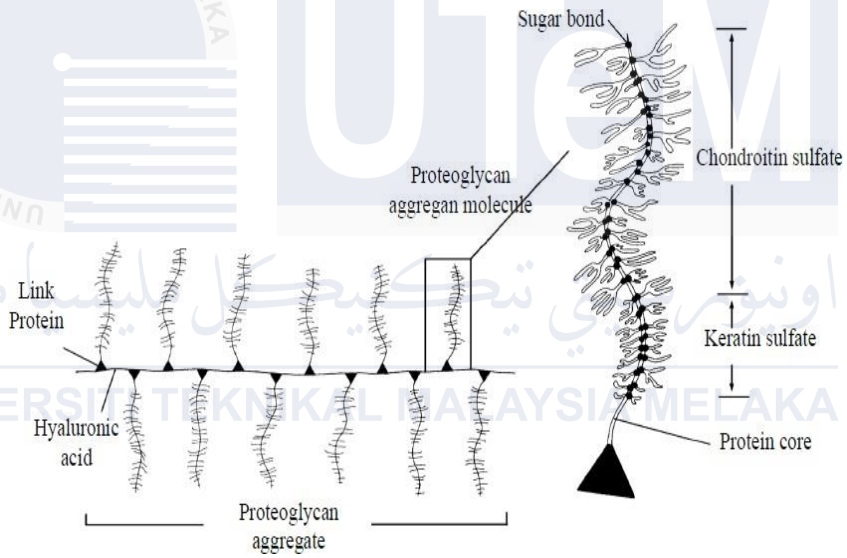

Figure 2.5: Diagram of PGs aggregate and aggrecan molecule (Pearle et al., 2005)

Chondrocytes were highly specialized cells that account for only about 1-5% of the volume and were sparsely embedded within the matrix. Chondrocytes synthesize matrix components, which include type II collagen and large PGs aggregates. The number, shape, and size of chondrocytes vary according to the anatomical region of cartilage. The balance between fluid and electrolytes in the cartilage tissue was maintained by PGs because the sulfated GAG chains were high in fixed negative charges and can draw water into the cartilage creating osmotic pressure gradient which provides compressive resistance to the cartilage tissue (Chen et al., 2006; Alcaide-Ruggiero et al., 2023). In a normal articular

cartilage, many aggrecan molecules binds to HA chain and the binding site was further stabilized by link protein. HA was a water retentive molecule that also responsible for the high-water content in cartilage tissue (Knudson et al., 2019). Thus, the Permeability of the cartilage tissue was fully controlled by the PGs concentration. It was worth pointing out that the biomechanical properties of articular cartilage depend mainly on the maintenance of high PGs and collagen concentrations within the ECM.

2.4.2 Structure

Besides that, articular cartilage can be divided into four distinct zones namely, superficial zone, transitional zone, deep zone, and calcified zone which consists of subchondral and cancellous bone. Figure 2.6 illustrates the zones and shape of the cells and their arrangement respectively.

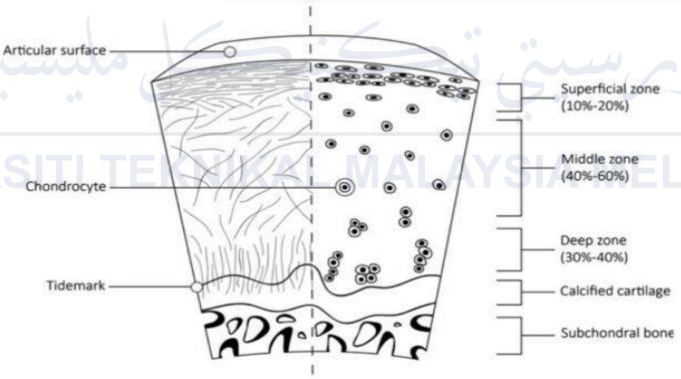

Figure 2.6*:* The zonal architecture and cells arrangement of articular cartilage (Schmidt, 2021)

Each zone was distinguished by the shape and orientation of the chondrocyte cells and the distribution of type II collagen fibrils and large aggregating PGs (Wong and Carter, 2003; Eschweiler et al., 2021). The superficial zone which has parallel oriented collagen fibrils and flat shaped chondrocytes were thought to act as a protector for the rest of the cartilage tissues below and makes up approximately 10% to 20% of the total cartilage thickness (Sophia Fox et al., 2009; Bartell et al., 2015; Guo et al., 2024). Water content

was highest on this zone with 80% of the total wet weight of the cartilage because it was said that chondrocytes on this zone actively synthesizes high concentration of collagens and low concentration of PGs especially aggrecan (Bhosale and Richardson, 2008; Takahata et al., 2020). This zone also secretes abundant lubricin, HA and phospholipids which were vital to lubricate joint articulatio (Kosinska et al., 2015; Takahata et al., 2020; Marian et al., 2021) n. Superficial zone can be stated as the thinnest zone compared with the other three zones and any injury that damages this surface will expose the underlying zones to shear and tensile forces (Guo et al., 2024).

The transitional zone takes up the largest portion in the cartilage structure where around 40% to 60% of the total cartilage thickness. In this zone, collagen fibrils start to bend and twist forming whimsical network and the chondrocyte cells were arranged randomly. The PGs concentration was higher in this zone (Eschweiler et al., 2021; Kafian-Attari et al., 2023). The deep zone comprises 30% of the total cartilage thickness and contrasts to the superficial zone, in deep zone the collagen fibrils were aligned perpendicularly to the surface and the chondrocytes were arranged in columns to provide the greatest resistance to compressive forces (Sophia Fox et al., 2009). This zone contains the largest diameter of collagen fibrils and highest concentration of PGs but poor in water content because chondrocytes density was lower in this zone (Bolog et al., 2015; Takada and Mizuno, 2018). In calcified zones the chondrocytes were hypertrophic and secretes mineralized matrix near the subchondral bone (Bhosale and Richardson, 2008; Sophia Fox et al., 2009; Fisher et al., 2019). The water content, PGs concentration, collagen fibrils concentration and orientation together with chondrocyte morphology vary throughout the depth of the cartilage tissue. This anisotropic structure of cartilage tissue has given the laminar appearance of cartilage in MRI images and makes the study on cartilage unique structure at molecular, macroscopic, histological and gross anatomic levels to be

interestingly demanding (Xia, 2000; Chahine et al., 2004; Puiggalí-Jou et al., 2024). Articular cartilage tissue was fragile, once damaged it were hard to heal itself and this was what makes OA a big clinical challenge as shown by the work of (Roseti et al., 2019).

2.4.3 Alteration in osteoarthritis

OA initiates with biochemical imbalances in articular cartilage, driven by the over expression of proteolytic enzymes that degrade the ECM. In early grade I OA, chondrocytes respond to mechanical stress or inflammatory cytokines by regulating collagenases such as matrix metalloproteinases (MMP) and stromelysin, which target collagen and PGs (Grenier et al., 2014). Collagenases cleave type II collagen fibrils, destabilizing the tensile network, while aggrecanases degrade the PGs core protein, aggrecan (Zhu et al., 2019). This enzymatic activity disrupts the ECM's structural integrity, increasing cartilage Permeability and reducing compressive stiffness. Despite chondrocytes attempting compensatory synthesis of ECM components, the overproduction of MMPs overwhelms endogenous inhibitors like tissue inhibitors of metalloproteinases, leading to progressive matrix breakdown (Mixon et al., 2021).

The transition to grade II OA was marked by visible cartilage fibrillation and erosion. As collagen degradation progresses, the superficial zone loses its protective lamina splendens, exposing the underlying collagen network to further enzymatic and mechanical damage. Fibrillation results in disjointed surface textures to promote wear and release of collagen and PGs fragments into synovial fluid. These fragments activate synovial inflammation, resulting in excessive production of cytokines that further activate chondrocytes to secrete MMPs. Degradation of collagen fibers leads to loss of the structural framework that allows for retention of PGs and therefore worsens the dehydration of the ECM and hampered load distribution. Conversely, this cycle of

bicondylar degeneration leads permanently damaged cartilage and its transformation toward a pathological joint with advanced OA.

Among PGs in AC, aggrecan was crucial for maintaining hydration and compressive resistance because its GAGs chains are negatively charged. This imbalance is driven by PGs in degenerating articular cartilage that is progressively degraded and bio-chemically altered during OA. Aggrecan are unique enzymes that cleave specific sequences in the core protein, which leads to the release of GAGs, and substantially reduces the fixed charge density. This loss makes it harder for the cartilage to draw in water, thereby reducing osmotic pressure and shock absorption. As PGs become exhausted, the collagen framework is subjected to excessive mechanical loading, hastening its degradation. This biomechanical failure leads to a feedforward cycle of ECM degradation, highlighting the critical role of PGs loss in the OA.

2.4.4 Thickness

Cartilage thickness is a critical factor influencing its load-bearing capacity and functional performance that are varies between different joints or within the same joint. (Nomura et al., 2017). Thinner cartilage areas which are more susceptible to stress accumulation, microstructural damage, surface fibrillation, erosion, localized loadings and regions of high curvature (Brown et al., 2022). In OA, cartilage thinning is one of the earliest changes, fibrillation mostly starts at the superficial zone before progressing deeper and thus relieving interstitial fluid retention and increasing tissue Permeability. By losing hydrostatic pressure, the collagen fibrillar networks is weakened, susceptible to tensile and shear forces which further contribute to the physical damage. In Grade I OA, the initial augmented water content, originating from PGs breakdown, leads to a general softening of the tissue, whose ability to bear load decreases, resulting in a reduced capacity to resist

deformation. Degeneration in Grade II OA is characterized by more pronounced superficial fibrillation features, leading to loss of PGs and collagen disorganization, which not only allow for increased Permeability but also compromised mechanical integrity. Even thicker cartilage at the femoral condyle or patellar surface may spare it from fibrillation but can be subject to rapid degeneration with abnormal mechanical loading.

2.5 Preparation of osteoarthritic cartilage

OA can lead to articular cartilage degradation both naturally and due to external factors. Primary OA typically results from the wear and tear of articular cartilage over time, while secondary OA arises from trauma, injury, or abnormalities. Since OA develops due to multiple factors rather than a single cause, obtaining samples at specific grades of progression is challenging, as they are often collected in the later grades. However, OA can be artificially induced which offer valuable approaches using preparation in vivo or in vitro methods. As it involve with degradation, the enzyme through in vitro preparation looks more promising in research as it can be convincing by preferred for targeted investigations and in vivo models for broader biological interactions. In vivo models involve surgical and enzymatic injections to induce degradation within a biological system, capturing natural tissue responses. In vitro preparation utilizes enzymes like collagenase, papain and others allowed precise control over concentration and exposure time. While in vivo methods reflect physiological conditions, in vitro approaches offer reproducibility and efficiency, making them ideal for controlled degradation studies. Animal models, including rodents, rabbits, and large animals like sheep or pigs, provide valuable platforms for studying OA progression (Zhou et al., 2025). These models help mimic human OA conditions by replicating mechanical loading, biochemical changes, and inflammatory responses seen in the disease (Esdaille et al., 2021).

2.5.1 In vivo degradation method

For many years, the basis of cartilage degeneration research has been through animals, and regulatory approval for the clinical application of biologics, devices, and procedures still depends on them (Mern et al., 2021). These have been utilized to comprehend the pathophysiology of OA and create effective degradation plans (Kuyinu et al., 2016). Drugs effects on the progression of OA have been investigated using induced (invasive) models. These were referred to as in vivo methods of inducing OA and can also be divided into chemically or surgically induced models. These models guarantee that the study may be completed in a shorter amount of time due to their quick induction of OA. However, induced models were flawed in and do not correspond to the organic degenerative changes in human degenerative OA (Lampropoulou-Adamidou et al., 2014). Subchondral bone alterations, for instance, have been employed to explore the pathophysiology of post-traumatic OA in surgically produced mice (Pauly et al., 2015).

In the past, small animal model, such as murine models represent a cornerstone of in vivo cartilage degradation research, offering significant advantages in terms of genetic manipulation capabilities, cost-effectiveness, and relatively rapid disease progression. One of the common types of research was the destabilization of the medial meniscus (DMM) mouse model that has emerged as a particularly valuable system for investigating OA pathogenesis and potential interventions (Wu et al., 2022). In this surgical model, transection of the medial meniscotibial ligament induces joint instability that leads to progressive cartilage degradation closely mimicking human OA (Temp et al., 2020). Even though this model have significant limitations, it can all be useful in determining the efficacy and potency of cartilage degeneration techniques.

Chemically induced models often require injecting an inflammatory or poisonous substance right into the joint. Using this model, researchers may examine how drugs

impact the pain or inflammation that these molecules cause. Collagenase, papain, sodium monoiodoacetate, and quinolone were a few of the drugs used to cause OA in animals. These eliminate the need for surgery and shield some animals from potential infection. These were helpful in the design of short-term studies due to their repeatability and ease of induction. Chemical models have a pathogenesis that was unrelated to that of post-traumatic OA, although being less invasive than surgical ones. In order to better understand the origins of pain, they were mostly used in this research (Lampropoulou-Adamidou et al., 2014).

A proteolytic enzyme called papain has historically been used to induce OA. It breaks down PGs, an important element of the cartilage that offers compressive resistance via water absorption (Glyn-Jones et al., 2015). Monosodium iodoacetate (MIA) is another well-studied method of cartilage degradation in the context of OA diseases (Pitcher et al., 2016). This agent prevents glyceraldehyde-3-phosphate dehydrogenase activity in chondrocytes, thus distorting their metabolism and causing degradation of tissue and matrix. In a recent study of artemisinin-in-loaded emulgel used MIA to induce knee OA in vivo which reported MIA injection resulted in an upsurge in inflammatory markers and simultaneously aggravated cartilage matrix degeneration (Sahin et al., 2021). Animal pain behavior was extensively evaluated and medicated using the MIA-induced OA paradigm. This pain model may be more accurate in predicting therapy success when compared to other pain models used to evaluate OA medicines (Fernihough et al., 2004). Mice and rats are common to study with as demonstrated (Guzman et al., 2003).

2.5.2 In vitro degradation method

Cartilage research of OA in animals often involves living animals, which was used to study the cartilage tissues. The cartilage of these animals was often degraded through in vivo means, meaning that OA was induced while the animals were still alive. There were also methods of in vitro degradation methods that offer controlled environments for studying biomechanical properties and degradation processes outside living organisms. Studies of OA involving the biomechanical properties of cartilage often use samples that were degraded through in vitro means. Three grades were used to categorize OA progression: 1) PGs degeneration followed by type II collagen degeneration, 2) cartilage surface fibrillation and erosion, and 3) the start of synovial inflammation (Wu et al., 2019). This indicates that PGs depletion was the first indication of OA development, making it a critical target for in vitro degradation studies.

Typically, total joint replacement, tissue explants or OA induction can be used to obtain OA samples. Chemicals used in chemical deterioration may vary depending on the intensity of the chemical. Most of these chemicals were enzymes that digest a particular component in the ECM. Some commonly used chemical enzymes include Collagenase, Pronase, Papain, Hyaluronidase and Chondroitinase (Laasanen et al., 2002; Nawaz et al., 2018). Degradative components were employed to simulate the breakdown of ECM components (Olivotto et al., 2015). In vivo experiments were chosen to focus on externally exerted mechanical properties rather than internal mechanical loading, as the aim of this research is to detect osteoarthritis through biomechanical properties rather than animal movement or other equivalents. Finally, OA can also be induced with the utilization of excessive mechanical loading on the target joints or samples.

2.5.2.1 Enzyme Degradation

OA is characterized by the loss of articular cartilage, the progressive degradation of cartilage, which has functional and structural consequences for the joint. Different enzymes are utilized in research to replicate this degradation and examine its impact on cartilage integrity. Histological cartilage destruction in OA research is commonly induced with Collagenase, Pronase, Papain, Hyaluronidase and Chondroitinase. Type II collagen fibrils form the key structural component of cartilaginous structures providing tensile strength and are specifically susceptible to collagenase cleavage. The degradation of ECM components, including basic units needed for cartilage integrity, was with a specific enzyme, Collagenase Type II which is known to selectively degrade collagen with the non-collagenous components of ECM remaining intact (Davidson et al., 2006; Mixon et al., 2021). This approach demonstrated that slight collagenase degradation induces early changes of OA specifically the discontinuities around collagen fibril networks and reorganization of chondrocytes without losing the entire ECM structure to enable the study of early changes in collagen networking (Mixon et al., 2021). The stronger activity of Pronase, a mix of proteolytic enzymes, makes it more comprehensive, the enzyme also acts on small collagens, glycoproteins, and PGs. In contrast to collagenase that only attacks the fibrillar network, Pronase digestion results in a more diffuse ECM degradation, leaving a relatively intact collagen scaffold. It has been applied to isolate chondrocytes with reduced ECM loss as well as studying the role of glycoprotein structures in the structural stability of cartilage (Gandy et al., 2017).

Papain, a cysteine protease, preferentially degrades PGs while sparing collagen fibrils in early digestion phases, effectively mimicking grade I -associated PG depletion, which reduces cartilage compressive stiffness (Yao et al., 2021). GAG loss precedes collagen network disruption in papain-treated cartilage; this is a known trait of grade I OA

pathology (Siebelt et al., 2014). Hyaluronidase and Chondroitinase specifically degrade hyaluronic acid and chondroitin sulfate major ECM components. Hyaluronidase is a naturally occurring enzyme that breaks down hyaluronic acid, a vital component of synovial fluid and ECM that promote lubrication and hydration. Its degradation causes an increase in cartilage Permeability and a decrease in resistance to compressive loads (Higuchi et al., 2017). Chondroitinase specifically cleaves chondroitin sulfate PGs, changing cartilage architecture in rats. This has been utilized to look at PGs functions in ECM maintenance as well as study how their degradation affects chondrocyte behavior and cartilage viscoelastic (Rieppo et al., 2003; Lin et al., 2020). As an overview, Table 2.2 compares enzymatic-based cartilage digestion used in OA research.

Table 2.2 Comparative overview of enzymatic cartilage digestion

Enzyme	Specificity	Mechanism of Action	Application in Cartilage Research	Reference
Collagenase	type II collagen fibrils	Cleaves triple-helical collagen regions, disrupting fibrillar network	To simulate early grade II OA-like collagen breakdown, preserving non-collagenous ECM	(Davidson et al., 2006; Mixon et al., 2021)
Pronase	Broad proteolytic activity	Degrades ECM proteins, including minor collagens, glycoproteins, and PGs	Partial ECM degradation for cell isolation and functional ECM analysis	Gandy et al., 2017
Papain	Prefers PGs degradation	Cleaves peptide bonds in PGs and glycoproteins, sparing fibrillar collagens	Mimics Grade I OA PGs depletion, useful for studying cartilage softening	(Siebelt et al., 2014; Yao et al., 2021)
Hyaluronidase	Degrades hyaluronic acid	Breaks down hyaluronic acid in ECM, increasing Permeability	Assesses cartilage lubrication loss and synovial fluid alterations	Higuchi et al., 2017
Chondroitinase	Targets chondroitin sulfate PGs	Degrades chondroitin sulfate, altering cartilage compressive and viscoelastic properties	Used to study the role of PGs in ECM stability	(Rieppo et al., 2003; Lin et al., 2020)

In contrast, the choice amongst types of enzymes can greatly determine the degradation pattern of cartilage, given that different collagenases choose their ECM targets (Jabłońska et al,. 2016). For Collagenase Type I, its main target is general Collagen Type I which results in non-specific collagen degradation and rapid breakdown. But it is not very suitable because of excessive degenerations of matrix (Sarkar et al., 2012). However, Collagenase Type II gained popularity in the OA field because of its ability to cleave native collagen fibrils while preserving significant concentrations of non-collagenous proteins. Such enzyme replicates the gradual natural degradation of collagen in OA cartilage thus it is one of the most used for such in vitro models (Stoop et al., 2001; Rangchian et al., 2019). Collagenase Type III, in contrast, has a wider substrate specificity, and can degrade both collagen and PGs, resulting in contributory excessive tissue degradation (Lui et al., 2010).

Type IV and Type V collagenase have also been studied in relation to cartilage degradation. Type IV is highly specific to the basement membrane, limiting its potential use in articular cartilage studies. Type IV has been used to assess cellular responses to matrix degradation, in models incorporating chondrocyte-matrix interactions (Jayadev et al., 2019). Type V collagenase was used infrequently as it has little activity on the fibrillar collagens, but it has been investigated in combination with other enzymes for controlled matrix digestion (Berchtold et al., 2015).

Histological and biochemical analyses have been used in comparative studies to assess the impacts of various types of enzymes on cartilage degradation. The use of Collagenase Type II most consistently yields controlled tissue fibrillation with minimal loss of PGs, while Type III results in more extensive matrix breakdown. Researchers need to carefully choose the type of enzyme and optimize the digestion conditions to create in vitro OA models that can accurately mimic the disease pathophysiology. Table 2.3 shows

comparison of cartilage fibrillation induced by different types of enzymes in the study of OA.

Table 2.3 Comparisons of cartilage fibrillation in different type of enzyme

Type of Enzyme	Effect on Cartilage	Suitability for OA Model
Type I	Non-specific collagen degradation, rapid breakdown	Less suitable due to excessive matrix degradation (Sarkar et al., 2012)
Type II	Controlled collagen fibrillation, preserves non-collagenous proteins, moderate degradation	Optimal for moderate OA replication, maintains tissue integrity (Stoop et al., 2001; Rangchian et al., 2019)
Type III	Broad substrate specificity, excessive matrix breakdown	Less suitable due to over-degradation (Lui et al., 2010)
Type IV	Limited effect on fibrillar collagen, targets basal membrane	Less applicable for articular cartilage (Jayadev et al., 2019)
Type V	Minimal activity on fibrillar collagens	Rarely used for OA models (Berchtold et al., 2015)

Most OA studies employed Collagenase Type II collagen, as it effectively degraded the fibrillar collagens that constitute AC. This mechanism involves the cleavage of peptide bonds of the collagen triple-helical structure, thus enabling controlled degradation while avoiding excessive tissue disruption. Type II preserves non-collagenous proteins, such as glycoproteins and PGs, compared to other collagenase types and thus maintains the integrity of the overall cartilage matrix to perform biomechanical studies.

In addition, the dosage of Collagenase Type II is a crucial factor in determining the degree of cartilage degradation. Collagenase Type II is a good mimic of moderate OA with 0.2% application of it leading to surface fibrillation and deeper matrix layers becoming exposed yet retaining important ECM components (Lian et al., 2019; Orhan et al., 2021). Conventional dissolution is not evident in this concentration, leading to progressive collagen disorganization suitable for studying early-to-moderate OA progression. The focus of this article is on the aspect of enzymatic efficiency and tissue preservation, which enables the investigation of regulated cartilage degradation with the evaluation of possible therapeutics (Davidson et al., 2006).

The activity of 0.2% collagenase Type II was influenced factors like incubation

time, temperature and buffer composition. This generally requires incubation of the sample at 37°C for 6–12 hours in a buffer containing calcium, which is known to be crucial to maintain enzyme stability and activity (Oseni et al., 2013). Extended exposure or increased concentrations can result in over-degradation, while insufficient concentrations may not reach the necessary fibrillatory state (Mixon et al., 2021). Standardization of these parameters is essential for establishing reproducibility in experimental OA models, hence the selection of collagenase (0.2%) for in vitro OA study (Kar et al., 2016).

Collagenase Type II at lower concentrations (0.01%–0.05%) causes mild fibrillation and limited loss of PGs suitable for the mechanical studies of Grade I OA changes (Wan et al., 2022). 0.1%–0.2% moderate concentrations produce exaggerated deposition like moderate OA; higher concentrations (>0.5%) can cause accelerated and significant degradation, predisposing tissue integrity (Oseni et al., 2013; Mixon et al., 2021). For example, studies have shown that a concentration range of 0.1%–0.2% is ideal for maintaining biomechanical properties akin to OA-infected cartilage as well as controlled fibrillation (Davidson et al., 2006).

However, the duration of interval for enzymatic digestion is a significant factor affecting the severity of cartilage injury. Digestion times of 15–30 min produce partial fibrillation with high preservation of the integrity of host tissue while longer incubations (>24 h) lead to excessive degradation and total collapse of the matrix (Kar et al., 2016; Wan et al., 2022). An incubation period of 6–12 h (0.2% collagenase) allows for moderate cartilage fibrillation without complete physical disintegration, and consequently, it is a widely used time frame in in vitro OA models (Oseni et al., 2013). The optimal incubation time is determined by factors such as enzyme concentration, thickness of the cartilage sample and the extent of degradation required (Mixon et al., 2021).

This study has been complemented by time-course studies showing that surface

changes associated with fibrillation can be observed early (1–3 h) after exposure to the proteolytic enzyme and are characterized by surface roughening and a decrease content of PG (Davidson et al., 2006). Deep fissures and clustering of chondrocytes appears by 6–12 hours, consistent with mild to moderate OA changes (Oseni et al., 2013). At 24 h, significant disruption of the collagen network occurs, followed by complete solubilization of the ECM (Kar et al., 2016; Mixon et al., 2021). Most protocols, however, optimize digestion times to fully digest cartilage without over-digesting proteins required for downstream applications such as biophysical characterization and biochemical assays (Yao et al., 2021).

The time dependent effects of enzymatic digestion are also dependent on cellular viability and metabolic activity. Digestive intervals can be in a shorter time span to maintain chondrocyte activity (Higuchi et al., 2017). In contrast, it has also been shown that longer incubation times can lead to extensive chondrocyte apoptosis and not applicable to early-grade OA (Lin et al., 2020). This makes the optimization of the incubation time a balancing act between matrix degradation and cell viability to create in vitro models that faithfully reproduce early-to-moderate OA cartilage features (Rieppo et al., 2003).

2.5.3 Animal models

Over the years, animal models have been widely used to examine cartilage fibrillation and OA progression, given that this research provides invaluable information on the underlying pathophysiological mechanisms and potential therapeutic interventions. The choice of the proper animal model considers multifactorial considerations including joint biomechanical aspects and cartilage and subchondral bone thickness, but also the pathophysiology of OA that we try to reproduce. Mice and rats, for instance, modeled

genetic and molecular studies due to their short life span and ease of genetic manipulation. But these models have serious drawbacks, because their cartilage was much thinner than in humans and lacks well-defined zonal architecture. Therefore, murine models frequently develop fibrillation in a way that is distinct from human OA and thus relatively ill-suited for study of the mechanical features of cartilage degradation (Das Neves Borges et al,. 2017; Kim et al., 2018; Ter et al,. 2019). Bigger animal models (rabbit, dog and sheep) demonstrate human cartilage fibrillation closer because of the wider zones of cartilage and a much more complex joint loading. For example, rabbits are often used for cartilage studies, since their cartilage has a degree of zonal organization and a similar response upon mechanical injury (Dai et al., 2014; Kim et al., 2018). Beagles and other canine models have also been commonly used in OA studies because of naturally occurring cartilage degeneration and fibrillation susceptibility (Chiu et al., 2020). Dogs exhibit a cartilage thickness profile that more closely resembles that of humans, providing the ability to assess mechanical fatigue and biochemical alterations due to fibrillation.

In large animal models, bovine and equine cartilages are closer in thickness, ECM composition, and load-bearing capacity to human cartilage. Cartilage from animals, mostly from femoral condyle of bovine, was frequent in vitro studies examining the viscous response to the fibrillated cartilage and the impact of enzymatic degradation (Laasanen et al., 2002; Teeple et al., 2016). The large mechanical loads experienced in weight-bearing joints particularly relevant for OA progression made equine models particularly useful (Malda et al., 2012). On the other hand, large animal models have their challenges, such as being more expensive, ethical issues, and the necessity for specialized accommodation and patient care. Despite these challenges, animal models remain indispensable in cartilage fibrillation research, providing a platform for testing novel therapies and advancing the understanding of OA pathogenesis. The comparisons of cartilage fibrillation in different

animal models in the study of OA were summarized in Table 2.4 below.

Table 2.4 Comparisons of cartilage fibrillation in different animal models

Animal Model	Cartilage Thickness (mm)	Vulnerability to Fibrillation	Key Considerations for Fibrillation Studies	Reference
Murine (Mouse)	< 0.1	Low	Extremely thin cartilage without distinct zones, limiting biomechanical studies. Suitable for genetic and molecular research on OA-related pathways.	Ter et al., 2019
Murine (Rat)	< 0.1	Low	Cartilage lacks zonal structure, making it unsuitable for mechanical studies but useful for chemically or surgically induced OA models.	(Das Neves Borges et al., 2017; Kim et al., 2018)
Guinea Pig	-	Moderate	Some strains develop spontaneous OA, making it a good model for naturally occurring cartilage degeneration, but species-specific patterns limit direct human comparison.	Gao et al., 2023
Rabbit	0.21 - 0.56	Moderate	Cartilage was thinner than human tissue but has some zonal organization. Suitable for focal defect study.	(Dai et al., 2014; Kim et al., 2018)
Canine (Dog)	0.95 - 1.30	High	Certain breeds show consistent joint mechanics, making ideal for OA and fibrillation progression studies. Prone to spontaneous OA development.	Chiu et al., 2020
Ovine (Sheep)	0.50 - 1.70	High	Cartilage thickness and subchondral bone properties resemble humans. Prone to subchondral cyst formation in OA, making it a valuable model for joint degeneration.	Oláh et al., 2019
Caprine (Goat)	0.80 - 2.00	High	Thick cartilage supports full-thickness defect studies. Susceptible to virus-induced joint degeneration, making it relevant for inflammatory OA	Schrauth et al., 2016

			models.	
Bovine (Cow)	0.50 - 3.30	High	Bovine cartilage, particularly from the patella, closely mimics human histology. Frequently used for in vitro mechanical fibrillation studies.	(Laasanen et al., 2002; Teeple et al., 2016)
Equine (Horse)	1.80 - 2.00	High	Thick cartilage with significant loading mechanics makes it ideal for large-scale OA and mechanical loading studies. Challenging to handle due to size.	Malda et al., 2012
Porcine (Pig)	1.50 - 2.00	High	Cartilage properties closely resemble human tissue. High growth velocity requires careful timing in studies.	Kheir et al., 2011

2.6 Magnetic Resonance Imaging

Magnetic Resonance Imaging (MRI) has long been recognized as a gold standard of non-invasive imaging diagnosis in which its working principle increased the spatial resolution and new windows into the anatomy, cell structure, and histopathology of living tissues. The high-field MRI has successfully been developed to provide measures of the macromolecular environment within cartilage tissue (Van et al., 2020). This was possible via the interaction between interstitial water, probed by MRI, and the macromolecular constituents that affect the nuclear magnetic relaxation properties characterizing the spin energetics of the water proton system. However, the diagnoses were mostly carried out at the progressive grade of OA because of the costly imaging procedure using high-field MRI. Recently, imaging on low-field MRI has gained interest due to its small size, low cost, and easily installed scanner (Wansin et al., 2017; Biggi and Dyson, 2018; Van et al., 2020). The low-field MRI also shows the potential of producing similar image quality to high-field MRI as shown in Figure 2.7.

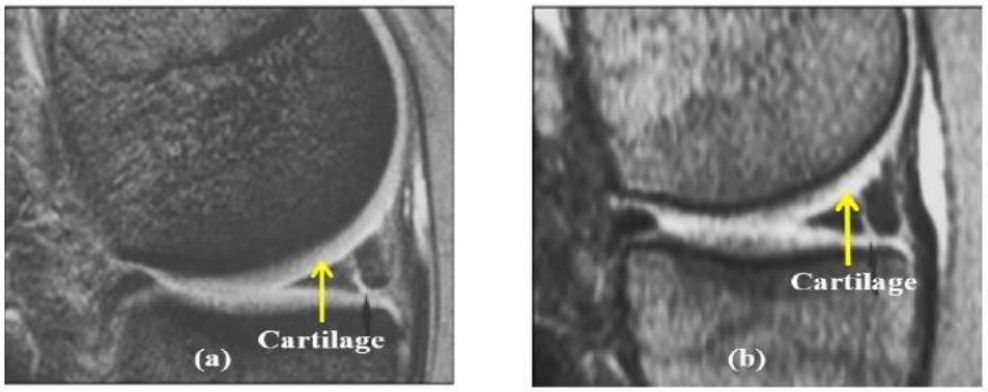

Figure 2.7: MRI images of cartilage (a) 1.5 T MRI and (b) 0.2 T (Wansin et al., 2017; Biggi and Dyson, 2018)

In previous quantitative MRI studies, cartilage was examined based on thickness, volume, and cartilage loss (Roemer et al., 2014; Hayashi et al., 2016). However, it has been reported that there were no significant differences in cartilage thickness in different grades of OA (Hayashi et al., 2016). Further quantitative MRI studies were also carried out to quantify the cartilage matrix composition particularly PGs using a contrast agent which was injected into the joint (Hafner et al., 2020). Although it was well known of the high-field MRI ability to describe the fluid phase behavior within the tissue, the cartilage correlation between quantitative low-field MRI image and biomechanical properties was yet to be fully understood because it appears that the morphological of the cartilage was mostly being investigated using healthy cartilage tissue and high-field MRI. Furthermore, the low-field MRI was only used to quantify the dimensional of the cartilage, and the potential of low-field MRI in cartilage imaging was also yet to be studied.

2.6.1 Studies of articular cartilage

Low-field MRI has been used actively for human and animal research since 1980s. In the beginning, ultra-low-field (<0.1T) scanners were studied before proceeding to use low-field MRIs (0.1 - 0.5T) extensively. Table 2.5 shows the cartilage studies using low-field MRI in previous studies:

Table 2.5 Cartilage studies using low-field MRI

Machine Type	Magnetic Field Strength (T)	Species	Cartilage Focus	References
Philips Achieva, Philips Healthcare, Best, Netherlands	7.0	Human	Measurements of patellar cartilage at 7T	Welsch et al., 2011
Bruker BioSpec, Bruker Corporation, Billerica, MA, USA	9.4	Porcine	Mechanical properties of articular cartilage using MRI	Zevenbergen et al., 2018
Hyperfine Swoop, Hyperfine Inc., Guilford, CT, USA	0.06	Human	Advancements and applications of modern low-field MRI in musculoskeletal radiology	Pogarell et al., 2024
General Electric Signa, GE Healthcare, Chicago, IL, USA	1.5	Human	MRI-based cartilage of platelet-rich plasma injections	Fatima et al., 2024
Siemens MAGNETOM Terra, Siemens Healthineers, Erlangen, Germany	7.0	Human	MRI of native knee cartilage delamination injuries	White et al., 2017
Esaote C-scan MRI system, Esaote S.p.A., Genoa, Italy	0.18	Bovine	MRI of cartilage layer differentiation	Wansin et al., 2017
Esaote E-scanner MRI system, Esaote S.p.A., Genoa, Italy	0.2	Human	MRI signal strengths of knee cartilage layers	Gudbergsen et al., 2011
MR750 3-Tesla MRI system with UTE-MT capability, GE Healthcare Tech., WI, USA	3.0	Human	MRI for functional cartilage assessment	Jerban et al., 2021

As shown in Table 2.5, Magnetic low-field strength is comparable to high-field in human cartilage study using low-field MRI. Esaote scanners have also become the brand of low-field MRI brand that were widely used by researchers. The C-scan was immobile low-field extremity scanners with MR qualities and physics like those of conventional whole-body systems. The C-scan, manufactured by the Esaote Company in Italy, was distributed by Hologic (previously distributed by General Electric). The system operates in a uniform 0.2 T and uses a permanent magnet that does not require magnetic shielding as shown in Figure 2.8, as well as images the extremities, including the elbow, wrist, hand, knee, ankle,

and foot (Ghazinoor et al., 2007; Nakagomi et al., 2019).

Figure 2.8: Esaote C-scanner (Ghazinoor and Crues, 2006)

2.6.2 Low-field magnetic resonance imaging

In the past decade has been rapid development of imaging on low-field strength (<0.5 T) MRI, be it on hardware development, or on the techniques employed to acquire more accurate imaging results. Improved imaging would not only produce good quality images but would deliver affordable scanners, be cost effective with low installation and maintenance costs where a room of ten-meter square in size was sufficient for installing the dedicated system and the RF shielding was incorporated into the magnet gantry, so no special shielding must be installed (Riel et al., 1999; Ejbjerg et al., 2005). Hayashi et al., (2004) discussed in detail the cost benefit of the low-field MRI through a model case comparison between 0.3 T scanner and 1.5 T scanner which costs 70 million yen and 120 million yen, respectively showing more than 41.7% of decrement in the total cost spent to purchase the systems (Hayashi et al., 2004). Other advantages of dedicated low-field MRI were providing exceptional patient comfort with removing problems associated with claustrophobia, minimal noise irritation, and continuous contact with the examiner.

2.7 Biomechanical properties of articular cartilage

Articular Cartilage is a specialized connective tissue that plays a crucial role in load distribution and joint lubrication, enabling smooth and pain-free movement. Its unique biomechanical properties stem from its biphasic nature, comprising a solid collagen PGs matrix and an interstitial fluid phase, which together creates its viscoelastic behavior. These properties can be understood through a combination of experimental mechanical testing methods such as compression, indentation and shear tests to quantify material responses and through theoretical modeling of biphasic and pyroclastic models that predict cartilage behavior under different loading conditions. Combining these approaches together yields important information about cartilage function and properties.

2.7.1 Mechanical testing

The biomechanical properties of the articular cartilage are foundational for the proper functioning of synovial joints. The mechanical properties of articular cartilage have been extensively characterized by using a wide range of mechanical testing techniques to evaluate the cartilage tissue response under different loading scenarios. Of the most used test methods, confined/unconfined compression, uniaxial tension, pure shear (torsion) and indentation were the most frequently utilized (DiSilvestro and Suh, 2001; Weizel et al,. 2020). These were performed on specimens after being extracted from them in vivo environment, and of those, the indentation test garnered the most preference for determining cartilage properties in an in-situ manner while preserving structural integrity (Mow et al., 1980). Cartilage is a biphasic material, with a solid ECM and an interstitial fluid phase, both contributing to its viscoelastic behavior when subject to mechanical testing (Cohen et al., 1998; Pearle et al., 2005). This effective biphasic model, widely adopted for in vivo studies, elucidates the crucial mechanics of how the cartilage faintly bears the applied mechanical loads while mitigating dissipater forces, as appropriate and

therefore represents a key framework for the interpretation of experimental data.

Among the various mechanical testing modalities, confined and unconfined compression assess the intrinsic stiffness and Permeability of cartilage. Confined compression testing consists of placing the cartilage sample in a chamber with a porous filter that allows fluid flow but constrains lateral deformation, a suitable approach to assess compressive Elastic Modulus and Permeability (Buschmann et al., 1998). In contrast, unconfined compression allows lateral deformation because the cartilage was compressed between two non-porous plates, thus measure the intrinsic stiffness and viscoelastic response of the tissue (Lu and Mow, 2008). However, confined compression testing has been criticized for potential inaccuracies arising from the assumption of zero boundary conditions at the cartilage-porous filter and radial-edge interfaces, potentially affecting the interpretation of mechanical properties (Buschmann et al., 1998). The distinction between these two methods was critical in selecting appropriate testing protocols for evaluating the biomechanical properties of cartilage.

From Figure 2.9, all three mechanical testing configurations presented the cartilage specimen was immersed in saline fluid throughout the tests to create physiological conditions. The main difference between these tests was only the indentation test was complete with the subchondral bone attached to the cartilage whereas the unconfined and confined compression tests were complete with the cartilage tissue detached from the subchondral bone. Also, in both confined and unconfined compression tests the load was transferred through a non-porous platen or indenter which was different from the indentation test that uses rigid porous indenter. Furthermore, exudation of fluid was encountered in the unconfined compression test since the cartilage specimen was compressed in between two non-porous loading platens which allow lateral deformation of the tissue. Whereas in confined compression testing there was a porous filter below the

cartilage specimen to allow fluid to flow through it. However, the problem with the interpretation of confined compression testing lies in the nature of the boundary conditions at the cartilage/porous filter interface and at the radial-edge/confining-wall interface where it was assumed to be nil by previous researchers (Buschmann et al., 1998). The indentation test was simplified in nature since the specimen used was attached to the subchondral bone and no boundary conditions come into importance to accounting for them.

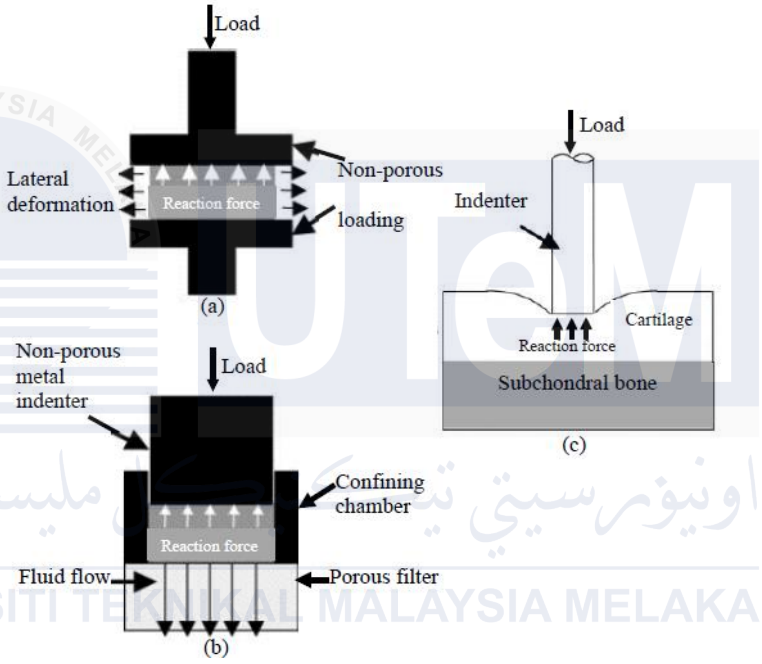

Figure 2.9: Mechanical testing configurations (a) Unconfined compression (b) Confined compression (c) Indentation (DiSilvestro and Suh, 2001)

The uniaxial tensile and pure shear (torsional) tests further elucidate the mechanical behavior of cartilage, particularly in relation to its collagen network. Uniaxial tensile testing was used to determine tensile strength and stiffness, which were heavily influenced by the anisotropic arrangement of collagen fibrils (Jurvelin et al., 2003). Furthermore, pure shear tests apply rotational forces to the cartilage sample for shear Modulus analysis, examining the interactions between the PGs matrix and collagen framework (Korhonen et al., 2002). These tests were vital for the understanding of how cartilage withstands shear forces in vivo, an important component of joint articulation and function. Nevertheless,

application of tensile and shear testing has historically been limited by simultaneous fragility and thinness of cartilage that introduces complexities in sample preparation and handling. The accuracy in these tests allows one to choose the experimental set-up needed to reduce the variation in different findings.

Of the various types of mechanical tests that can be performed, one particularly valuable test was the indentation test, which allows sampling of the cartilage in a minimally invasive manner and allows evaluation of in situ properties of the cartilage with the subchondral bone intact. Unlike in compression tests, where cartilage samples were cut and tested independently, indentation testing retains the natural structure meaning boundary condition artifacts are less likely (Mow et al., 1980). The indentation test used a relatively hard, porous indenter to measure the critical biomechanical parameters: the Elastic Modulus (E), Permeability (κ), and Poisson's ratio (ν), which were important for characterizing the biphasic property of total cartilage (Hayes et al., 1972; Lu and Mow, 2008; Kabir et al., 2021). Moreover, tests of indentation have been shown to produce higher Elastic Modulus values with respect to other testing methods and strengthens the interest in a localized mechanical property sensitivity and zonal variations within cartilage (Kabir et al., 2021). So, this variability, the understanding of those variability was important for accurate biomechanical models that would then account for the heterogeneity of AC. In Table 2.6, we summarize OA studies on biphasic biomechanical properties of synovial joints.

Table 2.6 Comparison of biphasic biomechanical properties in human synovial joints

Mechanical Testing	Synovial Joint	Elastic Modulus, E (MPa)	Permeability, κ ($\times 10^{-15}$ m^4/Ns)	Void Ratio, ν	Reference
Indentation	Hip	4.89 ± 0.76	0.19 ± 0.20	-	Taylor et al., 2011
Indentation	Knee	3.12 ± 0.55	0.22 ± 0.18	0.15 ± 0.08	Jin and Lewis, 2004
Unconfined	Knee	0.19 – 0.96	-	-	Nissi et al., 2007
Confined	Hip	1.64 ± 0.34	1.10 ± 0.60	0.14 ± 0.09	Démarteau et al., 2006
Confined/ Unconfined	Knee	1.24 ± 0.49	| 1.75 ± 1.82	0.16 ± 0.15	Jurvelin et al., 2003
Indentation	Shoulder	3.89 ± 1.02	0.17 ± 0.15	0.12 ± 0.09	Taffetani et al., 2014
Indentation	Ankle	2.54 ± 0.78	0.25 ± 0.21	0.18 ± 0.07	Ateshian et al., 1997)
Confined compression	Bovine humeral head	0.64 ± 0.22	3.62 ± 0.97	0.03 ± 0.01	Soltz and Ateshian, 2000

2.7.2 Theoretical modelling

Theoretical modelling has become a potent computational modality, particularly finite element analysis (FEA), in amplifying experimental mechanical testing, providing deeper insights into stress–strain distributions and predictions of mechanical behaviors, as articular cartilage is a complexly composed and structured tissue whose mechanical behavior is particularly challenging to investigate in the biomechanical research landscape. The biphasic organs were significant in describing the viscoelastic and poroelastic behavior of cartilage, coupling solid and fluid components during load-bearing situations (Mow et al., 1980). FEA simulations have been applied extensively to confirm aspects of experimental data and improve our understanding of the response of cartilage to a range of physiologically and pathologically relevant mechanical loading modes (DiSilvestro and Suh, 2001; Mellors et al., 2023). Fibril-reinforced frameworks of advanced FEA models can now simulate the complex anisotropic behavior of cartilage when subjected to

indentation and compression tests, thus improving micromechanical evaluations of cartilage (Sajjadinia et al., 2019).

A few studies successfully merged experimental and theoretical methods to advance the understanding of the biomechanical nature of cartilage. An example of this is demonstrated by Jin and Lewis (2004), where indentation testing was combined with FEA simulations to characterize the anisotropic nature of articular cartilage and the effect of collagen orientation on Elastic Modulus values. Entailed in such differences were global properties of cartilage which were examined via confined/unconfined compression and further indentation, with differing species, site, depth and age supported overall results from extended indentation tests on both human and animal cartilage around significant point localized mechanical property differences (Jurvelin et al,. 2003; Taylor et al,. 2011). The combined use of experimental testing and computational modelling has greatly improved the ability to properly characterize cartilage mechanics.

2.8 Summary

OA was a degenerative disease which was associated with the articular cartilage in the synovial joint. As this disease progresses, it will change the macromolecular structure inside the cartilage tissue by altering its biomechanical properties. Diagnosis was often identified by medical practitioners when this disease was already progressed into advanced grade and no specific treatment was available to stop the progression of this disease until the disease becomes severe and need to do joint replacement. Hence, study on early detection of this disease was crucial to identify the biomarkers for the onset of OA.

Morphological changes in the synovial joints caused by progression of OA were visible through non-invasive imaging modality. From the vast selection of imaging modalities available to image the structure of the articular cartilage however MRI becomes

the most suitable candidate to produce reliable images with high spatial resolution and excellent soft tissue contrast without ionizing radiation. Furthermore, cartilage was a complex structure which shows anisotropic characteristics and requires further mechanical testing and computational modeling to get accurate results on its biomechanical properties. Additionally, proper setting of mechanical testing and storage protocols were crucial to obtain reliable results on cartilage biomechanical properties.

Previously, most of the studies performed correlation between quantitative MRI parameters with the cartilage biomechanical properties using high-field MRI. A major gap in current research was the limited comparative analysis of low-field versus high-field MRI in assessing early-grade cartilage fibrillation. Conventional low-field systems were only used to measure geometrical data of the articular cartilage such as thickness and volume. However, this study aimed to bridge that gap through a dedicated low-field MRI system, which shows promising capability to enhance patient comfort along with other beneficial factors, ultimately offering better results and reliable diagnostic information on progressive-grade II OA.

CHAPTER 3

METHODOLOGY

3.1 Introduction

This chapter outlines the comprehensive methodology implemented to study the biomechanical properties of articular cartilage focusing on the effects of progressive fibrillation. The methodology includes materials and sample preparation, microscopic assessment, measurement of water content, low-field MRI scanning, and various mechanical tests such as creep and thickness tests using an indentation apparatus. Healthy cartilage samples were extracted through drilling and subsequently subjected to progressive fibrillation using Collagenase type II. Microscopic evaluation was conducted to observe physical changes in the cartilage tissue at the ECM levels. The water content of cartilage samples was then measured to calculate the water percentage, a key parameter influencing the mechanical properties of cartilage. Subsequently, creep indentation tests were conducted to evaluate the deformation behavior of the cartilage tissue. The characterized biomechanical properties were finally correlated with greyscale images from low-field MRI scans. Figure 3.1 illustrates an overview of the study workflow.

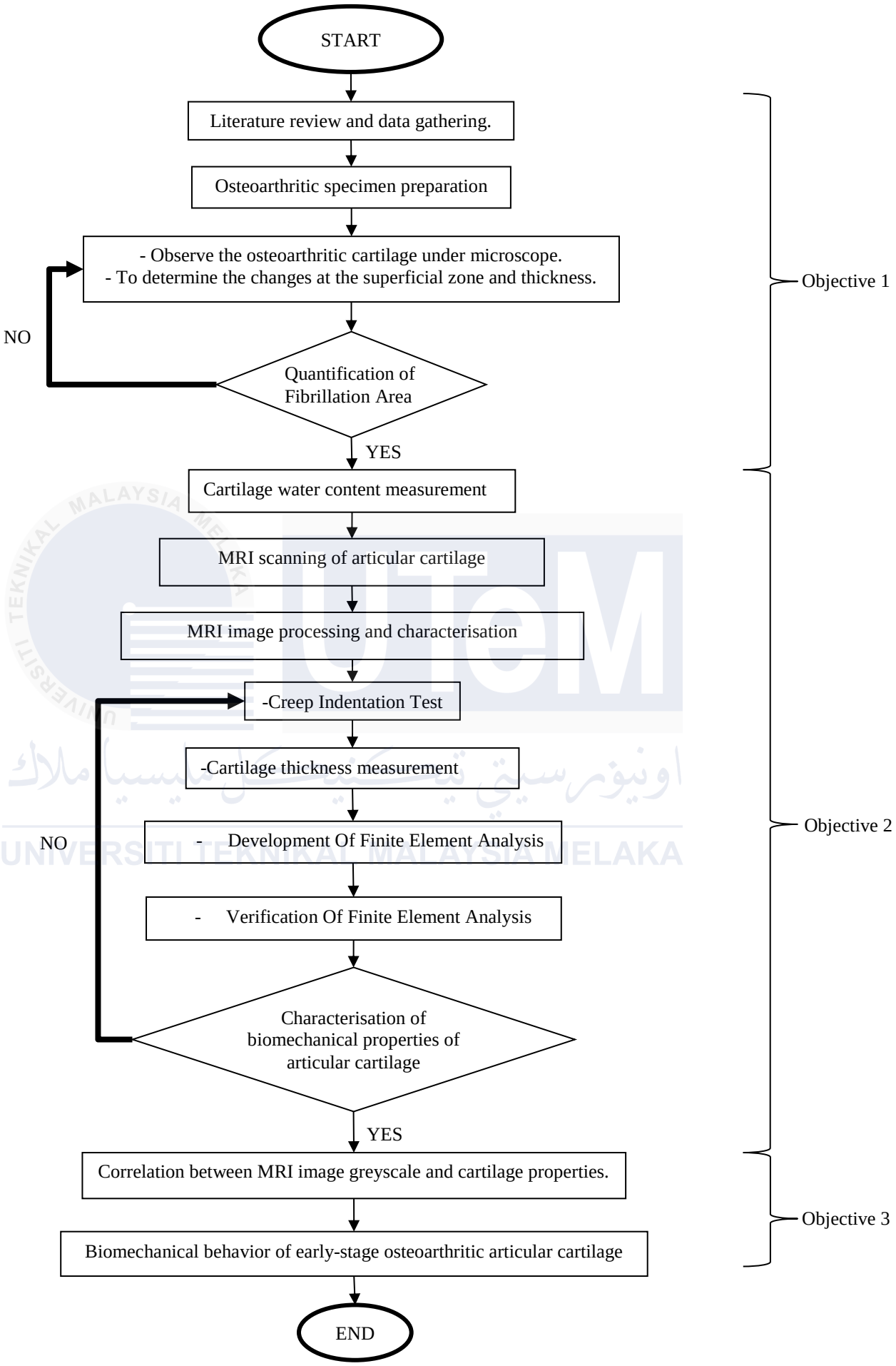

Figure 3.1 Methodology flow chart

3.2 Material Preparation

3.2.1 Phosphate-buffered saline

Phosphate Buffered Saline (PBS) was a physiological buffer extensively used to maintain the hydration and preserve the native mechanical properties of cartilage tissues during sample preparation, storage, and testing in vitro conditions. PBS was a buffered solution composed of 0.9% sodium chloride, 0.0795% sodium phosphate dibasic, and 0.0144% potassium phosphate monobasic with a pH range of 6.6–7.6 as per previous study (Safa et al., 2017).

In this study, PBS was supplied in tablet form, as shown in Figure 3.2. To prepare the solution, each tablet was dissolved in 100 mL of sterile distilled water as instructed by manufacturer (Wright et al., 2014). The PBS was used throughout the experimental procedures to replicate physiological conditions and ensure the preservation of the cartilage mechanical properties as prior studies (Safa et al., 2017; Farnham et al., 2021). This practice was crucial for studies such as OA research especially examining the fibrillation of articular cartilage.

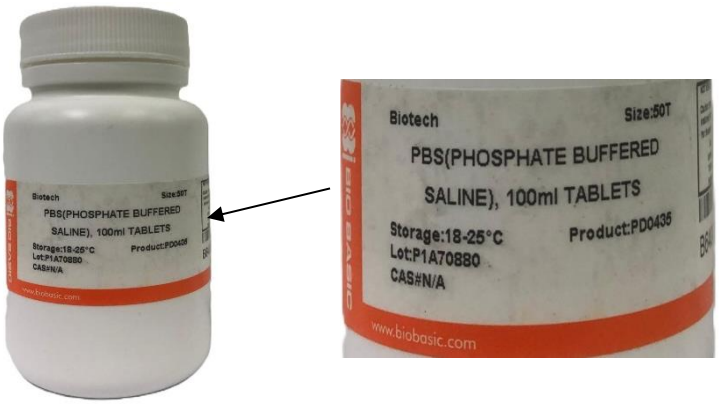

Figure 3.2 100 ml PBS tablet (Bio Basic Inc.)

3.2.2 Trypsin Solution

In this context of cartilage studies, a 0.05% Trypsin solution as per shown was Figure 3.3 plays a significant role in the enzymatic digestion of ECM components

particularly collagen and PGs in earlier studies (Gao et al., 2021; Wan et al., 2022). It contained 0.02% EDTA, a chelating agent that bound divalent cations, thereby weakening cell adhesion by disrupting cell-cell and cell-matrix interactions (Kirillova et al., 2023). The pH was typically adjusted to a range of 7.2–7.4 to ensure optimal compatibility with the cells (Kirillova et al., 2023). This digestion was crucial for isolating chondrocytes from the cartilage matrix with the intention to study the cellular responses and biochemical changes associated with OA. By breaking down the matrix, Trypsin facilitates the examination of cellular behavior in a controlled environment which was essential in understanding the mechanisms of cartilage degradation and the progression of OA.

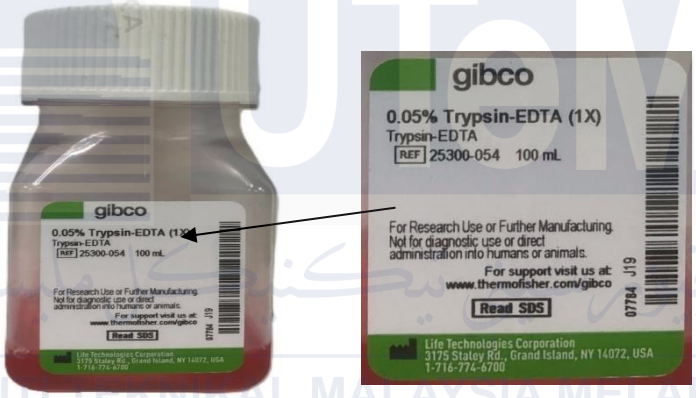

Figure 3.3 0.05% Trypsin (Gibco)

3.2.3 Collagenase Type II

Collagenase Type II was an enzymatic preparation extensively used for digesting ECM components particularly collagen in tissue dissociation procedures (Cruz et al., 2023). Collagenase Type II contained a mixture of proteolytic enzymes, including collagenase 125 CDU/mg, caseinase 200 units/mg, and clostripain 3.5 units/mg. The enzyme preparation had a molecular weight ranging from 68 to 130 kDa and functioned optimally within a pH range of 6.3–8.5 as reported in previous study (Satish et al., 2015). Collagenase Type II at 0.2% concentration was frequently utilized in cartilage study for its ability to degrade collagen, a primary physical protein in the ECM of cartilage. This

enzymatic activity was valuable in studies focused on cartilage fibrillation. Collagenase breaks down collagen fibrils simulating the degradation observed in disease states and enable them to analyze the subsequent biochemical and cellular responses of cartilage tissue. In this research, cartilage specimens were degraded with a 0.2% concentration of Collagenase type II as illustrate in Figure 3.4 to simulate the progressive grades of fibrillation grade II observed in OA.

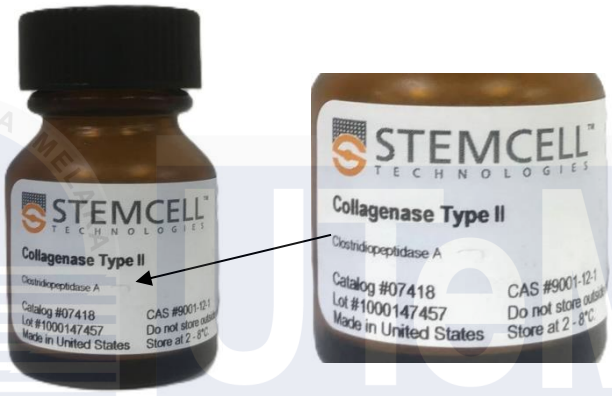

Figure 3.4 0.2% Collagenase Type II (STEMCELL Technologies.)

3.2.4 Hank's Balanced Salt Solution

Hank's Balanced Salt Solution (HBSS) was a physiological buffer extensively used to maintain the osmotic balance, provide essential ions, and support cell viability during tissue processing and cell isolation procedures. HBSS was a buffered solution composed of 0.137% sodium chloride, 0.0067% potassium chloride, 0.0005% magnesium sulfate, 0.0006% monobasic potassium phosphate, 0.0035% sodium bicarbonate, 0.0048% glucose, 0.0014% calcium chloride, and 0.0006% dibasic sodium phosphate, with a pH range of 7.0–7.4, as reported in previous study (Fagundes et al., 2018).

HBSS serves as a commonly used buffer medium in tissue and cell studies, including those involving collagenase degradation. When collagenase at 0.2% was dissolved in HBSS, the solution provides an optimal ionic environment to maintain tissue viability and enzyme activity during cartilage fibrillation experiments. The balanced salt

composition of HBSS ensures essential ions like calcium and magnesium which were cofactors for collagenase were present to facilitate its enzymatic function as shown in Figure 3.5.

Figure 3.5 HBSS (Thermo Fisher Scientific)

3.3 Sample Preparation

Animal models have been widely used in OA research since the early 1970s and these models were able to reproduce the pattern and progression of OA at a controlled rate as evidenced by earlier study (Biggi and Dyson 2018). In this research, cartilage samples were prepared using bovine hip joints whereby it were extracted from bovine hip joints, specifically the femoral head part. The hip joint was chosen since its large size allows maximum sample collection and its wide availability in the market makes the process more economical and efficient. The hip joints were obtained from cows retrieved at Pusat Sembelih Jasin, Melaka within 24 hours after slaughter. The hip joints were dissected to separate the femoral head from the rest of the joint. The cartilages were then be visually inspected and discarded if there were any signs of damage or disease. Samples were obtained by drilling the femoral head using 8 mm diameter hollow diamond drill bit as shown in Figure 3.6. Cartilage tissues were obtained by carefully separating the tissue from the subchondral bone using a scalpel. Throughout the process, the cartilage surfaces were

kept hydrated with regular PBS washes. The tissue samples were immersed in PBS and stored in the refrigerator at 10℃ until further testing.

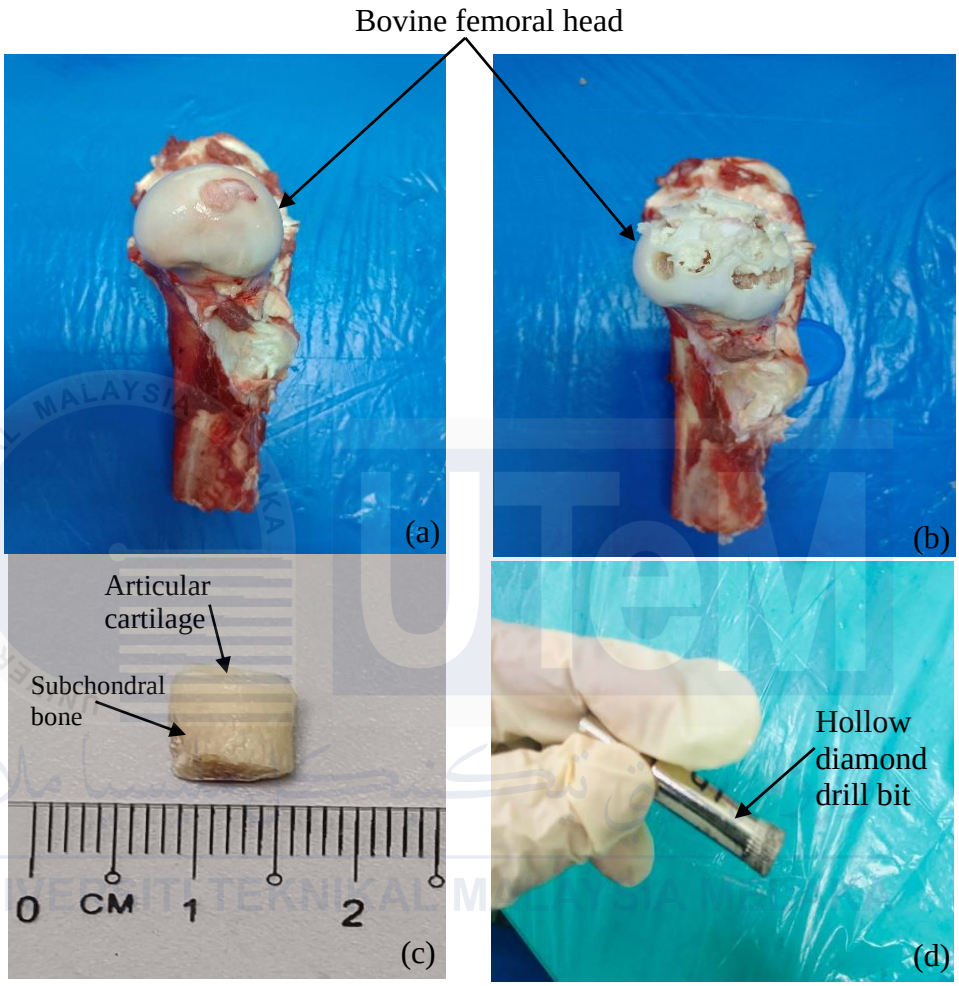

Figure 3.6: (a) before drilling and (b) after drilling; (c) drilled sample with intact subchondral bone (d) Used 8 mm bore diameter hollow diamond drill bit

3.3.1 Grade II Cartilage

Based on previous studies, it was established that the depletion of PGs was one of theearly signs of OA (Loeser et al., 2012). Therefore, osteoarthritic cartilage samples can be prepared by depleting PGs from the cartilage through enzymatic digestion. The enzyme used to degrade the samples was trypsin. The samples that were previously kept in the fridge were taken out and then be heated at 37℃ in a water bath for 1 hour to equilibrate the cartilage as evidenced by (June and Fyhrie 2010; Abdel-Sayed et al., 2013). This

equilibration process ensured that the cartilage reaches a stable temperature conducive to subsequent enzymatic degradation. During this time, the trypsin was also heated at the same temperature, but for only 30 mins. 0.5ml of 0.05% trypsin was then be pipetted into test tubes and be dipped inside the water bath. Following preparation, the samples were degraded in trypsin with the duration of 120 mins.

Following that, the fibrillation process was initiated and the preparation started by dissolving 20 mg Collagenase Type II (lyophilized powder) in 1 ml HBSS in a sterile tube. The tube was vortexed gently, the collagenase powder was completely dissolved and ensured homogenous mixing without foam formation. The fully dissolved collagenase solution was transferred to a clean sterile tube for subsequent use in the fibrillation protocol. Pre-equilibrated cartilage samples were placed into the prepared collagenase solution and were incubated at the following time: 30, 60, 90, and 120 mins, in accordance with methods established in previous studies (Nahar et al., 2018; Yan et al., 2021; Shajib et al., 2022). The cartilage samples were then transferred out of the collagenase solution and washed with PBS solution in 5 mins to ensure that the residual enzyme activity was eliminated at the end of each selected incubation period. Then, the washed samples were soaked in a new container with PBS solution and held there for another 30 mins according to the previous works (Zhou et al., 2018; Kilmer et al., 2020; Arlk et al., 2021). This allowed for the stabilization of the cartilage matrix post-enzymatic digestion and rendering the samples amenable to downstream biochemical assays.

3.4 Microscopic Assessment of Fibrillated Cartilage

The cartilage containing intact subchondral bone was cut to fit on a glass slide. The micro-photographs of the physical structures of the trimmed cartilages were taken using Zeiss Axioscope 2 MAT microscope with 50x magnification as shown in Figure 3.7. Then,

the cartilage underwent fibrillation enzyme process to observe the changes occur. These images were processed with Solution Lite Software for accurate scaling and then analyzed with ImageJ to extract data for physical observations.

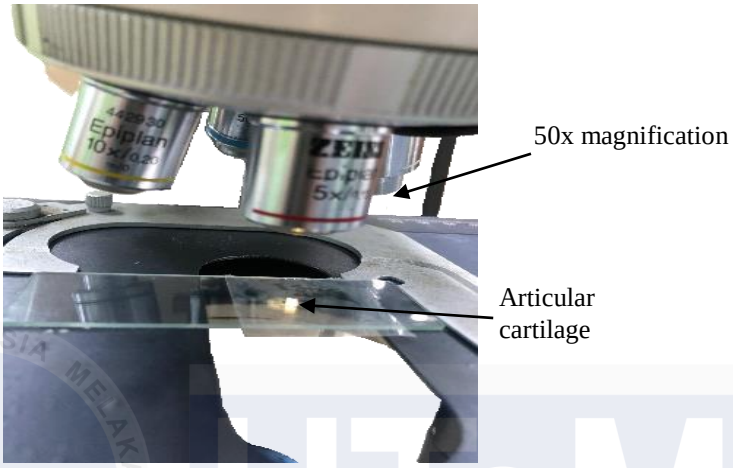

Figure 3.7: A trimmed cartilage had been observed under microscope

The articular cartilage was then analyse based on the microscopic image using ImageJ software. Articular cartilage specimens were obtained for microscopic analysis; the indentation centre as it provided a consistent relevant reference. This reduced variability originating from the superficial zone ensuring reproducible results (Mansfield et al., 2015; Bergholt et al., 2016). The cross-section at this site facilitated the examination of components essential for tissue integrity such as collagen fibers and PGs. It also contributed to the detection of early degenerative changes like Grade I and Grade II that associated with OA worsening.

Figure 3.8 showed a cross-sectional view through the articular cartilage and subchondral bone where one line serves as the reference point, further standardising the cross-sections to remove another element of variability. The cartilage area could clearly be seen superior to subchondral bone with the vertical reference lines symmetrically positioned at 0.65 mm intervals to the left and right of the center reference point. A total of 5 mm horizontal was defined across the cartilage and subchondral bone to facilitate appropriate orientation during image segmentation and analysis.

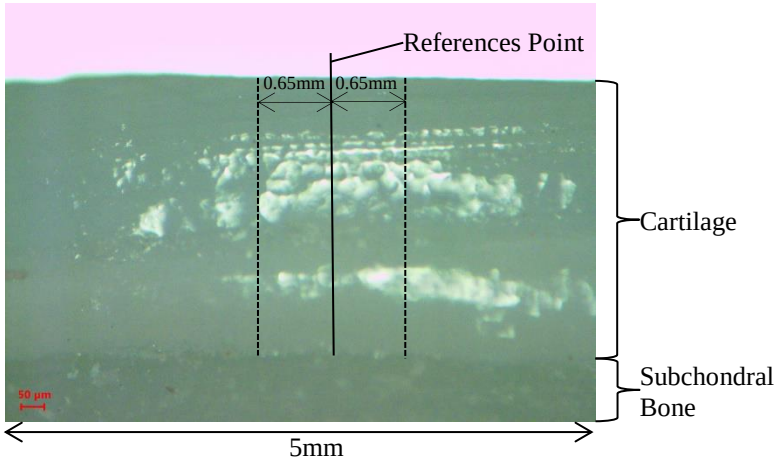

Figure 3.8: Reference area for the microscope image

The study of the articular cartilage will now proceed using the Reference area from the microscopic image. The individual image dataset was captured with a low powered microscope and brought into the software for measurement and segmentation. The measuring scale within the image was enhanced and carefully adjusted to make optimization for viewing easy for the measurement precision.

Spatial calibration entailed establishing the relationship between the distances measured in pixels and those in real life. A reference mark was set over the scale bar for 50 µm. Thereafter, calibration parameters had to be adjusted with the 'Set Scale' option. Within the entire session's analysis, all measurements needed to be seamless spatially, hence the global calibration option checked. The comparison between the outputs of the measurement against validation mark using the calibration check was sufficient. After calibrating, the imaging tools available in ImageJ were employed to measure the region of interest (ROI) dimensions, which consist of length and width. The measurements taken were written in micrometres (µm) and converted to millimetres (mm) whenever necessary to conform to engineering standards.

Subsequently, the software MATLAB (v7.12.0 R2024a, MathWorks Inc., MA, USA) was used as shown in Figure 3.9 to emphasize the greyscale MRI for fibrillation

assessment on the cartilage structure within the ROI as shown by Saitou et al., (2018). Appendix A outlines the custom-made algorithms developed to transmute photographs captured under a microscope to greyscale images. From there, using the Semi-Auto feature along with moving through the ROI permits the counting of black pixels within the defined region. This crucial step was executed through the command window, where meticulous computations were conducted to quantify and analyze the pertinent data. Thus, navigating the ROI, and performing calculations within the command window representing a comprehensive approach towards effectively delineating and analyzing the boundary between bone and cartilage. The outcome also revealed that fibrillation caused a quantifiable increase in both the distance and size of gaps present within the ROI.

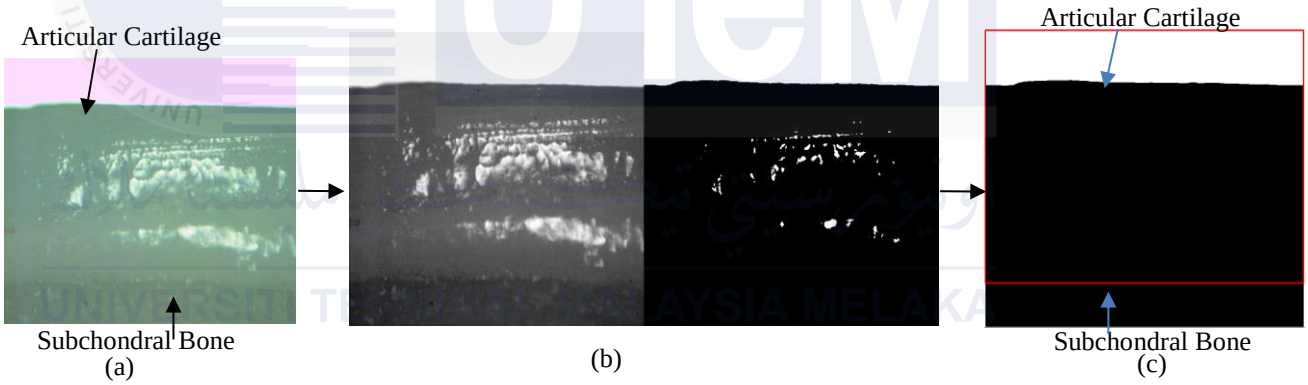

Figure 3.9: (a) Image of the cartilage that had been captured through microscope (b) Converted image into grayscale (c) ROI of cartilage from the grayscale image in (b)

3.5 Measurement of Water Content

Cartilage samples (*n*=36) were separated from the subchondral bone to measure the initial wet weight. At every interval, the samples were washed in PBS solution for 5 mins and then immersed in normal saline for 60 mins. Subsequently, the wet weight of the articular cartilage was measured using a digital balance weighing scale. The fibrillated samples were dried at room temperature for 48 hours before measuring their dry weight. The water content was calculated based on the percentage of the difference between the

wet weight at each interval and the dry weight divided by the initial wet weight as shown in the following Equation 3.1 (Roemer et al., 2014; Hayashi et al., 2016):

$$Percentage\ of\ water\ content = \frac{wet\ weight - dry\ weight}{wet\ weight}\ x\ 100\% \qquad (3.1)$$

3.6 Magnetic Resonance Imaging Image Analysis

Articular Cartilage samples (n=36) were imaged using a 0.18 T Esaote C-scan MRI system (Genova, Italy). Unlike conventional MRI systems that require a dedicated radiofrequency (RF) shielding room, this system were designed with copper shielding collars which were simplifies the setup but increases susceptibility to environmental noise. To address this, RF shielding was achieved using a flexible material encircling the magnet's aperture ensuring sufficient protection against external interference. The system incorporates a receiving coil housed within the gantry that was responsible for transmitting RF signals to the sample. The simplified accessibility of the C-scan MRI system allows for diverse usage since it operates at standard room temperature and requires only a 110-volt power supply. The C-scan MRI system utilized is shown in Figure 3.10 (a), while 3.10(b) illustrates the articular cartilage sample situated in the center of the receiving coil. The position was chosen to optimize the imaging of the articular cartilage samples.

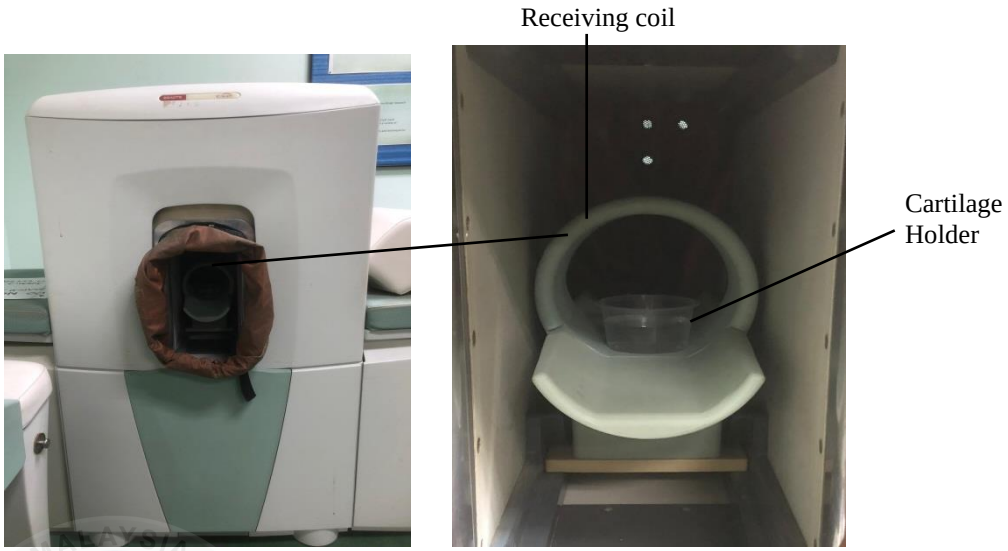

Figure 3.10: (a) C-scan MRI system (b) Cartilage sample set-up at receiving coil

The intact hip joint was scanned using one imaging pulse sequence in the MRI system. The Gradient Echo (GE) sequence was selected for this study because of its effectiveness in low-field MRI systems for visualizing intact joints, as demonstrated in prior research efforts (Eliasson et al., 2009; Arencibia et al., 2015; Wansin et al., 2017; Schmaranzer et al., 2021; Del Vecchio 2021). This sequence was particularly advantageous for imaging cartilage owing to its sensitivity in detecting changes in the tissues which enhances the contrast and detail of the cartilage visualization. Also, the Esaote C-scan MRI system which operates under a low magnetic field of 0.18 T was well suited for the GE sequence. High-quality visualization of the cartilage samples positioned centrally within the receiving coil was achieved by the optimization of the imaging parameters for the GE sequence as described in Table 3.1.

Table 3.1 Imaging parameter of pulse sequence in low-field MRI (Zhang et al., 2023)

Parameters	Imaging pulse sequences
	GRADIENT ECHO (GE)
Echo time, TE (ms)	18
Repetition time, TR (ms)	2660
No. of slices	7
Field of view, FOV (mm)	180
Matrix	256
Thickness (mm)	2

The images from the MRI scan were saved in the DICOM format (Digital Imaging and Communication in Medicine) and were processed using MATLAB. A custom MATLAB program (Appendix B) was developed to evaluate the greyscale intensity of individual pixels within the cartilage MRI images. These results were then utilized to establish correlations between greyscale intensity and the biomechanical properties of cartilage.

Greyscale intensity corresponds to a numerical scale representing pixel values that range from black to white. In this study, the MRI images featured a 12-bit resolution per pixel, providing greyscale intensity values between 0 and 4,096. To assess greyscale intensity, a rectangular ROI was selected in transverse views, aligned with the location of the indentation tests. The greyscale intensity for the chosen region was computed by averaging pixel column values across the cartilage depth as shown in Figure 3.11 ensuring precise characterization of the cartilage within the targeted area. The evaluation of MRI images included a visual assessment of the cartilage and its corresponding greyscale intensity range.

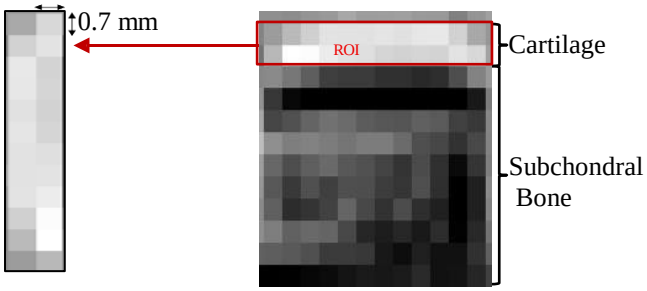

Figure 3.11 MRI image of the cartilage sample at the sagittal view through GE sequence

3.7 Experimental Methods

The experimental methodology involved two primary tests, the creep indentation test and cartilage thickness measurement. The thickness data was used to develop finite

element (FE) model of the cartilage while the creep indentation test data was incorporated into the computational simulation to determine key biomechanical properties of the cartilage specifically the Elastic Modulus and Permeability.

3.7.1 Indentation Test Apparatus

The biomechanical properties were characterized based on the time-dependent deformation response of the cartilage during the indentation test. These tests were performed using a custom-designed indentation apparatus depicted in Figure 3.12 that supported both the creep indentation test and cartilage thickness measurements.

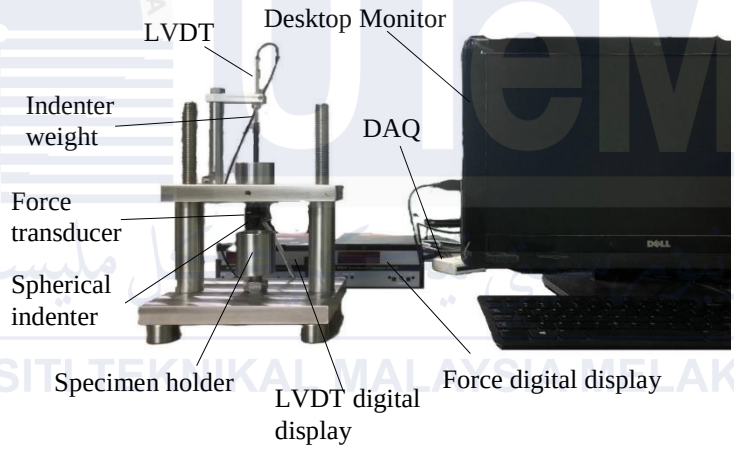

Figure 3.12 Indentation test apparatus

The indentation apparatus included several key components: a linear variable differential transformer (LVDT), a force transducer, a stainless-steel frame, a 4-mm diameter spherical indenter, and a sample holder. The spherical indenter was fabricated using Delrin which a material was selected as a lightweight alternative to aluminum due to its enhanced properties. Delrin offers superior weight reduction compared to the previously used aluminum contributing to improved efficiency and handling at the cartilages (Schmidt et al., 2015; Ingale 2016; Arshad et al., 2021). The force transducer measured the force exerted by the indenter on the cartilage surface with the total weight of the transducer shaft assembly being 0.11 N. The LVDT recorded cartilage deformation by tracking the shaft

displacement during contact between the indenter and the cartilage. Data from the LVDT and force transducer were displayed on a digital interface and recorded via a data acquisition (DAQ) system. LabVIEW 8.5.1 software (National Instruments Corporation, Austin, TX, USA) was used for data recording and analysis.

3.7.2 Calibration Procedure

As a preliminary step, the LVDT was calibrated to ensure measurement accuracy and reliability. Calibration was performed using stainless steel gauge blocks of varying thicknesses. The indenter was released onto the gauge blocks from different heights as illustrated in Figure 3.13.

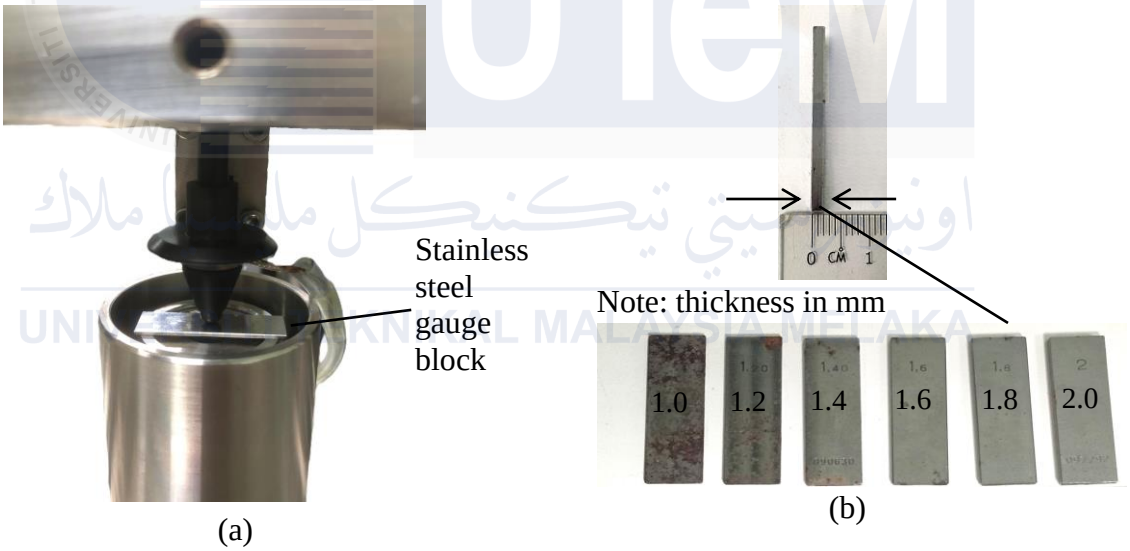

Figure 3.13 (a) Calibration test set-up (b) Different heights of gauge blocks

The shaft weight remained constant during calibration and changes in the LVDT's output voltage were recorded as gauge blocks were added or removed. This process was repeated three times to calculate the average values and assess repeatability. The resulting calibration factor was used to convert recorded displacement data from voltage to millimeters. Displacement data was documented and a linear regression fit graph was generated as shown in Figure 3.14.

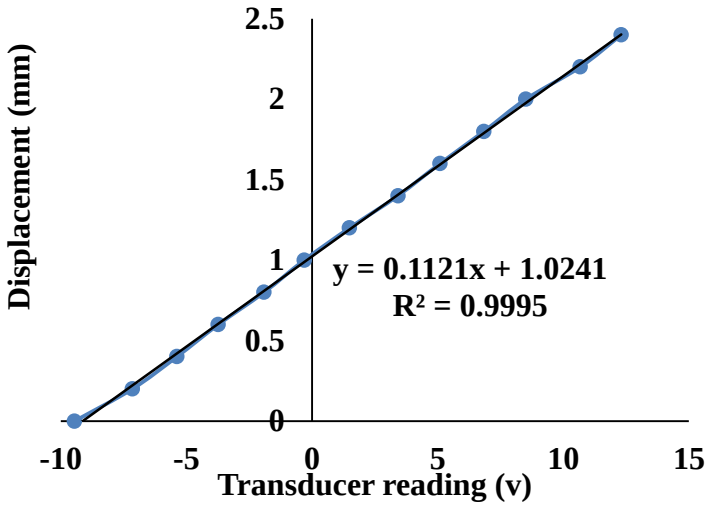

Figure 3.14 Graph shows measurements in load calibration

3.7.3 Creep Indentation Test

The creep indentation test provided data on cartilage deformation over time which was used to characterize the biomechanical properties of Elastic Modulus and Permeability. Tests were conducted for each cartilage sample at the ROI, as previously described in Section 3.7. An impermeable 4-mm diameter spherical indenter was positioned as close as possible to the cartilage surface and released with a 0.11 N compression load inducing 10-20% strain relative to cartilage thickness evidenced by earlier studies (Abd Latif et al., 2012; Hashim et al., 2017). The test apparatus was shown in Figure 3.15.

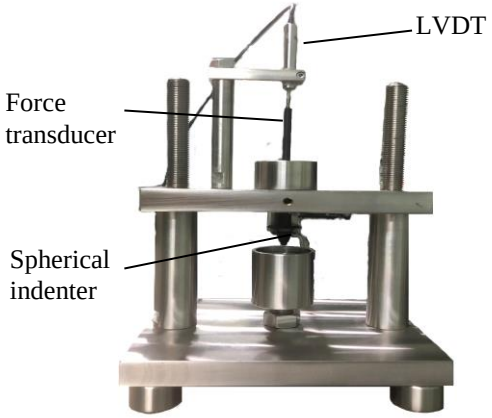

Figure 3.15 Creep indentation test apparatus

During testing, the cartilage samples were immersed in PBS solution to prevent dehydration and maintain physiological conditions. Displacement data was recorded continuously at 0.01-second intervals for over 2000 seconds reaching equilibrium at approximately 2500 seconds (Ateshian et al., 1997; Pierce et al., 2013; Gilbert and Blain 2018). Data acquisition was performed using LabVIEW 8.5.1 software.

3.7.4 Cartilage Thickness Measurement

Following the creep indentation test, cartilage samples were equilibrated in PBS solution for 60 mins to restore their original shape as reported in previous works (Abd Latif et al., 2012). A sharp needle indenter was then used to penetrate the cartilage tissue until it reached the underlying subchondral bone. The thickness measurement test involved applying a 3.18 N load to a designated point on the cartilage surface as shown in Figure 3.16. Displacement of the needle indenter and applied load were recorded at 0.001-second intervals enabling precise measurement of cartilage thickness (Ibramsa et al., 2022).

Figure 3.16 Apparatus for indentation thickness test (a) Close-view on the thickness test (b) Needle indenter

Cartilage thickness was determined by calculating the difference between the contact points of the needle on the cartilage surface (point A) and the subchondral bone

(point B) as illustrated in Figure 3.17. To ensure accuracy the cartilage samples were fully submerged in PBS solution throughout the thickness testing process.

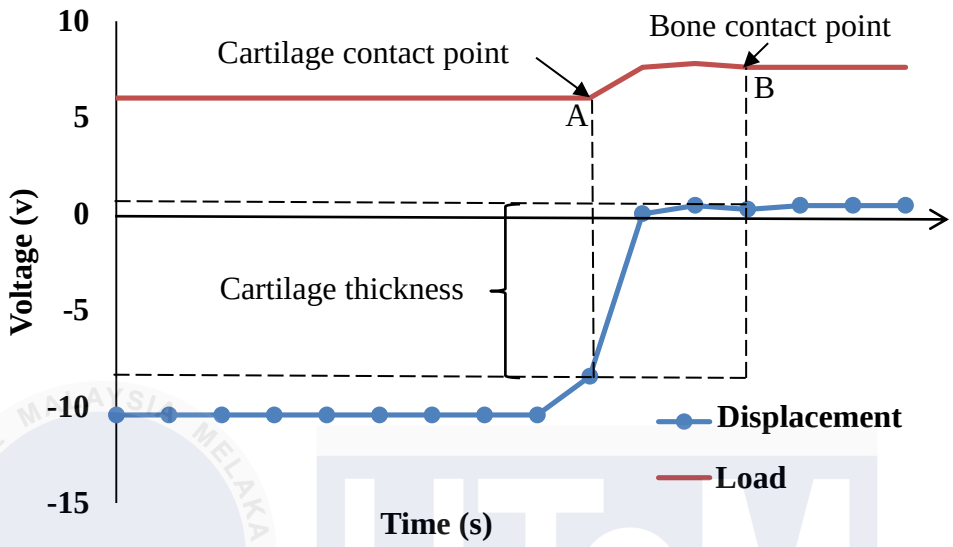

Figure 3.17 Schematic of cartilage thickness measurement

3.8 Computational Methods

The computational method incorporated data from the creep indentation tests to characterize cartilage's biphasic properties. These properties including Elastic Modulus (E) and Permeability (κ) were determined using an idealized axisymmetric biphasic poroelastic FE model. All FE models were developed in ABAQUS 6.9 software (DS Simulia Corp., Providence, RI, USA).

3.8.1 Modelling of Contact-Dependent Flow

The model was reconstructed with identical interface and boundary conditions, element types, and cartilage properties to implement and validate a contact-dependent flow algorithm. This algorithm determines flow conditions based on contact stress at the cartilage surface nodes as evidenced by earlier study (Pawaskar et al., 2010). The cartilage was modeled as an axisymmetric FE structure with a 3-mm thickness and a 20-mm radius while the rigid spherical indenter had a 5-mm radius. The FE element type was four-node

bilinear displacement and pore pressure (CAX4P) elements. Boundary conditions included fixing the bottom nodes of the cartilage in both horizontal and vertical directions, constraining horizontal motion along the axis, and allowing the spherical indenter to move vertically. The cartilage surface in contact with the indenter was assigned a contact-dependent flow condition while the bottom and vertical symmetry axis were set to no fluid flow. The outer edge of the cartilage was assigned zero pore pressure to the unrestricted fluid flow as shown in Figure 3.18.

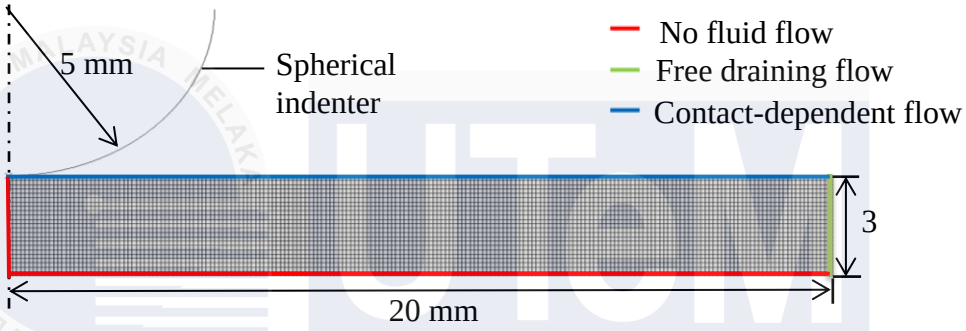

Figure 3.18 Axisymmetric FE model of a cartilage

Deformation phenomenon was simulated in creep-deformation and stress-relaxation to verify the cartilage behavior. The creep-deformation simulation was performed by applying a ramp load of 0.11 N on the indenter for two seconds with the load maintained for a further 1000 seconds. The stress-relaxation was performed by applying 10% of deformation over a ramp time for two seconds and then the indenter position was maintained for a further 1000 seconds. Table 3.2 shows the cartilage properties that were applied in previous study.

Table 3.2: Material properties of articular cartilage (Lian et al., 2015)

Parameter	Value
Elastic Modulus, E	0.54 MPa
Poisson's ratio, υ	0.08
Permeability, k	4.0×10^{-15} m^4/Ns
Void ratio, e	4.0 (80% interstitial fluid)

3.8.2 Finite Element Model

FE models were developed to account for variations in cartilage thickness as shown in Figure 3.19 significantly influenced the mechanical behavior of cartilage under loading conditions. A single model would not have accurately represented the mechanical response across different thicknesses since both thinner and thicker cartilage exhibited modulus deformation characteristics. Hence, by constructing models for varying thicknesses, it was possible to analyze these differences and determine the impact on Elastic Modulus and Permeability of the articular cartilage.

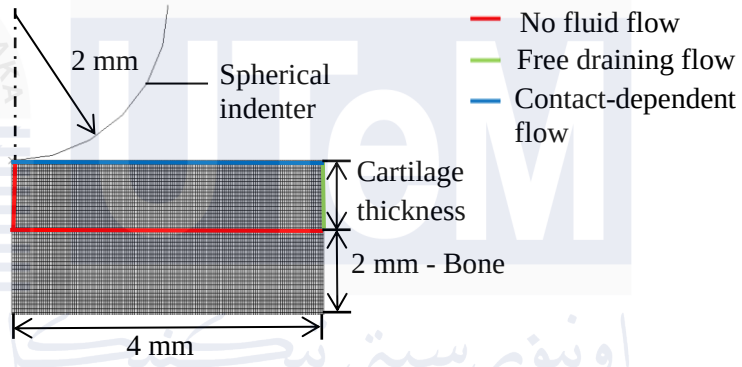

Figure 3.19 Axisymmetric FE model of a cartilage

3.9 Characterization of Biomechanical Properties of Articular Cartilage

The biphasic biomechanical properties of cartilage, namely the Elastic Modulus and Permeability, were determined by matching the deformation curve generated from the FE model with the experimental deformation curve through sequential adjustment of these properties, as shown in Figure 3.20. The red circles represent the experimental curve obtained during indentation, while the blue line corresponds to the FE model output. Parameter values were iteratively modified until the deformation-time curve from the FE model closely matched the experimental data. A non-linear least-square method, using the 'lsqnonlin' function in Matlab software (V7.12.0 R2011a, MathWorks Inc, MA, USA), was employed following the procedure described by Pawaskar (2010), with curve

fitting performed to minimise the sum of squared errors. After curve fitting, the resulting elastic modulus and permeability values were taken as the biomechanical properties of the tested cartilage specimen. Iterations began with initial estimates of elastic modulus and permeability, and the final optimised values were obtained when the function reached either the minimum squared error or the predefined convergence criteria between the two curves. Automatic time increments with the UTOL parameter, which restricted the maximum allowable change in pore pressure per increment at 600 kPa, were applied to ensure acceptable results (Pawaskar, 2010 Latif et al., 2013; Hashim et al., 2017).

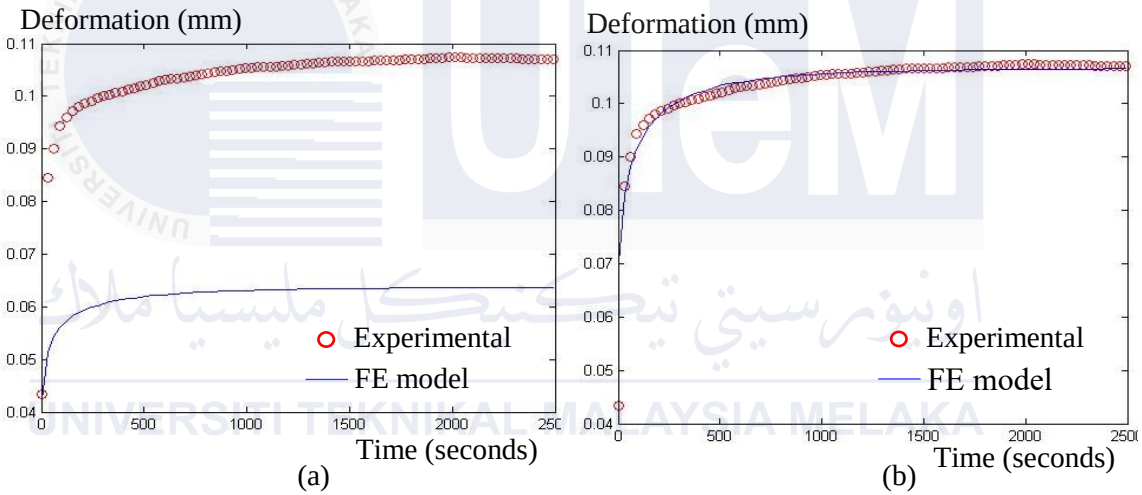

Figure 3.20 Cartilage deformation curve (a) before matching and (b) after matching

3.10 Summary

This chapter outlines the biomechanical properties and progressive fibrillation of articular cartilage using a combination of experimental and computational approaches. Cartilage samples were enzymatically degraded with 0.05% trypsin and 0.2% Collagenase Type II at various intervals to simulate osteoarthritic fibrillation followed by microscopic imaging using the Zeiss Axioscope 2 MAT and further analyzed using ImageJ to evaluate dimension scale of surface area. These methods provided insights into the physical integrity of the articular cartilage. Biomechanical assessments included creep indentation tests and cartilage thickness measurements which were incorporated into FE modeling in Abaqus were used to determine the Elastic Modulus and Permeability. Additionally, low-field MRI imaging using a 0.18 T Esaote C-scan MRI system was employed to analyze cartilage samples with MATLAB processing the grayscale intensities assessed using linear Pearson Correlation analysis link to the cartilage fibrillation physical and mechanical properties. The findings highlight the relationship between physical fibrillation and biomechanical performance offering critical insights into cartilage behavior under progressive osteoarthritic conditions.

CHAPTER 4

RESULT AND DISCUSSION

4.1 Introduction

This chapter presents the results and discussion of the experiment study. The quantification assessment involves the cartilage thickness and microscopic cartilage area. After that, measurement of cartilage water content was observed to assess the degradation of PGs leading to higher water molecules within the tissue. The greyscale values were obtained from the MRI sequence image with better quality of articular cartilage image. The biomechanical properties of the articular cartilage were characterized using a combination of creep indentation test and computational axisymmetric FE model. Then, providing the correlation between the greyscale values and biomechanical properties of the articular cartilage fibrillated articular cartilage was studied to show the effect enzyme degradation on cartilage biomechanical properties.

4.2 Fibrillation Assessment of OA Cartilage

Cartilage thickness and microscopic cartilage area were assessed through experimental measurements as part of the quantification assessment. Cartilage thickness serves as a foundation for developing the FE model in this study. The cartilage thickness for the specimens (n=36) obtained via the indentation test was 0.97 ± 0.10 mm as shown in Figure 4.1 for the control samples which aligned with the range reported in previous study (Temple et al., 2016). The results indicate that Grade I cartilage initially measured 0.90 ± 0.08 mm. However, after 30 mins of fibrillation, the thickness decreased to 0.62 ± 0.08 mm, and by 120 mins, it further declined to 0.39 ± 0.05 mm. This represents a 57% reduction in thickness over the enzymatic degradation period.

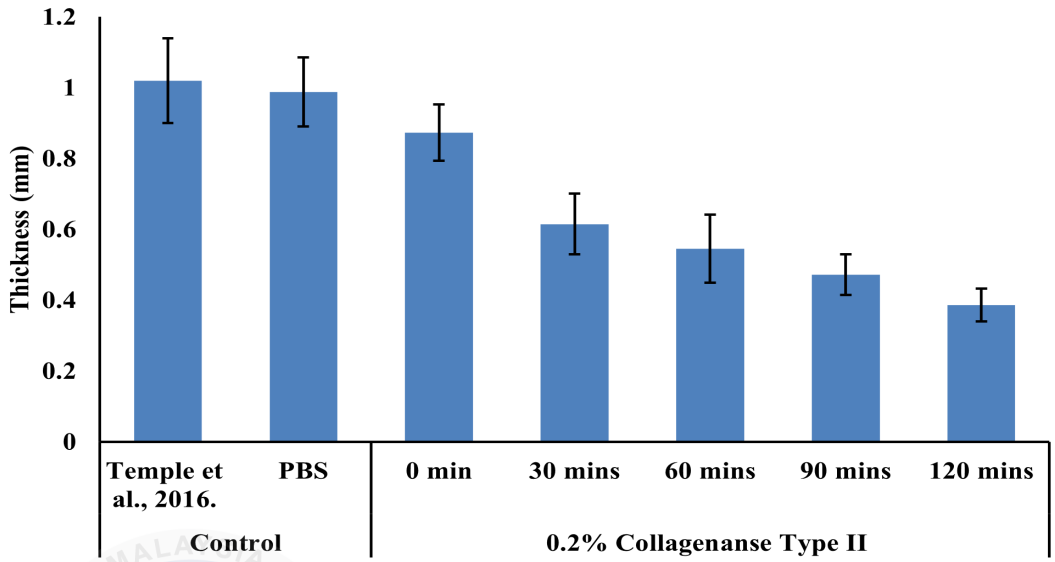

Figure 4.1 Mean cartilage thicknesses of bovine femoral head with different interval time

The study investigated cartilage thickness variations across the bovine femoral head revealed that cartilage thickness was not uniform across the surface. This emphasizing the necessity of region-specific assessments aligns with previous researches (Athanasiou et al., 1991; Sadeghi et al., 2015; Temple et al., 2016).

This initial state of the cartilage 0.05% Trypsin with its consistent thickness can be the representation of Grade I OA. At Grade I, the cartilage maintains its physical integrity with minimal degradation, and the thickness was close to its normal physiological range as highlighted in prior studies (Krakowski et al., 2024). The surface of the cartilage was smooth with no significant evidence of fibrillation or physical compromise. The baseline measurements of cartilage thickness across the bovine femoral head in the control samples served as a valuable reference point for evaluating the progression of OA.

At 30 mins, after exposure to 0.2% Collagenase Type II the cartilage thickness had already begun to decline significantly reducing from 0.90 ± 0.08 mm to 0.62 ± 0.08 mm indicate early grade of fibrillation. The once relatively smooth cartilage surface exhibited visible structural irregularities where thickness analysis revealed the initial formation of micro fissures and roughened textures along the surface suggested the early breakdown of collagen fibers. The collagen network started to lose its original organized structure as

fibrils began to separate and extend outward forming a disorganized pattern within the ECM.

The study observed a significant reduction in cartilage thickness following exposure of Grade I, marking a transition towards Grade II OA**.** After 120 mins of degradation, the cartilage thickness decreased to 0.39 ± 0.05 mm, representing a 57% reduction. Grade II OA was characterized by the appearance of fibrillation on the cartilage surface, indicate the breakdown of collagen fibres and a reduction in thickness as the matrix loses its physical organization. The cartilage surface becomes uneven, with superficial cracks or fissures as confirmed by previous work (Ouyang et al., 2023). The loss of physical organization of the cartilage was accompanied by enzymatic activity of collagenase that makes reduction in its biomechanical integrity.

Although the study did not progress to Grade III, the consistent thinning and fibrillation of the cartilage through this study suggested that it has a potential to progress to Grade III if the enzymatic degradation had been allowed to continue. The degradation process would continue beyond the 120 mins timeframe, with the cartilage exhibiting changes consistent with severe OA potentially reaching Grade III. Grade III OA was typified by deep fibrillation of the cartilage extending into deeper layers and loss of the underlying bone (Wang et al., 2020).

In addition, Figure 4.2 illustrates the cartilage area reduction during the fibrillation process, analyzed using MATLAB and ImageJ. Based on the figure, the mean control samples using PBS 0.85 ± 0.17 mm² similar with previous reported values (Youssef et al., 2021). The figure illustrates a significant decline in cartilage area over time, decreasing from 0.81 ± 0.16 mm² at 0 mins in Grade I to 0.72 ± 0.15 mm² after 30 mins, and further to 0.63 ± 0.15 mm² after 120 mins of fibrillation in Grade II. The whole declination from Grade I to Grade II decreasing with trend of 22%. This reduction in area showed that

cartilage becomes thinner and reflects the loss of cartilage integrity during the process of fibrillation.

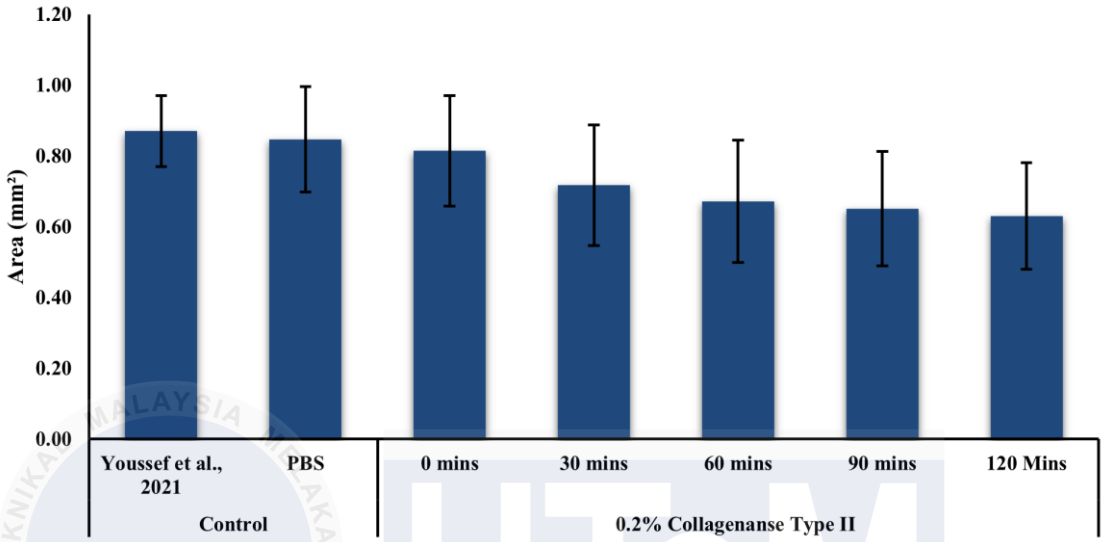

Figure 4.2 Area changes in fibrillation of progressive cartilage

The microscopic images from Figure 4.3 clearly showed these physical area changes. From the microscopic view, fibrillation process began with degraded cartilage preserved in its original form at the superficial zone.

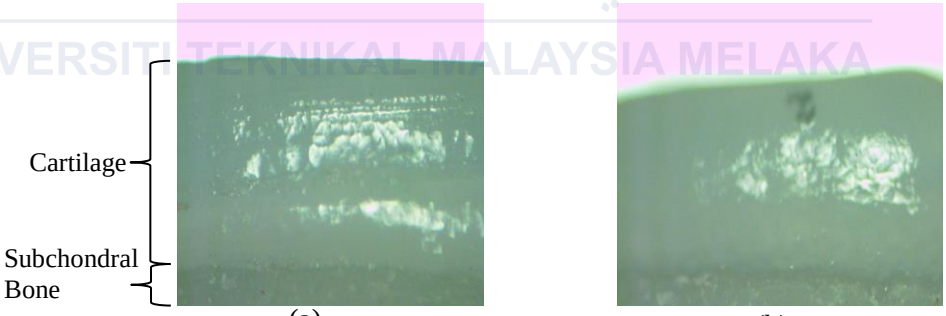

Figure 4.3 Superficial zone of articular cartilage decrease (a) Grade I (b) Grade II after fibrillated 120 mins.

At Grade I OA**,** the cartilage surface was smooth and intact, with minimal evidence of fibrillation or physical compromise. The collagen fibres maintain their organized alignment, and the ECM showed no significant disruptions as supported by (Goldring and Goldring 2016). Also, the cartilage thickness was within its normal physiological range, and its biomechanical integrity was maintained as affirmed by (Krakowski et al., 2024).

There might be subtle changes that were not visible without microscopic examination. However, the overall structure of the cartilage was still remarkably close to its healthy condition state (Kleemann et al., 2005).

At 30 mins, the microscopic cartilage area also showed a reduction decrease from 0.81 ± 0.16 mm² to 0.72 ± 0.15 mm² as a result of collagenase induced degradation which caused the cartilage slowly exposed towards fibrillation progresses within Grade II OA and microscopic observation started to reveal a distinct physical change. The progressive grade of cartilage thinning were evident in cross sectional views, where superficial disruptions extended into deeper layers, with localized areas showing early signs of delamination. The surface began showing signs of uneven stress distribution as sections of the ECM started to lose their cohesive integrity as these early changes demonstrated the progressive weakening of the cartilage allowing for further deterioration with prolonged enzyme exposure. The smooth surfaces also develop micro fissures and roughened textures indicate the breakdown of collagen fibres as prior study (Ouyang et al., 2023). The collagen network starts to become increasingly disorganized, with collagen fibres losing their uniform alignment. This disorganization was seen as thin, thread like fibrils that extend from the surface into deeper layers as evidenced by (Gottardi et al., 2016).

At 120 mins, the superficial zone at Grade II cartilage also possessed significant changes reflecting 38% reduction compared to Grade I through the thinning and physical changes. The fibrillated cartilage surface displayed an extensive delamination with visible peeling particularly in superficial zone where collagen fibers had unraveled and lost their mechanical interconnections. The continuous fibrillated cartilage structure was now interrupted by irregular gaps and uneven depressions indicating a severe loss of its load bearing capacity, showing a deep fibrillation and surface degradation. This fibrillation in these areas often align parallel to the surface, forming elongated disruptions that extend

circumferentially around the cartilage edge. These physical changes at the superficial zone can lead to uneven stress distribution, increasing its vulnerability for further mechanical wear as per previous study (Mohammadi et al., 2013).

Overall, Grade II OA was marked by the emergence of fibrillation, micro fissures, disorganized collagen fibres, and a reduction in both thickness and area compared to Grade I that has a smooth and intact cartilage surface as confirmed by previous studies (Lee and Xia, 2013; Chaudhary et al., 2015; Ouyang et al., 2023). These changes, as observed in microscopic images and supported by quantitative result changes in thickness and area illustrate the physical breakdown of cartilage during the progressive grades of OA.

4.3 Measurement of Cartilage Water Content

The study examined water content in cartilage at two distinct Grades of OA early Grade I and progressive Grade II. Figure 4.4 showed the control samples water content at 76% had been use resemblances to the past study research (Crolla et al., 2022).This figure also revealed the water content at Grade I cartilage was 87%. After 30 mins of fibrillation, the water content reached 88%, and by 120 mins, it increased to 92%. This represents a 5% rise in water content over the enzymatic period. Interestingly, the plateau observed in the figure suggests that after 60 mins of fibrillation, the water content stabilize indicate that the enzymatic reactions have reached its equilibrium state with no significant changes in water retention as reported in earlier investigations (Liu and Wang 2020; Lim et al., 2023).

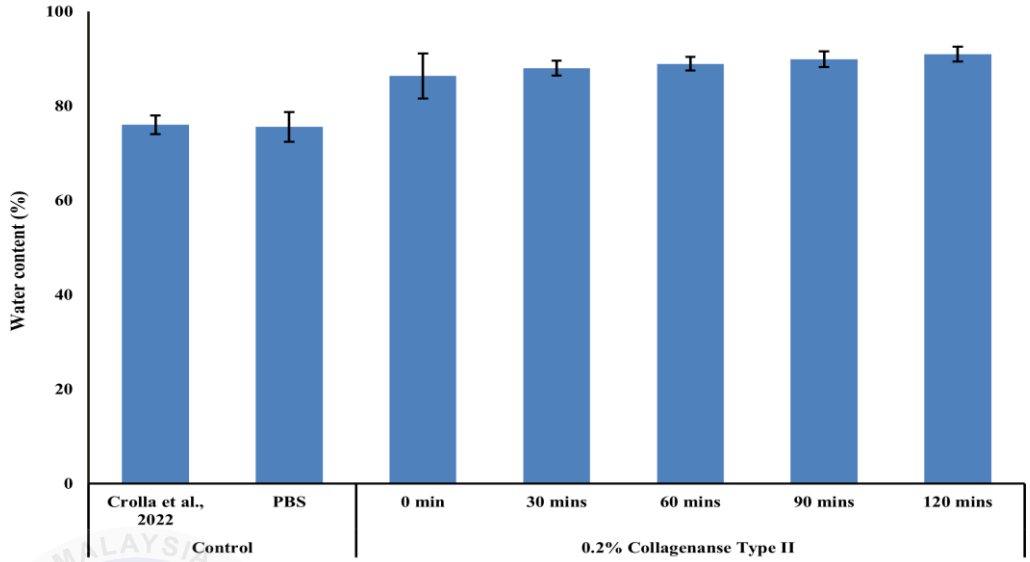

Figure 4.4 Mean water content for control, degraded and fibrillated samples

The rise in water content between control samples and initial Grade I, 0 min, was linked to the degradation of PGs and their GAGs side chains as shown in early OA Grade I. As OA progresses, PGs particularly, aggrecans, were broken down leading to the loss of their negatively charged GAGs. This degradation disrupts the osmotic balance, causing previously bound water molecules to become free within the tissue (Wright et al., 2014; Athanasiou et al., 2017). While the overall water content increases, the free water lose the physical organization necessary for hydrostatic support compromising the tissue biomechanical function (Gao et al., 2014).

At 30 mins of enzymatic exposure, the cartilage water content showed a slight but notable increase from 87% in Grade I cartilage to 88%. This change was associated with the early breakdown of PGs which resulted in the loss of GAGs responsible for binding water molecules. As PGs degraded the bounded water within the ECM started transitioning into free water leading to an initial rise in hydration levels, however, the increase in water content was not yet drastic but analysis revealed localized swelling in regions where PGs loss was pronounced. The superficial layer of the cartilage appeared to retain to its original integrity, but early fibrillation had already begun altering its ability to regulate fluid distribution. This imbalance in water retention affected the cartilage capacity to maintain

osmotic pressure with certain regions experiencing increased water absorption while others started to lose their structural moisture stability.

At 120 mins, the water content increased dramatically reaching 92% indicate a significant shift in the hydration state of the cartilage. The breakdown of PGs had progressed extensively allowing for a greater flow of free water into the cartilage ECM. The degradation of PGs and the associated changes in water content were closely tied to the physical deterioration of cartilage particularly the development of Grade II fibrillation. The interplay between PGs degradation, GAGs loss, increased free water, and collagen fibrillation creates a vicious cycle of cartilage degradation driving the progression of Grade II OA (Lotz et al., 2013). This has led to the further disorganization of collagen fibers as the osmotic imbalance created excessive swelling within the tissue. The cartilage structure appeared viscous with larger gaps forming between disorganized collagen fibrils where the increased fluid intake further weakened the cartilage mechanical integrity, allowing the ability of the cartilage to retain its structural water to be compromised as the balance between bound and free water was lost. The elevated hydration level at this grade suggested that the cartilage had reached a point where the degradation of PGs and the unstructured distribution of water had made it highly susceptible to further mechanical breakdown.

4.4 Evaluation of Low-field MRI Grayscale

Figure 4.5 showed that greyscale intensity variations changes over time. According to the result, control samples cartilages grayscale intensity value 1604 ± 90 aligned with prior experimental study (Ibramsa et al., 2022). Whereas the imaging results identified noteworthy changes in greyscale intensity for Grade I cartilage showed the value of 2076 ±

68. The next fibrillated 30 mins showed 2110 ± 79 until 120 mins Grade II at 2237 ± 113. The whole incline from Grade I to Grade II was within increasing trend of 5%.

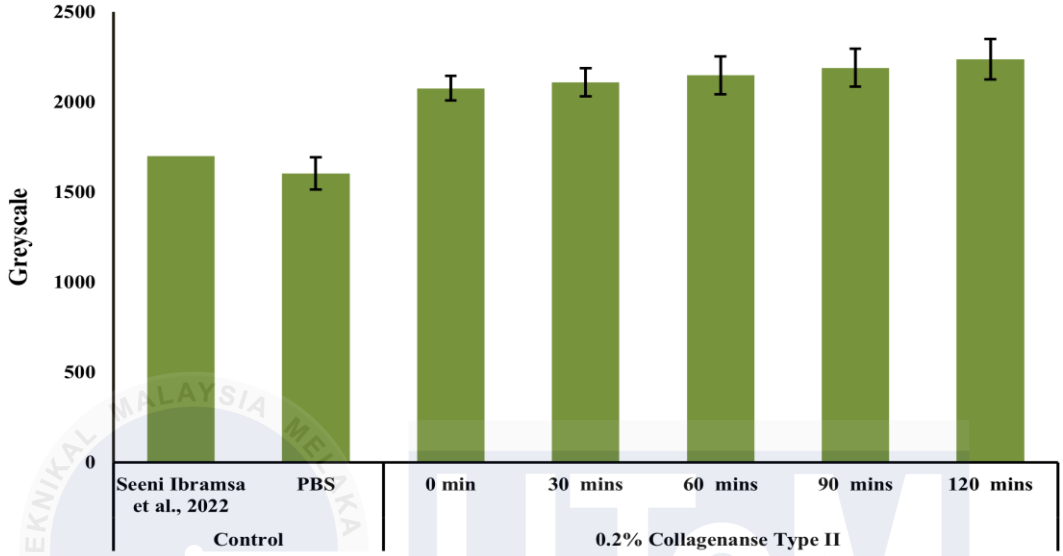

Figure 4.5 Mean greyscale intensity for control, degraded and fibrillated samples.

The choice of MRI imaging sequence was crucial for accurately assessing the integrity of cartilage, as it directly impacts signal contrast and tissue differentiation. GE sequences have demonstrated superior contrast between cartilage, joint fluid, and subchondral bone due to their ability to enhance (Signal-to-noise ratio) SNR and (Contrast-to-noise ratio) CNR at low-field strengths (Paunipagar and Rasalkar 2014; Afsahi et al., 2022).

At 30 mins, the low-field MRI grayscale intensity showed an increase from 2076 ± 68 to 2110 ± 79. This change attributed to the progressive increase in cartilage hydration as water content continued to rise due to PGs degradation. MRI images revealed that the cartilage structure appeared with variations in grayscale intensity corresponding to regions where fibrillation and water accumulation had begun to disrupt tissue uniformity. The early breakdown of collagen fibers and the localized accumulation of free water contributed to the slight but measurable increase in grayscale values indicate that the structural degradation was becoming detectable at intensity level. The grayscale variation indicated

that the cartilage ECM had lost part of its original uniformity, with changes in signal intensity reflecting differences in hydration levels and collagen integrity across the tissue.

At 120 mins, the MRI grayscale intensity increased further reaching 2237 ± 113 confirming the substantial progression of cartilage degradation. The increased water content contributed to a higher MRI signal as the cartilage ECM became saturated with free water. The imaging results revealed widespread variations in grayscale intensity with distinct high intensity regions corresponding to areas where collagen breakdown had led to significant tissue hydration. The transition from bounded to free water was evident in the MRI scans where the cartilage structure appeared increasingly fragmented within areas of high contrast highlighting extensive fibrillation and structural weakening showing a strong correlation between MRI grayscale intensity and water content, indicated that the imaging technique effectively captured the progressive degradation of the cartilage as fibrillation continued and hydration levels increased.

The study reveals a strong correlation with r=0.94 as shown in Figure 4.6 between cartilage water content and MRI greyscale intensity. This finding was significant because it demonstrates that the information provided by MRI scans accurately reflects the biomechanical state of the cartilage. Specifically, as the water content of cartilage increases due to fibrillation, the MRI signal intensity also elevates. This correlation indicates that the MRI signal was sensitive to changes in the hydration level of the tissue, making it a reliable tool for assessing the degree of cartilage degradation.

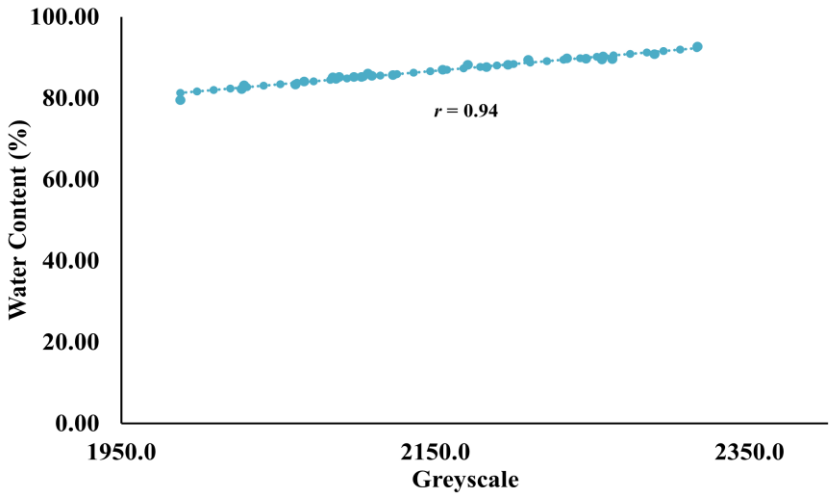

Figure 4.6 Correlation between greyscale and water content

GE sequence relied on proton density and magnetic susceptibility differences to generate image contrast, with minimal influence from relaxation times. In degraded articular cartilage, the breakdown of the collagen-PGs matrix disrupted the tissue's structural integrity, leading to increased water mobility and content. This rise in free water elevated the local proton density, which directly contributed to increased signal intensity in GE images. The increase in greyscale values in degenerated cartilage corresponded to the increased water-associated signal under GE acquisition, which was sensitive to changes in magnetic field inhomogeneities caused by tissue degradation. Therefore, the plot captured the GE-based MRI principle where signal intensity increased with water content due to loss of matrix organization in osteoarthritic cartilage.

4.5 Biomechanical Properties of Articular Cartilage

The characterized Elastic Modulus and Permeability were shown in Figure 4.7. There were significant changes between early degraded Grade I and fibrillated cartilage Grade II at different grades of time interval in the context of mechanical behavior. The Elastic Modulus at illustrate in Figure 4.7(a) for the control samples was measured 1.81 ± 0.32 MPa consistent within the range of previous findings (Temple et al., 2016). According

to the result, the Grade I cartilage was 0.47 ± 0.10 MPa. The next fibrillated 30 mins was 0.40 ± 0.13 MPa until 120 mins Grade II, 0.26 ± 0.07 MPa exhibited a reduced of Elastic Modulus. The whole declination of Grade I to Grade II represented a 48% decrease. This indicates a reduced in the cartilage ability to withstand mechanical loads. The reduction of Elastic Modulus in the cartilage becomes less able to withstand the forces it normally experiences and was prone to deformation and damage. In contrast, cartilage Permeability exhibited in Figure 4.7(b), shows an increasing trend as fibrillation progressed. The Permeability of control sample was 1.38 ± 0.55×10^{-15} m^4/Ns aligning with previously reported value (Démarteau et al., 2006). Notably, the increase in Permeability from degradation Grade I 3.47 ± 1.08×10^{-15} m^4/Ns to the first 30 mins fibrillated was 4.18 ± 1.04×10^{-15} m^4/Ns and further to fibrillated Grade II 120 mins 5.26 ± 1.72×10^{-15} m^4/Ns reflecting a 34% increase from Grade I to Grade II. This progressive degradation increases Permeability, with significant implications for overall cartilage function. Result at the 0 mins fibrillated or 120 mins degrade had been supporting the through observations reported by Salehuddin et al. (2024). The outcomes at 0 mins fibrillated or 120 mins degraded for Elastic Modulus and Permeability demonstrate agreement with the findings reported by Salehuddin et al. (2024)

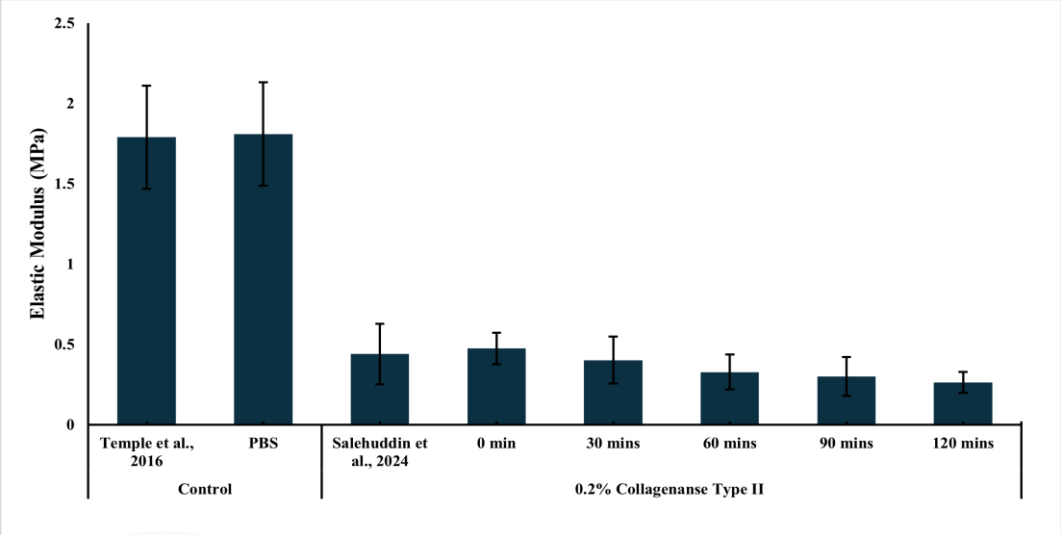

(a)

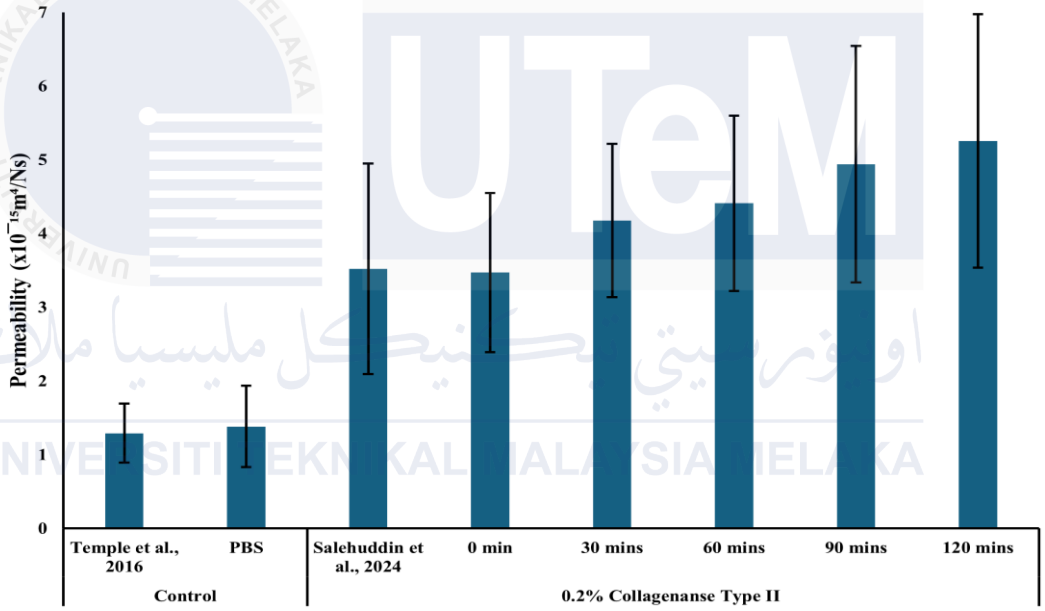

(b)

Figure 4.7 Biomechanical properties of progressive OA cartilage (a) Elastic Modulus, (b) Permeability

At 30 mins, the biomechanical properties of the cartilage showed early signs of deterioration. The Elastic Modulus decreased from 0.47 ± 0.10 MPa in Grade I cartilage to 0.40 ± 0.13 MPa indicated a loss of stiffness as the collagen network began to break down. The ability of the cartilage to resist compressive forces was already compromised as the disorganization of collagen fibrils reduced its structural support. Biomechanical evaluation showed that the superficial layer of the cartilage was beginning to exhibit increased

deformation under mechanical stress suggesting that early fibrillation had started affecting its load bearing capacity. The Permeability increased from $3.47 \pm 1.08 \times 10^{-15}$ m^4/Ns to $4.18 \pm 1.04 \times 10^{-15}$ m^4/Ns reflecting early breakdown of the collagen fiber network. The Permeability of the cartilage also increased reflecting the progressive loss of ECM integrity as enzyme activity allowed for greater fluid exchange within Pgs. This increase in Permeability was associated with the early disintegration of collagen fiber interconnections making the cartilage susceptible to fluid and structural weakening.

After 120 mins, the decline in biomechanical properties became more pronounced, as the Elastic Modulus further decreased to 0.26 ± 0.07 MPa, representing a 48% total reduction from Grade I. The cartilage became significantly softer and less capable of withstanding mechanical loads due to the breakdown of the collagen network, which led to widespread fibrillation. The increased water content, combined with collagen fiber disorganization, caused the tissue to become more deformable under compressive forces. Whereas, the Permeability continued reaching $5.26 \pm 1.72 \times 10^{-15}$ m^4/Ns, marking a 34% increase from Grade I cartilage. This significant rise in Permeability indicated that the cartilage ECM had become viscous and less capable of retaining its original hydration balance the advanced degradation observed at 120 mins, confirmed that prolonged enzymatic exposure had led to severe biomechanical weakening creating the cartilage to become highly vulnerable for further mechanical damage within OA progression.

Modulus and Permeability-based biomarkers offer clear, quantitative insights into cartilage degradation and OA progression. A decline in Elastic Modulus reflects reduced stiffness and structural integrity, signaling early damage to collagen fibrils and loss of PGs from Grade I to II. This decline weakens the tissue's ability to resist compressive loads and increases the risk of mechanical failure. Similarly, rising Permeability points to a compromised ECM where collagen and PGs breakdown allows more fluid flow, triggers

swelling, and lowers load-bearing capacity. Increased porosity and poor synovial fluid retention further disrupt cartilage function. Together, these biomechanical markers help detect early structural changes before permanent damage occurs.

4.6 Correlation of Cartilage Greyscale and Biomechanical Properties

Linear Pearson correlation coefficient was performed to evaluate the relationship between the greyscale obtained from MRI and the biomechanical properties of the articular cartilage. The linear correlation coefficient, *r* was used to measure the strength and the direction of the linear relationship between cartilage greyscale and biomechanical properties. The correlation was classified as weak at $0.1 \leq r < 0.3$, indicating minimal association; moderate at $0.3 \leq r < 0.7$, suggesting a noticeable relationship with some variability; and strong at $r \geq 0.7$, representing a clear and significant connection between variables, as reported in previous research (Schober et al., 2018).

This study includes graphs of the correlations between Elastic Modulus within greyscale intensity as shown Figure 4.8 (a) and the correlation between Permeability with greyscale intensity in Figure 4.8 (b). The analysis reveals that lower greyscale values were associated with decreased Elastic Modulus and increased Permeability. The degraded cartilage had become less stiff and less resistant to deformation, becoming more permeable. This finding supports the hypothesis that physical degradation has a direct effect on mechanical function.

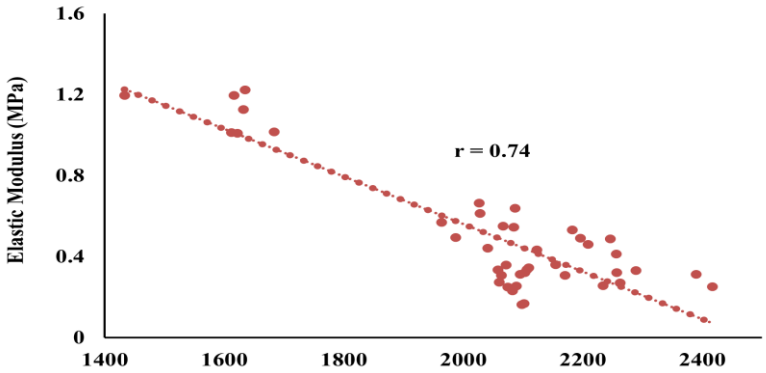

(a)

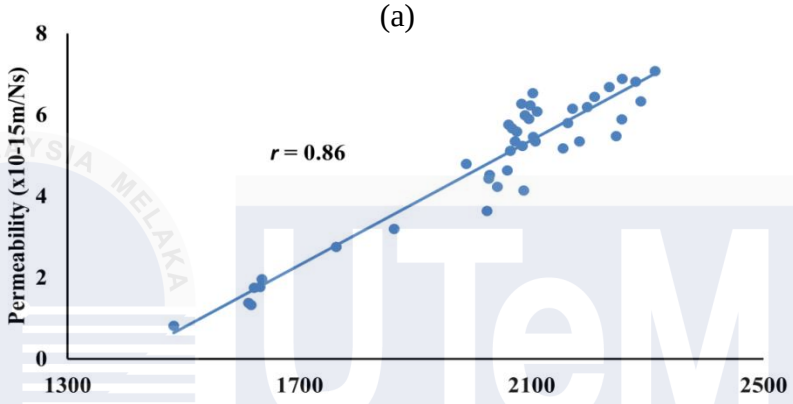

(b)

Figure 4.8 Linear Pearson correlations between greyscale intensity and (a) Elastic Modulus, and (b) Permeability of cartilage

This analysis provided the statistical relationship between greyscale intensity and the Elastic Modulus, which was r=0.74. This value indicated a strong relationship, where an increase in greyscale intensity signified severe fibrillation, while the modulus of the cartilage decreased. These findings indicate that as the cartilage becomes damaged, it also becomes softer and less resilient. This further supports the idea that physical degradation leads to a reduction of its physical breakdown.

Additionally, the study examines the correlation between greyscale intensity and cartilage Permeability. The results revealed a correlation coefficient of r = 0.86 between greyscale intensity and Permeability, indicating an even stronger relationship as according to the correlation value stated in previous chapter. This high correlation further supports evidence of the weaken mechanical integrity of the cartilage.

The compressive stiffness of cartilage, particularly its intrinsic properties, is linked to its biochemical composition. Cartilage's compressive stiffness is directly proportional to PGs and collagen content and inversely proportional to the water content (Jurvelin et al., 1994). On the other hand, Permeability has a positive relationship with water content while inversely correlating to PGs and collagen content.

4.7 Summary

This study emphasizes the significant effects of fibrillation on the biomechanical properties of articular cartilage in OA progression from Grade I to Grade II. The interplay of cartilage fibrillation with structural degradation was assessed through the quantitative analysis of cartilage thickness, concentration of water and Permeability. Cartilage thickness was found to significantly decline along with an increase in fibrillation, micro-fissures, and disorderly array of collagen, indicative of structural degradation. There was a trend for an increasing loss of water content because of the loss of PGs, resulting the loss of cartilage's biomechanical control due to osmotic balance. All these factors contributed to the reduced capability of cartilage to bear mechanical loads which accelerates OA progression.

Low-field MRI accurately depicted these degenerative changes, with pebble intensity increasing with the progression of cartilage damage. A strong correlation was seen between MRI greyscale intensity and water content, proving the weak sensitivity to cartilage hydration and fibrillation. Increasing MRI greyscale values was also correlated with increasing Permeability, which was associated with progressive OA changes. The images effectively demonstrated the change from Grade I to Grade II OA within the OA imaging changes framework, delineating the capability of MRI to evaluate cartilage loss non-invasively. In addition, biomechanical evaluations showed that Grade II cartilage had

a significantly lower Elastic Modulus, pointing to reduced stiffness and mechanical strength. In turn, increased Permeability pointed to diminished control of interstitial fluid flow due to fibrillation. The unchanged relationship of the three variables has reinforced the increase capture of MRI greyscale intensity, the modulus and Permeability portraying OA's known changes which shifts the potential for these markers in clinical OA progression determined surveillance.

The findings reinforce the value of low-field MRI in tracking the condition of cartilage and set the grade for the early detection of OA and its treatment. The biomechanically observed weakening described by high Permeability reflects an advance grade of loss in cartilage function. Collectively, these findings broaden the understanding of the processes involved in the degeneration of cartilage and suggest new avenues for non-invasive OA evaluation and treatment approaches. The research illustrates that the physical and biomechanical changes are profound and highlight the potential of low-field MRI in the diagnosis and surveillance of OA.

CHAPTER 5

CONCLUSION

5.1 Introduction

This chapter presents the research findings and outlines recommendations for future investigations. It provides a comprehensive summary of the research objectives and their achievement with highlights the key contributions of the study. Additionally, it addresses the limitations encountered during the study and proposes directions for future research to build upon the current work.

5.2 Research Summary

This study investigated the potential of low-field (0.18 T) MRI as a sensitive imaging tool to monitor enzyme-induced fibrillation in articular cartilage. Using a gradient echo sequence, the MRI clearly distinguished cartilage from surrounding soft tissues and revealed distinct greyscale layering, especially in the superficial zone. A 5% increase in greyscale intensity was observed in Grade II specimens compared to Grade I, indicating early structural changes. Creep indentation data were integrated with an axisymmetric poroelastic FE model to estimate the Elastic Modulus and Permeability which is key biomechanical properties of cartilage. These properties varied across anatomical locations and were significantly altered by fibrillation: Grade II specimens showed a 48% decrease in Modulus and a 34% increase in Permeability, suggesting a weakened extracellular matrix and increased fluid flow due to collagen network disruption.

A strong correlation was found between MRI greyscale values and cartilage biomechanics, confirming the reliability of low-field MRI in capturing functional tissue changes. This highlights the potential of MRI-derived greyscale as a non-invasive biomarker for cartilage integrity. If biomechanical properties can be accurately inferred from MRI data, it could eliminate the need for mechanical testing, offering a more efficient diagnostic pathway. These findings may support the development of cost-effective, clinically applicable imaging protocols for early OA detection and monitoring.

5.3 Research Contributions

This thesis makes a significant contribution to the biomechanical evaluation of articular cartilage in the context of OA, particularly by leveraging low-field MRI in correlate with FEA. It bridges imaging and computational biomechanics by extracting geometrically accurate cartilage models from low-field MRI scans, an approach that is both cost-effective and clinically accessible. By employing bovine cartilage with a thickness range of 0.5–3.3 mm, this study provides a relevant model for comparison with human cartilage of 2–4 mm, strengthening its applicability to human osteoarthritis research. The study advances the current understanding of cartilage mechanical behavior by simulating key parameters such as Elastic Modulus and hydraulic Permeability, which are critical indicators of tissue integrity and degeneration. Unlike conventional diagnostic approaches that rely solely on morphological observations or biochemical markers, this work brings biomechanical degradation to the forefront of OA assessment. The inclusion of subject-specific cartilage geometry, combined with a well-validated biphasic material model, allows for the prediction of stress distribution and fluid dynamics under physiological loading. This dual focus on solid and fluid phase interactions within the cartilage matrix offers a more comprehensive representation of the early degenerative

changes occurring in OA, potentially before they become visible on standard radiographic images.

In addition, this study aimed to bridge that gap through a dedicated low-field MRI system, which shows promising capability to enhance patient comfort along with other beneficial factors, ultimately offering better results and reliable diagnostic information on progressive-grade II OA. The combination of low-field MRI with appropriate post-processing and meshing techniques enables robust biomechanical modeling, even though many consider low-field MRI systems devoid of resolution mastery relative to high-field systems. This expansion enhances the clinical usefulness of the proposed approach, particularly in effort-driven environments. Critical to note is that the thesis does not limit itself to creating simulation models; rather, it vividly outlines translatable diagnostic applications. The research enables higher sensitivity for detecting OA by proposing hitherto unavailable thresholds for mechanical properties associated with early-grade cartilage softening. In this manner, the research substantially contributes to the accurate medicine paradigm in musculoskeletal healthcare by shifting the focus from diagnosis and treatment to disease prevention and tailor-made intervention planning.

5.4 Limitations of the Present Study

While this study shows particular advances in the biomechanics of cartilage, there are limitations that come correlated with the imaging method used and the modelling assumptions. Firstly, low-field MRI has a practical application, but the ease does come at the cost of spatial resolution. The contrast-to-noise ratio can interfere with cartilage boundary segmentation, therefore impacting precision and adding uncertainty to the 3D reconstruction of cartilage geometry, especially in lumpy or thin regions such as the patellofemoral compartment. The errors in segmentation affect the FE model, while the

stress fields and mechanical properties of the model undergo the most change. The selected biphasic model makes an accurate prediction of how the solid-fluid interactions are carried out in cartilage but does not take into consideration the zonal microstructure of the tissue as an additional complexity. Likewise, estimating a tissue's properties such as Elastic Modulus and Permeability through inverse modelling remains limited, as parameter fitting is often influenced by assumptions in the loading scenario. The absence of in vivo data and the use of idealised boundary conditions can further yield estimations inconsistent with physiological states. Moreover, the lack of biochemical degradation or cellular changes in the model leaves it biomechanically rich but biologically silent, restricting its capacity to capture the early onset of OA.

From a clinical standpoint, these limitations highlight the balance between promise and practicality in adopting low-field MRI for progressive-grade II OA assessment. Compared with high-field MRI, low-field systems offer greater comfort, affordability, and accessibility but at the expense of spatial resolution and contrast fidelity. When set against conventional radiography or ultrasound, which remain common in clinical diagnosis but offer limited biomechanical detail, the modelling approach presented here provides deeper mechanistic insights but lacks the validation required for clinical reliability. Thus, future research should pursue multimodal integration, combining MRI-based mechanical modelling with histological validation or biochemical biomarkers, to generate a more holistic and clinically meaningful evaluation of cartilage. Such integration would not only strengthen diagnostic confidence but also help position this methodology as a complementary tool alongside established imaging and grading modalities in OA management.

5.5 Future Works

To enhance the findings and extend the scope of the study, the following approaches are recommended:

i. Human articular cartilage

One of the most promising extensions of this research is the application of the current biomechanical assessment framework to human articular cartilage**,** particularly from patients at different grade of OA. This will allow for direct comparisons and validation of the mechanical thresholds established in this study using bovine models. Future investigations can focus on integrating clinical imaging data through arthroscopic grading with mechanical testing outcomes to bridge experimental findings with diagnostic relevance in a healthcare setting.

ii. Imaging modalities

A second avenue involves advancing the imaging modalities used in cartilage evaluation. The incorporation of low-field MRI, for example, can complement mechanical testing by offering non-invasive, high-resolution visualization of structural changes within cartilage. Combining MRI-based thickness and T2 relaxation mapping with mechanical parameters like Elastic Modulus and Permeability could allow for the creation of predictive models that detect early OA-related changes without tissue excision, facilitating longitudinal studies in both clinical and preclinical environments.

iii. Dynamic mechanical analysis

Thirdly, dynamic mechanical analysis should be incorporated to better understand the time-dependent viscoelastic properties of cartilage, which are not fully captured through equilibrium indentation alone. Frequency-dependent testing and stress-relaxation protocols can provide insights into how degenerated cartilage responds

under real-time joint loading conditions. These parameters are especially crucial for developing subject-specific FE models and simulating gait-cycle–relevant stresses in joint cartilage during movement.

iv. Biochemical and microstructural correlates

Lastly, biochemical and microstructural correlates of mechanical properties should be studied more comprehensively. Future work can include biochemical assays (sulfated glycosaminoglycan content, collagen crosslinking) and microscopic imaging techniques such as polarized light microscopy or second harmonic generation to assess collagen fiber organization. These analyses will offer deeper insights into how molecular-level changes drive mechanical degradation, potentially leading to biomarkers or therapeutic targets for early-grade OA intervention.

REFERENCES

Abd Latif, M.J., Jin, Z. and Wilcox, R.K., 2012. Biomechanical characterisation of ovine spinal facet joint cartilage, Journal of biomechanics, 45(8), pp. 1346-1352.

Abdel-Sayed, P., Vogel, A., Nassajian Moghadam, M. and Pioletti, D., 2013. Cartilage self-heating contributes to chondrogenic expression, European Cells and Materials, 26, pp. 171-178.

Abd Rahim, K.N.K., Kamaruzaman, H.F., Dahlui, M. and Puteh, S.E.W., 2020. From evidence to policy: economic evaluations of healthcare in Malaysia: a systematic review. *Value in health regional issues*, *21*, pp. 91-99.

Abramoff, B. and Caldera, F.E., 2020. Osteoarthritis: pathology, diagnosis, and treatment options. *Medical Clinics*, *104*(2), pp. 293-311.

Afsahi, A.M., Sedaghat, S., Moazamian, D., Afsahi, G., Athertya, J.S., Jang, H. and Ma, Y.J., 2022. Articular cartilage assessment using ultrashort echo time MRI: a review. Frontiers in Endocrinology, 13, p. 892961.

Alcaide-Ruggiero, L., Molina-Hernández, V., Granados, M.M. and Domínguez, J.M., 2021. Main and minor types of collagens in the articular cartilage: The role of collagens in repair tissue evaluation in chondral defects, International Journal of Molecular Sciences, 22(24), p. 13329.

Alcaide-Ruggiero, L., Cugat, R. and Domínguez, J.M., 2023. Proteoglycans in articular cartilage and their contribution to chondral injury and repair mechanisms, International journal of molecular sciences, 24(13), p. 10824.

Antony, J., McGuinness, K., Moran, K. and O'Connor, N.E., 2020. Feature learning to automatically assess radiographic knee osteoarthritis severity. *Deep Learners and Deep Learner Descriptors for Medical Applications*, pp. 9-93.

Arencibia, A., Encinoso, M., Jáber, J.R., Morales, D., Blanco, D., Artiles, A. and Vázquez, J.M., 2015. Magnetic resonance imaging study in a normal Bengal tiger (Panthera tigris) stifle joint, BMC Veterinary Research, 11, pp. 1-9.

Arlk, Y.B., de Sa Vivas, A., Laarveld, D., Van Laar, N., Gemser, J., Visscher, T., van den Berg, A., Passier, R. and van der Meer, A.D., 2021. Collagen I based enzymatically degradable membranes for organ-on-a-chip barrier models, ACS biomaterials science & engineering, 7(7), pp. 2998-3005.

Arnold, T.C., Freeman, C.W., Litt, B. and Stein, J.M., 2023. Low-field MRI: clinical promise and challenges. Journal of Magnetic Resonance Imaging, 57(1), pp. 25-44.

Arshad, A., Cong, P., Elsayed Elmenshawy, A.A.A. and Blumbergs, I., 2021. Design optimization for the weight reduction of 2-cylinder reciprocating compressor crankshaft, Archive of Mechanical Engineering, 68(4), pp. 449-471.

Ateshian, G.A., Warden, W.H., Kim, J.J., Grelsamer, R.P. and Mow, V.C., 1997. Finite deformation biphasic material properties of bovine articular cartilage from confined compression experiments, Journal of biomechanics, 30(11-12), pp. 1157-1164.

Athanasiou, A.E., Toutountzakis, N., Mavreas, D., Ritzau, M. and Wenzel, A., 1991. Alterations of hyoid bone position and pharyngeal depth and their relationship after surgical correction of mandibular prognathism, American Journal of Orthodontics and Dentofacial Orthopedics, 100(3), pp. 259-265.

Athanasiou, K.A., Darling, E.M., Hu, J.C., DuRaine, G.D. and Reddi, A.H., 2017. Articular cartilage. Crc Press.

Bartell, L.R., Fortier, L.A., Bonassar, L.J. and Cohen, I., 2015. Measuring microscale strain fields in articular cartilage during rapid impact reveals thresholds for chondrocyte death and a protective role for the superficial layer, Journal of biomechanics, 48(12), pp. 3440-3446.

Belluzzi, E., Todros, S., Pozzuoli, A., Ruggieri, P., Carniel, E.L. and Berardo, A., 2023. Human cartilage biomechanics: experimental and theoretical approaches towards the identification of mechanical properties in healthy and osteoarthritic conditions, Processes, 11(4), p. 1014.

Berchtold, S., Grünwald, B., Krüger, A., Reithmeier, A., Hähl, T., Cheng, T., Feuchtinger, A., Born, D., Erkan, M., Kleeff, J. and Esposito, I., 2015. Collagen type V promotes the malignant phenotype of pancreatic ductal adenocarcinoma, Cancer letters, 356(2), pp. 721-732.

Bergholt, M.S., St-Pierre, J.P., Offeddu, G.S., Parmar, P.A., Albro, M.B., Puetzer, J.L., Oyen, M.L. and Stevens, M.M., 2016. Raman spectroscopy reveals new insights into the zonal organization of native and tissue-engineered articular cartilage. ACS central science, 2(12), pp. 885-895.

Bhosale, A.M. and Richardson, J.B., 2008. Articular cartilage: structure, injuries and review of management, British medical bulletin, 87(1), pp. 77-95.

Biggi, M. and Dyson, S.J., 2018. Use of high-field and low-field magnetic resonance imaging to describe the anatomy of the proximal portion of the tarsal region of nonlame horses, American Journal of Veterinary Research, 79(3), pp. 299-310.

Bolog, N.V., Andreisek, G., Ulbrich, E.J., Bolog, N.V., Andreisek, G. and Ulbrich, E.J., 2015. Articular cartilage and subchondral bone. MRI of the Knee: A Guide to Evaluation and Reporting, pp. 95-112.

Brown, E.T.T., Simons, J.M. and Thambyah, A., 2022. The ultrastructure of cartilage tissue and its swelling response in relation to matrix health. Journal of Anatomy, 240(1), pp. 107-119.

Buckwalter, J.A. and Mankin, H.J., 1997. Articular cartilage: part II. Journal of bone and joint surgery, 79(4), p. 612.

Buschmann, M. D., Soulhat, J., Shirazi-Adl, A., Jurvelin, J. S. and Hunziker, E. B., 1998. Confined Compression of Articular Cartilage: Linearity in Ramp and Sinusoidal Tests and the Importance of interdigitation and Incomplete Confinement, Journal of Biomechanics, 31(2), pp. 171–178.

Campbell-Washburn, A.E., Varghese, J., Nayak, K.S., Ramasawmy, R. and Simonetti, O.P., 2024. Cardiac MRI at low field strengths. Journal of Magnetic Resonance Imaging, 59(2), pp. 412-430.

Chalian, M., Roemer, F.W. and Guermazi, A., 2023. Advances in osteoarthritis imaging. *Current Opinion in Rheumatology*, *35*(1), pp. 44-54.

Chaudhary, R., Campbell, K.R., Tilbury, K.B., Vanderby Jr, R., Block, W.F., Kijowski, R. and Campagnola, P. J., 2015. Articular cartilage zonal differentiation via 3D Second-Harmonic Generation imaging microscopy. Connective tissue research, 56(2), pp. 76-86.

Chen, F.H., Rousche, K.T. and Tuan, R.S., 2006. Technology Insight: adult stem cells in cartilage regeneration and tissue engineering, Nature clinical practice rheumatology, 2(7), pp. 373-382.

Chery, D.R., Han, B., Li, Q., Zhou, Y., Heo, S.J., Kwok, B., Chandrasekaran, P., Wang, C., Qin, L., Lu, X.L. and Kong, D., 2020. Early changes in cartilage pericellular matrix micromechanobiology portend the onset of post-traumatic osteoarthritis. Acta biomaterialia, 111, pp. 267-278.

Chiu, K.W., Hash, J., Meyers, R. and Lascelles, B.D.X., 2020. The effect of spontaneous osteoarthritis on conditioned pain modulation in the canine model, Scientific Reports, 10(1), p. 1694.

Coaccioli, S., Sarzi-Puttini, P., Zis, P., Rinonapoli, G. and Varrassi, G., 2022. Osteoarthritis: new insight on its pathophysiology. *Journal of clinical medicine*, *11*(20), p. 6013.

Cohen, N. P., Foster, R. J. and Mow, V. C., 1998. Composition and Dynamics of Articular Cartilage: Structure , Function , and Maintaining Healthy State, Journal of Orthopadic and Sports Physical Therapy, 28(4), pp. 203–215.

Cotten, A., Delfaut, E., Demondion, X., Lapegue, F., Boukhelifa, M., Boutry, N., Chastanet,P. and Gougeon, F., 2000. MR Imaging of the Knee at 0.2 and 1.5T: Correlation with Surgery, American Journal of Roentgenology, 174, pp. 1093–1097.

Crolla, J.P., Lawless, B.M., Cederlund, A.A., Aspden, R.M. and Espino, D.M., 2022. Analysis of hydration and subchondral bone density on the viscoelastic properties of bovine articular cartilage, BMC Musculoskeletal Disorders, 23(1), p. 228.

Cruz, M.A., Gonzalez, Y., Vélez Toro, J.A., Karimzadeh, M., Rubbo, A., Morris, L., Medam, R., Splawn, T., Archer, M., Fernandes, R.J. and Dennis, J.E., 2023. Micronutrient optimization for tissue engineered articular cartilage production of type II collagen, Frontiers in Bioengineering and Biotechnology, 11, p. 1179332.

Cui, A., Li, H., Wang, D., Zhong, J., Chen, Y. & Lu, H., 2020, 'Global, regional prevalence, incidence and risk factors of knee osteoarthritis in population-based studies', EClinicalMedicine, 29–30, p. 100587.

D'Agostino, V., Sorriento, A., Cafarelli, A., Donati, D., Papalexis, N., Russo, A., Lisignoli, G., Ricotti, L. and Spinnato, P., 2024. Ultrasound imaging in knee osteoarthritis: current role, recent advancements, and future perspectives. *Journal of Clinical Medicine*, *13*(16), p. 4930.

Dai, L., He, Z., Zhang, X., Hu, X., Yuan, L., Qiang, M., Zhu, J., Shao, Z., Zhou, C. and Ao, Y., 2014. One-step repair for cartilage defects in a rabbit model: a technique combining the perforated decalcified cortical-cancellous bone matrix scaffold with microfracture. The American journal of sports medicine, 42(3), pp. 583-591.

Das Neves Borges, P., Vincent, T.L. and Marenzana, M., 2017. Application of autofluorescence robotic histology for quantitative evaluation of the 3-dimensional morphology of murine articular cartilage. Microscopy Research and Technique, 80(12), pp. 1351-1360.

Davidson, R.K., Waters, J.G., Kevorkian, L., Darrah, C., Cooper, A., Donell, S.T. and Clark, I.M., 2006. Expression profiling of metalloproteinases and their inhibitors in synovium and cartilage. Arthritis research & therapy, 8, pp. 1-10.

Del Vecchio, O.V., 2021. Magnetic resonance imaging findings in a cat with cranial cruciate ligament rupture, Veterinary Record Case Reports, 9(3), p. 91.

Demarteau, O., Pillet, L., Inaebnit, A., Borens, O. and Quinn, T.M., 2006. Biomechanical characterization and in vitro mechanical injury of elderly human femoral head cartilage: comparison to adult bovine humeral head cartilage. Osteoarthritis and cartilage, 14(6), pp. 589-596.

DiSilvestro, M.R. and Suh, J.K.F., 2001. A cross-validation of the biphasic poroviscoelastic model of articular cartilage in unconfined compression, indentation, and confined compression, Journal of biomechanics, 34(4), pp. 519-525.

Driban, J.B., Harkey, M.S., Liu, S.H., Salzler, M. and McAlindon, T.E., 2020. Osteoarthritis and aging: young adults with osteoarthritis, Current Epidemiology Reports, 7, pp. 9-15.

Eck, B.L., Yang, M., Elias, J.J., Winalski, C.S., Altahawi, F., Subhas, N. & Li, X., 2023, 'Quantitative MRI for Evaluation of Musculoskeletal Disease', Investigative Radiology, 58(1), pp. 60–75.

Edd, S.N., Omoumi, P., Jolles, B.M. and Favre, J., 2021. Longitudinal femoral cartilage T2 relaxation time and thickness changes with fast sequential radiographic progression of

medial knee osteoarthritis—data from the osteoarthritis initiative (OAI). Journal of Clinical Medicine, 10(6), p. 1294.

Ejbjerg, B. J., Narvestad, E., Jacobsen, S., Thomsen, H. S. and Østergaard, M., 2005. Optimised, Low Cost, Low Field Dedicated Extremity MRI is Highly Specific and Sensitive for Synovitis and Bone Erosions in Rheumatoid Arthritis Wrist and Finger Joints: Comparison with Conventional High Field MRI and Radiography, Annals of the Rheumatic Diseases, 64(9), pp. 1280–1287.

Eliasson, G.J., Bjorgvinsson, E. and Jonsson, H., 2009. Low-Field Magnetic Resonance Imaging of the Thumb Base in Severe Symptomatic Osteoarthritis: A Comparison with Radiographs and Clini-cal Symptoms, The Open Arthritis Journal, 2(1).

Emanuel, K.S., Kellner, L.J., Peters, M.J.M., Haartmans, M.J.J., Hooijmans, M.T. & Emans, P.J., 2022, 'The relation between the biochemical composition of knee articular cartilage and quantitative MRI: a systematic review and meta-analysis', Osteoarthritis and Cartilage, 30(5), pp. 650–662.

Eschweiler, J., Horn, N., Rath, B., Betsch, M., Baroncini, A., Tingart, M. and Migliorini, F., 2021. The biomechanics of cartilage—An overview, Life, 11(4), p. 302.

Esdaille, C.J., Ude, C.C. and Laurencin, C.T., 2022. Regenerative engineering animal models for knee osteoarthritis. Regenerative engineering and translational medicine, 8(2), pp.284-297.

Fagundes, N.C.F., Bittencourt, L.O., Magno, M.B., Marques, M.M., Maia, L.C. and Lima, R.R., 2018. Efficacy of Hank's balanced salt solution compared to other solutions in the preservation of the periodontal ligament. A systematic review and meta-analysis, PLoS One, 13(7), p. 0200467.

Farnham, M.S., Ortved, K.F., Burris, D.L. and Price, C., 2021. Articular cartilage friction, strain, and viability under physiological to pathological benchtop sliding conditions, Cellular and Molecular Bioengineering, 14(4), pp. 349-363.

Fatima, S.A., Ganai, A.A., Jehangir, M., Parry, A.H., Sath, S. and Qayoom, S., 2024. MRI-based cartilage changes and clinical effectiveness of autologous intra-articular platelet-rich plasma injections in symptomatic patients with moderate osteoarthritis of the knee. Egyptian Journal of Radiology and Nuclear Medicine, 55(1), p. 30.

Fernihough, J., Gentry, C., Malcangio, M., Fox, A., Rediske, J., Pellas, T., Kidd, B., Bevan, S. and Winter, J., 2004. Pain related behaviour in two models of osteoarthritis in the rat knee, Pain, 112(1-2), pp. 83-93.

Fisher, M., Ackley, T., Richard, K., Oei, B. & Dealy, C.N., 2019, Osteoarthritis at the cellular level: Mechanisms, clinical perspectives, and insights from development, Encyclopedia of Biomedical Engineering, vols 1–3, pp. 660–676, Elsevier.

Foo, C.N., Manohar, A., Rampal, L., Lye, M.S., Mohd-Sidik, S. and Osman, Z.J., 2017. Knee Pain and Functional Disability of Knee Osteoarthritis Patients Seen at Malaysian Government Hospitals. *Malaysian Journal of Medicine & Health Sciences*, *13*(2).

French, D. and Vigne, S., 2019. The causes and consequences of household financial strain: A systematic review. *International Review of Financial Analysis*, *62*, pp.150-156.

Gahunia, H.K. and Pritzker, K.P., 2020. Structure and function of articular cartilage, Articular Cartilage of the Knee: Health, Disease and Therapy, pp. 3-70.

Gandy, J.R., Foulad, A., Chao, K.K. and Wong, B.J.F., 2017. Injectable chondroplasty: Enzymatic reshaping of cartilage grafts, European Annals of Otorhinolaryngology, Head and Neck Diseases, 134(4), pp. 217-220.

Gao, L.L., Zhang, C.Q., Gao, H., Liu, Z.D. and Xiao, P. P., 2014. Depth and rate dependent mechanical behaviors for articular cartilage: experiments and theoretical predictions, Materials Science and Engineering: C, 38, pp. 244-251.

Gao, T., Boys, A.J., Zhao, C., Chan, K., Estroff, L.A. and Bonassar, L.J., 2021. Non-destructive spatial mapping of glycosaminoglycan loss in native and degraded articular cartilage using confocal raman microspectroscopy, Frontiers in Bioengineering and Biotechnology, 9, p. 744197.

Gao, J., Ren, P. and Gong, H., 2023. Morphological and mechanical alterations in articular cartilage and subchondral bone during spontaneous hip osteoarthritis in guinea pigs, Frontiers in Bioengineering and Biotechnology, 11, p. 1080241.

Gao, L.L., Wei, Y., Tan, Y.S., Li, R.X., Zhang, C.Q. and Gao, H., 2023. Irrigating degradation properties of silk fibroin–collagen type II composite cartilage scaffold in vitro and in vivo. Biomaterials Advances, 149, p. 213389.

Ghazinoor, S. and Crues, J.V., 2006. Low field MRI: a review of the literature and our experience in upper extremity imaging, Clinics in sports medicine, 25(3), pp. 591-606.

Ghazinoor, S., Crues III, J.V. and Crowley, C., 2007. Low-field musculoskeletal MRI, Journal of Magnetic Resonance Imaging: An Official Journal of the International Society for Magnetic Resonance in Medicine, 25(2), pp. 234-244.

Gilbert, S.J. and Blain, E.J., 2018. Cartilage mechanobiology: How chondrocytes respond to mechanical load, In Mechanobiology in health and disease pp. 99-126. Academic Press.

Glyn-Jones, S. and Palmer, A.J., 2015. Agricola, R.; Price, AJ; Vincent, TL; Weinans, H.; Carr, AJ Osteoarthritis. Lancet, 386(9991), pp. 376-387.

Goldring, S.R. and Goldring, M.B., 2016. Changes in the osteochondral unit during osteoarthritis: structure, function and cartilage–bone crosstalk. Nature Reviews Rheumatology, 12(11), pp. 632-644.

Gottardi, R., Hansen, U., Raiteri, R., Loparic, M., Düggelin, M., Mathys, D., Friederich, N.F., Bruckner, P. and Stolz, M., 2016. Supramolecular organization of collagen fibrils in healthy and osteoarthritic human knee and hip joint cartilage. PloS one, 11(10), p. 0163552.

Grenier, S., Bhargava, M.M. and Torzilli, P. A., 2014. An in vitro model for the pathological degradation of articular cartilage in osteoarthritis, Journal of biomechanics, 47(3), pp. 645-652.

Gudbergsen, H., Boesen, M., Christensen, R., Astrup, A. and Bliddal, H., 2011. Radiographs and low field MRI (0.2 T) as predictors of efficacy in a weight loss trial in obese women with knee osteoarthritis. BMC musculoskeletal disorders, 12, pp. 1-7.

Guo, L., Li, P., Rong, X. and Wei, X., 2024. Key roles of the superficial zone in articular cartilage physiology, pathology, and regeneration, Chinese Medical Journal, pp. 10-1097.

Guzman, R.E., Evans, M.G., Bove, S., Morenko, B. and Kilgore, K., 2003. Mono-iodoacetate-induced histologic changes in subchondral bone and articular cartilage of rat femorotibial joints: an animal model of osteoarthritis, Toxicologic pathology, 31(6), pp. 619-624.

Hafner, T., Post, M., Said, O., Schad, P., Schock, J., Abrar, D.B., Knobe, M., Kuhl, C., Truhn, D. and Nebelung, S., 2020. Identifying the imaging correlates of cartilage functionality based on quantitative MRI mapping-the collagenase exposure model. Acta Biomaterialia, 117, pp. 310-321.

Hall, A.C., 2019. The role of chondrocyte morphology and volume in controlling phenotype—implications for osteoarthritis, cartilage repair, and cartilage engineering, Current Rheumatology Reports, 21, pp. 1-13.

Hani, A. F. M., Kumar, D., Malik, A. S., Ahmad, R. M. K. R., Razak, R. and Kiflie, A., 2015. Non-Invasive and In Vivo Assessment of Osteoarthritic Articular Cartilage: A Review on MRI Investigations, Rheumatology International, 35(1), pp. 1–16.

Hänninen, N.E., Nykänen, O., Prakash, M., Hanni, M., Nieminen, M.T. and Nissi, M.J., 2021. Orientation anisotropy of quantitative MRI parameters in degenerated human articular cartilage. Journal of Orthopaedic Research®, 39(4), pp. 861-870.

Hashim, N.H., Latif, M.J.A., Jaafar, Y.L., Ramlan, R. and Mahmud, J., 2017. Computational and experimental study of articular cartilage thickness on biomechanical behavior, Int J Appl Eng Res, 12(16), pp. 5849-5856.

Hayashi, N., Watanabe, Y., Masumoto, T., Mori, H., Aoki, S., Ohtomo, K., Okitsu, O. and Takahashi, T., 2004. Utilization of Low-Field MR Scanners, Magnetic Resonance in Medical Sciences, 3(1), pp. 27–38.

Hayashi, D., Roemer, F.W. & Guermazi, A., 2016, Imaging for osteoarthritis, Annals of Physical and Rehabilitation Medicine, 59(3), pp. 161–169.

Hayes, W.C., Keer, L.M., Herrmann, G. and Mockros, L.F., 1972. A mathematical analysis for indentation tests of articular cartilage, Journal of biomechanics, 5(5), pp. 541-551.

He, Y., Li, Z., Alexander, P.G., Ocasio-Nieves, B.D., Yocum, L., Lin, H. and Tuan, R.S., 2020. Pathogenesis of osteoarthritis: risk factors, regulatory pathways in chondrocytes, and experimental models. *Biology*, *9*(8), p. 194.

Higuchi, Y., Nishida, Y., Kozawa, E., Zhuo, L., Arai, E., Hamada, S., Morita, D., Ikuta, K., Kimata, K., Ushida, T. and Ishiguro, N., 2017. Conditional knockdown of hyaluronidase 2 in articular cartilage stimulates osteoarthritic progression in a mice model, Scientific reports, 7(1), p. 7028.

Hollander, A.P., Heathfield, T.F., Webber, C., Iwata, Y., Bourne, R., Rorabeck, C. and Poole, A.R., 1994. Increased damage to type II collagen in osteoarthritic articular cartilage

detected by a new immunoassay, The Journal of clinical investigation, 93(4), pp. 1722-1732.

Horkay, F., Basser, P.J. and Geissler, E., 2024. Cartilage extracellular matrix polymers: hierarchical structure, osmotic properties, and function. Soft Matter, 20(30), pp. 6033-6043.

Ibramsa, R.S., Abd Latif, M.J., Zakaria, M.S., Harun, M.N. and Mahmud, J., 2022. Quantitative study of articular cartilage based on greyscale assessment using low-field MRI, Int J Adv Sci Eng Inform Technol, 12(1), p. 231.

Ingale, Y.A., Kadam, A.P. and Bhosale, D.G., 2016. Comparative study of steel, nylon 66 and delrin helical gears used in steering gearbox, Int J Res Eng Technol, 5(06).

Jabłońska-Trypuć, A., Matejczyk, M. and Rosochacki, S., 2016. Matrix metalloproteinases (MMPs), the main extracellular matrix (ECM) enzymes in collagen degradation, as a target for anticancer drugs. Journal of enzyme inhibition and medicinal chemistry, 31(sup1), pp. 177-183.

Jayadev, R., Chi, Q., Keeley, D.P., Hastie, E.L., Kelley, L.C. and Sherwood, D.R., 2019. α-Integrins dictate distinct modes of type IV collagen recruitment to basement membranes, Journal of Cell Biology, 218(9), pp. 3098-3116.

Jerban, S., Kasibhatla, A., Ma, Y., Wu, M., Chen, Y., Guo, T., Wan, L., Szeverenyi, N., Chang, E.Y. and Du, J., 2021. Detecting articular cartilage and meniscus deformation effects using magnetization transfer ultrashort echo time (MT-UTE) modeling during mechanical load application: ex vivo feasibility study. Cartilage, 13(1_suppl), pp. 665-673.

Jin, H. and Lewis, J. L., 2004. Determination of Poisson's Ratio of Articular Cartilage by Indentation Using Different-Sized Indenters, Journal of Biomechanical Engineering, 126(2), pp. 138–145.

June, R.K. and Fyhrie, D.P., 2010. Temperature effects in articular cartilage biomechanics, Journal of Experimental Biology, 213(22), pp. 3934-3940.

Jurvelin, J. S., Buschmann, M. D. and Hunziker, E. B., 2003. Mechanical Anisotropy of the Human Knee Articular Cartilage in Compression, Proceedings of the Institution of Mechanical Engineers, Part H: Journal of Engineering in Medicine, 217(3), pp. 215–219.

Kabir, W., Di Bella, C., Choong, P. F. and O'Connell, C.D., 2021. Assessment of native human articular cartilage: a biomechanical protocol, Cartilage, 13(2_suppl), pp. 427-437.

Kafian-Attari, I., Nippolainen, E., Bergmann, F., George, A., Paakkari, P., Mirhashemi, A., Foschum, F., Kienle, A., Töyräs, J. and Afara, I.O., 2023. Broadband scattering properties of articular cartilage zones and their relationship with the heterogenous structure of articular cartilage extracellular matrix, Journal of biomedical optics, 28(12), pp. 125003-125003.

Kar, S., Smith, D.W., Gardiner, B.S., Li, Y., Wang, Y. and Grodzinsky, A.J., 2016. Modeling IL-1 induced degradation of articular cartilage, Archives of biochemistry and biophysics, 594, pp. 37-53.

Kheir, E., Stapleton, T., Shaw, D., Jin, Z., Fisher, J. and Ingham, E., 2011. Development and characterization of an acellular porcine cartilage bone matrix for use in tissue engineering, Journal of biomedical materials research Part A, 99(2), pp. 283-294.

Kilmer, C.E., Battistoni, C.M., Cox, A., Breur, G.J., Panitch, A. and Liu, J.C., 2020. Collagen type I and II blend hydrogel with autologous mesenchymal stem cells as a scaffold for articular cartilage defect repair, ACS biomaterials science & engineering, 6(6), pp. 3464-3476.

Kim, J.E., Song, D.H., Kim, S.H., Jung, Y. and Kim, S.J., 2018. Development and characterization of various osteoarthritis models for tissue engineering, PLoS One, 13(3), p. 0194288.

Kirillova, A.D., Nemets, E.A., Grigoriev, A.M., Kirsanova, L.A., Ryzhikova, V.A., Volkova, E.A., Basok, Yu.B. & Sevastianov, V.I., 2023, Effect of trypsin on biochemical and functional properties of decellularized porcine articular cartilage, Russian Journal of Transplantology and Artificial Organs, 25(3), pp. 76–86.

Kleemann, R.U., Krocker, D., Cedraro, A., Tuischer, J. and Duda, G.N., 2005. Altered cartilage mechanics and histology in knee osteoarthritis: relation to clinical assessment (ICRS Grade). Osteoarthritis and cartilage, 13(11), pp. 958-963.

Knudson, W., Ishizuka, S., Terabe, K., Askew, E.B. and Knudson, C.B., 2019. The pericellular hyaluronan of articular chondrocytes, Matrix Biology, 78, pp. 32-46.

Korhonen, R. K., Laasanen, M. S., Töyräs, J., Rieppo, J., Hirvonen, J., Helminen, H. J. and Jurvelin, J. S., 2002. Comparison of the Equilibrium Response of Articular Cartilage in Unconfined Compression, Confined Compression and Indentation, Journal of Biomechanics, 35(7), pp. 903–909.

Kosinska, M.K., Ludwig, T.E., Liebisch, G., Zhang, R., Siebert, H.C., Wilhelm, J., Kaesser, U., Dettmeyer, R.B., Klein, H., Ishaque, B. and Rickert, M., 2015. Articular joint lubricants during osteoarthritis and rheumatoid arthritis display altered levels and molecular species, PloS one, 10(5), p. 0125192.

Kosonen, J.P., Eskelinen, A.S., Orozco, G.A., Nieminen, P., Anderson, D.D., Grodzinsky, A.J., Korhonen, R.K. and Tanska, P., 2023. Injury-related cell death and proteoglycan loss in articular cartilage: Numerical model combining necrosis, reactive oxygen species, and inflammatory cytokines. *PLoS computational biology*, *19*(1), p. 1010337.

Krakowski, P., Rejniak, A., Sobczyk, J. and Karpiński, R., 2024, August. Cartilage integrity: A review of mechanical and frictional properties and repair approaches in osteoarthritis. In Healthcare (Vol. 12, No. 16, p. 1648). MDPI.

Kung, M.S., Markantonis, J., Nelson, S.D. and Campbell, P., 2015. The synovial lining and synovial fluid properties after joint arthroplasty, Lubricants, 3(2), pp. 394-412.

Kuş, G., Yasaci, Z., Boz, C. & Türkmen, E., 2023, 'Association of Osteoarthritis Prevalence with Age and Obesity Factors in OECD Countries: Panel Regression Model', American Journal of Physical Medicine & Rehabilitation.

Kuyinu, E.L., Narayanan, G., Nair, L.S. and Laurencin, C.T., 2016. Animal models of osteoarthritis: classification, update, and measurement of outcomes, Journal of orthopaedic surgery and research, 11, pp. 1-27.

Laasanen, M.S., Töyräs, J., Hirvonen, J., Saarakkala, S., Korhonen, R.K., Nieminen, M.T., Kiviranta, I. and Jurvelin, J.S., 2002. Novel mechano-acoustic technique and instrument for diagnosis of cartilage degeneration, Physiological measurement, 23(3), p. 491.

Lampropoulou-Adamidou, K., Lelovas, P., Karadimas, E.V., Liakou, C., Triantafillopoulos, I.K., Dontas, I. and Papaioannou, N.A., 2014. Useful animal models for the research of osteoarthritis, European Journal of Orthopaedic Surgery & Traumatology, 24, pp. 263-271.

Laronha, H. and Caldeira, J., 2020. Structure and function of human matrix metalloproteinases, Cells, 9(5), p. 1076.

Lee, J.H. and Xia, Y., 2013. Quantitative zonal differentiation of articular cartilage by microscopic magnetic resonance imaging, polarized light microscopy, and Fourier-transform infrared imaging, Microscopy research and technique, 76(6), pp. 625-632.

Leifer, V.P., Katz, J.N. & Losina, E., 2022, 'The burden of OA-health services and economics', Osteoarthritis and Cartilage, 30(1), pp. 10–16.

Li, X., Roemer, F.W., Cicuttini, F., MacKay, J.W., Turmezei, T. and Link, T.M., 2023. Early knee OA definition–what do we know at this stage? An imaging perspective. *Therapeutic Advances in Musculoskeletal Disease*, *15*, p. 1759720X231158204.

Lian, Q., Chen, C., Uwayezu, M.C., Zhang, W., Bian, W., Wang, J. and Jin, Z., 2015. Biphasic mechanical properties of in vivo repaired cartilage, Journal of Bionic Engineering, 12(3), pp. 473-482.

Lian, C., Wang, X., Qiu, X., Wu, Z., Gao, B., Liu, L., Liang, G., Zhou, H., Yang, X., Peng, Y. and Liang, A., 2019. Collagen type II suppresses articular chondrocyte hypertrophy and osteoarthritis progression by promoting integrin β1− SMAD1 interaction. Bone research, 7(1), p. 8.

Lim, R., Martin, T.L., Chae, J., Kim, W.J., Ghim, C.M. and Kim, P. J., 2023. Generalized Michaelis–Menten rate law with time-varying molecular concentrations, PLoS Computational Biology, 19(12), p. 1011711.

Lin, T.S., Hsieh, C.H., Kuo, C., Juang, Y.P., Hsieh, Y.S., Chiang, H., Hung, S.C., Jiang, C.C. and Liang, P. H., 2020. Sulfation pattern of chondroitin sulfate in human osteoarthritis cartilages reveals a lower level of chondroitin-4-sulfate, Carbohydrate Polymers, 229, p. 115496.

Lin, W. and Klein, J., 2021. Recent progress in cartilage lubrication, Advanced Materials, 33(18), p. 2005513.

Linus, A., Tanska, P., Nippolainen, E., Tiitu, V., Töyras, J., Korhonen, R.K., Afara, I.O. and Mononen, M.E., 2024. Site-specific elastic and viscoelastic biomechanical properties of healthy and osteoarthritic human knee joint articular cartilage. Journal of Biomechanics, 169, p. 112135.

Liphardt, A.M., Godonou, E.T., Dreiner, M., Mündermann, A., Tascilar, K., Djalal, N., Heer, M., Schett, G., Zaucke, F. and Niehoff, A., 2024. Immobilization by 21 days of bed rest results in type II collagen degradation in healthy individuals. Osteoarthritis and Cartilage, 32(2), pp. 177-186.

Liu, F., Zhou, Z., Samsonov, A., Blankenbaker, D., Larison, W., Kanarek, A., Lian, K., Kambhampati, S. and Kijowski, R., 2018. Deep learning approach for evaluating knee MR images: achieving high diagnostic performance for cartilage lesion detection. Radiology, 289(1), pp. 160-169.

Liu, Q. and Wang, J., 2020. Quantifying the flux as the driving force for nonequilibrium dynamics and thermodynamics in non-Michaelis–Menten enzyme kinetics, Proceedings of the National Academy of Sciences, 117(2), pp. 923-930.

Loeser, R.F., Goldring, S.R., Scanzello, C.R. and Goldring, M.B., 2012. Osteoarthritis: a disease of the joint as an organ, Arthritis and rheumatism, 64(6), p. 1697.

Lotz, M., Martel-Pelletier, J., Christiansen, C., Brandi, M.L., Bruyère, O., Chapurlat, R., Collette, J., Cooper, C., Giacovelli, G., Kanis, J.A., Karsdal, M.A., Kraus, V., Lems, W.F., Meulenbelt, I., Pelletier, J.P., Raynauld, J.P., Reiter-Niesert, S., Rizzoli, R., Sandell, L.J., Spil, W.E. Van & Reginster, J.Y., 2013, Value of biomarkers in osteoarthritis: Current status and perspectives, Annals of the Rheumatic Diseases, 72(11), pp. 1756–1763.

Lu, X.L. and Mow, V.C., 2008. Biomechanics of articular cartilage and determination of material properties, Medicine & Science in Sports & Exercise, 40(2), pp. 193-199.

Lui, P. P. Y., Chan, L.S., Lee, Y.W., Fu, S.C. and Chan, K.M., 2010. Sustained expression of proteoglycans and collagen type III/type I ratio in a calcified tendinopathy model, Rheumatology, 49(2), pp. 231-239.

Malda, J., Benders, K.E.M., Klein, T.J., De Grauw, J.C., Kik, M.J.L., Hutmacher, D.W., Saris, D.B.F., Van Weeren, P. R. and Dhert, W.J.A., 2012. Comparative study of depth-dependent characteristics of equine and human osteochondral tissue from the medial and lateral femoral condyles, Osteoarthritis and cartilage, 20(10), pp. 1147-1151.

Mansfield, J.C., Bell, J.S. and Winlove, C.P., 2015. The micromechanics of the superficial zone of articular cartilage. Osteoarthritis and cartilage, 23(10), pp. 1806-1816.

Marian, M., Shah, R., Gashi, B., Zhang, S., Bhavnani, K., Wartzack, S. and Rosenkranz, A., 2021. Exploring the lubrication mechanisms of synovial fluids for joint longevity–a perspective, Colloids and Surfaces B: Biointerfaces, 206, p. 111926.

Marks, R., 2014. Osteoarthritis and Articular Cartilage: Biomechanics and Novel Treatment Paradigms, Advances in Aging Research, 03(04), pp. 297–309.

Mat, S., Jaafar, M.H., Ng, C.T., Sockalingam, S., Raja, J., Kamaruzzaman, S.B., Chin, A.V., Abbas, A.A., Chan, C.K., Hairi, N.N. and Othman, S., 2019. Ethnic differences in the prevalence, socioeconomic and health related risk factors of knee pain and osteoarthritis symptoms in older Malaysians. *PloS one*, *14*(11), p. 0225075.

Mellors, B., Allen, P., Lavecchia, C.E., Mountcastle, S., Cooke, M.E., Lawless, B.M., Cox, S.C., Jones, S. and Espino, D.M., 2023. Development and experimental validation of a dynamic numerical model for human articular cartilage, Proceedings of the Institution of Mechanical Engineers, Part H: Journal of Engineering in Medicine, 237(7), pp. 879-889.

Mern, D.S., Walsen, T., Beierfuß, A. and Thomé, C., 2021. Animal models of regenerative medicine for biological treatment approaches of degenerative disc diseases. Experimental Biology and Medicine, 246(4), pp. 483-512.

Mixon, A., Savage, A., Bahar-Moni, A.S., Adouni, M. and Faisal, T., 2021. An in vitro investigation to understand the synergistic role of MMPs-1 and 9 on articular cartilage biomechanical properties, Scientific reports, 11(1), p. 14409.

Mohammadi, H., Mequanint, K. and Herzog, W., 2013. Computational aspects in mechanical modeling of the articular cartilage tissue. Proceedings of the Institution of Mechanical Engineers, Part H: Journal of Engineering in Medicine, 227(4), pp. 402-420.

Mow, V.C., Kuei, S.C., Lai, W.M. and Armstrong, C.G., 1980. Biphasic creep and stress relaxation of articular cartilage in compression: theory and experiments.

Nahar, S., Nakashima, Y., Miyagi-Shiohira, C., Kinjo, T., Kobayashi, N., Saitoh, I., Watanabe, M., Noguchi, H. and Fujita, J., 2018. A Comparison of the Preservation of Mouse Adipose Tissue-Derived Mesenchymal Stem Cells Using the University of Wisconsin Solution and Hank's Balanced Salt Solution, Stem cells international, 2018(1), p. 1625464.

Nakagomi, M., Kajiwara, M., Matsuzaki, J., Tanabe, K., Hoshiai, S., Okamoto, Y. and Terada, Y., 2019. Development of a small car-mounted magnetic resonance imaging system for human elbows using a 0.2 T permanent magnet, Journal of Magnetic Resonance, 304, pp. 1-6.

Namiranian, B., Jerban, S., Ma, Y., Dorthe, E.W., Masoud-Afsahi, A., Wong, J., Wei, Z., Chen, Y., D'Lima, D., Chang, E.Y. & Du, J., 2020, 'Assessment of mechanical properties of articular cartilage with quantitative three-dimensional ultrashort echo time (UTE) cones magnetic resonance imaging', Journal of Biomechanics, 113, p. 110085.

Nawaz, M., Shah, N., Zanetti, B.R., Maugeri, M., Silvestre, R.N., Fatima, F., Neder, L. and Valadi, H., 2018. Extracellular vesicles and matrix remodeling enzymes: the emerging roles in extracellular matrix remodeling, progression of diseases and tissue repair. Cells, 7(10), p. 167.

Nissi, M. J., Rieppo, J., Töyräs, J., Laasanen, M. S., Kiviranta, I., Nieminen, M. T. and Jurvelin, J. S., 2007, Estimation of Mechanical Properties of Articular Cartilage with MRI – dGEMRIC, T2 and T1 Imaging in Different Species with Variable Stages of Maturation, Osteoarthritis and Cartilage, 15(10), pp. 1141–1148.

Nomura, M., Sakitani, N., Iwasawa, H., Kohara, Y., Takano, S., Wakimoto, Y., Kuroki, H. and Moriyama, H., 2017. Thinning of articular cartilage after joint unloading or immobilization. An experimental investigation of the pathogenesis in mice. Osteoarthritis and cartilage, 25(5), pp. 727-736.

Oláh, T., Reinhard, J., Gao, L., Haberkamp, S., Goebel, L.K., Cucchiarini, M. and Madry, H., 2019. Topographic modeling of early human osteoarthritis in sheep, Science Translational Medicine, 11(508), p. 6775.

Olivotto, E., Otero, M., Marcu, K.B. and Goldring, M.B., 2015. Pathophysiology of osteoarthritis: canonical NF-κB/IKKβ-dependent and kinase-independent effects of IKKα in cartilage degradation and chondrocyte differentiation. RMD open, 1(Suppl 1), p.000061.

O'Neill, T.W. and Felson, D.T., 2018. Mechanisms of osteoarthritis (OA) pain. *Current osteoporosis reports*, *16*, pp. 611-616.

Orhan, C., Juturu, V., Sahin, E., Tuzcu, M., Ozercan, I.H., Durmus, A.S., Sahin, N. and Sahin, K., 2021. Undenatured type II collagen ameliorates inflammatory responses and articular cartilage damage in the rat model of osteoarthritis. Frontiers in veterinary science, 8, p. 617789.

Oseni, A.O., Butler, P. E. and Seifalian, A.M., 2013. Optimization of chondrocyte isolation and characterization for large-scale cartilage tissue engineering, journal of surgical research, 181(1), pp. 41-48.

Ouyang, Z., Dong, L., Yao, F., Wang, K., Chen, Y., Li, S., Zhou, R., Zhao, Y. & Hu, W., 2023, Cartilage-Related Collagens in Osteoarthritis and Rheumatoid Arthritis: From Pathogenesis to Therapeutics, International Journal of Molecular Sciences, 24(12), p. 9841.

Park, H.J., Chang, M.J., Kim, T.W., Chang, C.B., Kang, K.S. and Kang, S.B., 2022. Subchondral bone condition and intraoperative grading of cartilage degeneration underneath patella unrelated to the clinical outcome after TKA with unresurfaced patella. *The Journal of Knee Surgery*, *35*(13), pp. 1417-1424.

Pap, T., Dankbar, B., Wehmeyer, C., Korb-Pap, A. and Sherwood, J., 2020, May. Synovial fibroblasts and articular tissue remodelling: role and mechanisms, In Seminars in cell & developmental biology (Vol. 101, pp. 140-145). Academic Press.

Pauly, H.M., Larson, B.E., Coatney, G.A., Button, K.D., DeCamp, C.E., Fajardo, R.S., Haut, R.C. and Haut Donahue, T.L., 2015. Assessment of cortical and trabecular bone changes in two models of post-traumatic osteoarthritis, Journal of orthopaedic research, 33(12), pp. 1835-1845.

Paunipagar, B.K. and Rasalkar, D.D., 2014. Imaging of articular cartilage, Indian Journal of Radiology and Imaging, 24(03), pp. 237-248.

Pawaskar, S.S., Fisher, J. and Jin, Z., 2010. Robust and general method for determining surface fluid flow boundary conditions in articular cartilage contact mechanics modeling, Journal of Biomechanical Engineering, 132(3), p. 031001.

Pearle, A.D., Warren, R.F. and Rodeo, S.A., 2005. Basic science of articular cartilage and osteoarthritis, Clinics in sports medicine, 24(1), pp. 1-12.

Petitjean, N., Canadas, P., Royer, P., Noël, D. and Le Floc'h, S., 2023. Cartilage biomechanics: From the basic facts to the challenges of tissue engineering, Journal of Biomedical Materials Research Part A, 111(7), pp. 1067-1089.

Pierce, D.M., Ricken, T. and Holzapfel, G.A., 2013. A hyperelastic biphasic fibre-reinforced model of articular cartilage considering distributed collagen fibre orientations: continuum basis, computational aspects and applications, Computer methods in biomechanics and biomedical engineering, 16(12), pp. 1344-1361.

Pitcher, T., Sousa-Valente, J. and Malcangio, M., 2016. The monoiodoacetate model of osteoarthritis pain in the mouse, Journal of visualized experiments: JoVE, (111), p. 53746.

Pogarell, T., Heiss, R., Janka, R., Nagel, A.M., Uder, M. and Roemer, F.W., 2024. Modern low-field MRI. Skeletal radiology, 53(9), pp. 1751-1760.

Popov, V.L., Poliakov, A.M. and Pakhaliuk, V.I., 2021. Synovial joints. Tribology, regeneration, regenerative rehabilitation and arthroplasty, Lubricants, 9(2), p. 15.

Puiggalí-Jou, A., Rizzo, R., Bonato, A., Fisch, P., Ponta, S., Weber, D.M. and Zenobi-Wong, M., 2024. Flight biofabrication supports maturation of articular cartilage with anisotropic properties, Advanced Healthcare Materials, 13(12), p. 2302179.

Rangchian, A., Francone, A., Farajzadeh, M., Hosseini, H., Connelly, K., Hubschman, J.P. and Kavehpour, H.P., 2019. Effects of collagenase type ii on vitreous humor—an in situ rheological study, Journal of biomechanical engineering, 141(8), p. 081007.

Redondo, M.L., Christian, D.R. and Yanke, A.B., 2019. The role of synovium and synovial fluid in joint hemostasis, Joint Preservation of the Knee: A Clinical Casebook, pp. 57-67.

Riel, K. A., Reinisch, M., Kersting-Sommerhoff, B., Hof, N. and Merl, T., 1999. 0.2-Tesla Magnetic Resonance Imaging of Internal Lesions of the Knee Joint : a Prospective Arthroscopically Controlled Clinical Study, Knee Surgery, Sports Traumatology, Arthroscopy, 7, pp. 37–41.

Rieppo, J., Töyräs, J., Nieminen, M.T., Kovanen, V., Hyttinen, M.M., Korhonen, R.K., Jurvelin, J.S. and Helminen, H.J., 2003. Structure-function relationships in enzymatically modified articular cartilage, Cells Tissues Organs, 175(3), pp. 121-132.

Roemer, F.W., Eckstein, F., Hayashi, D. and Guermazi, A., 2014. The role of imaging in osteoarthritis, Best practice & research Clinical rheumatology, 28(1), pp. 31-60.

Roseti, L., Desando, G., Cavallo, C., Petretta, M. and Grigolo, B., 2019. Articular cartilage regeneration in osteoarthritis. Cells, 8(11), p. 1305.

Roškar, S. and Hafner-Bratkovič, I., 2022. The role of inflammasomes in osteoarthritis and secondary joint degeneration diseases, Life, 12(5), p. 731.

Sadeghi, H., Espino, D.M. & Shepherd, D.E., 2015. Variation in viscoelastic properties of bovine articular cartilage below, up to and above healthy gait-relevant loading frequencies, Proceedings of the Institution of Mechanical Engineers, Part H: Journal of Engineering in Medicine, 229(2), pp. 115-123.

Safa, B.N., Meadows, K.D., Szczesny, S.E. and Elliott, D.M., 2017. Exposure to buffer solution alters tendon hydration and mechanics, Journal of biomechanics, 61, pp. 18-25.

Sahin, K., Kucuk, O., Orhan, C., Tuzcu, M., Durmus, A.S., Ozercan, I.H., Sahin, N. and Juturu, V., 2021. Niacinamide and undenatured type II collagen modulates the inflammatory response in rats with monoiodoacetate-induced osteoarthritis. Scientific reports, 11(1), p. 14724.

Sajjadinia, S.S., Haghpanahi, M. and Razi, M., 2019. Computational simulation of the multiphasic degeneration of the bone-cartilage unit during osteoarthritis via indentation and unconfined compression tests, Proceedings of the Institution of Mechanical Engineers, Part H: Journal of Engineering in Medicine, 233(9), pp. 871-882.

Salehuddin, S.S., Latif, M.J.A., Zakaria, M.S., Harun, M.N. and Sha'ban, M., 2024, December. Alteration of Biomechanical Properties in Early-Stage Osteoarthritis: A Study on Elastic Modulus and Permeability of Articular Cartilage. In International Conference on Biomedical Engineering pp. 69-78. Cham: Springer Nature Switzerland.

Sarkar, S.K., Marmer, B., Goldberg, G. and Neuman, K.C., 2012. Single-molecule tracking of collagenase on native type I collagen fibrils reveals degradation mechanism, Current Biology, 22(12), pp. 1047-1056.

Satish, L., Krill-Burger, J.M., Gallo, P. H., Etages, S.D., Liu, F., Philips, B.J., Ravuri, S., Marra, K.G., LaFramboise, W.A., Kathju, S. and Rubin, J.P., 2015. Expression analysis of human adipose-derived stem cells during in vitro differentiation to an adipocyte lineage, BMC Medical Genomics, 8, pp. 1-12.

Schmaranzer, F., Afacan, O., Lerch, T.D., Kim, Y.J., Siebenrock, K.A., Ith, M., Cullmann, J.L., Kober, T., Klarhoefer, M., Tannast, M. and Bixby, S.D., 2021. Magnetization-prepared 2 rapid gradient-echo MRI for B1 insensitive 3D T1 mapping of hip cartilage: an experimental and clinical validation, Radiology, 299(1), pp. 150-158.

Schmidt, U.S., Koch, L., Rentschler, C., Kurz, T., Endreß, H.U. and Schuchmann, H.P., 2015. Effect of molecular weight reduction, acetylation and esterification on the emulsification properties of citrus pectin, Food biophysics, 10, pp. 217-227.

Schmidt, S., 2021. Cartilage Tissue Engineering–Comparison of Articular Cartilage Progenitor Cells and Mesenchymal Stromal Cells in Agarose and Hyaluronic Acid-Based Hydrogels (Doctoral dissertation, Universität Würzburg).

Schmidt, I.L., Haag, N., Shahzadi, I., Frohwein, L.J., Schneider, C., Niehoff, J.H., Kroeger, J.R., Borggrefe, J. and Moenninghoff, C., 2023. Diagnostic image quality of a low-field (0.55 T) knee MRI protocol using deep learning image reconstruction compared with a standard (1.5 T) knee MRI protocol. Journal of clinical medicine, 12(5), p.1916.

Schober, P., Boer, C. & Schwarte, L.A., 2018, Correlation Coefficients: Appropriate Use and Interpretation, Anesthesia & Analgesia, 126(5), pp. 1763–1768.

Schrauth, J.H., Lykowsky, G., Hemberger, K., Kreutner, J., Weber, D., Rackwitz, L., Nöth, U., Jakob, P. M. and Haddad, D., 2016. Comparison of multiple quantitative MRI parameters for characterization of the goat cartilage in an ongoing osteoarthritis: DGEMRIC, T1ρ and sodium, Zeitschrift für Medizinische Physik, 26(3), pp. 270-282.

Shajib, M.S., Futrega, K., Jacob Klein, T., Crawford, R.W. and Doran, M.R., 2022. Collagenase treatment appears to improve cartilage tissue integration but damage to collagen networks is likely permanent, Journal of Tissue Engineering, 13, p. 20417314221074207.

Siddaiah, A. and Menezes, P. L., 2016. Advances in bio-inspired tribology for engineering applications, Journal of bio-and tribo-corrosion, 2, pp. 1-19.

Sidharthan, S., Yau, A., Almeida, B.A., Shea, K.G., Greditzer IV, H.G., Jones, K.J. and Fabricant, P.D., 2021. Patterns of articular cartilage thickness in pediatric and adolescent

knees: a magnetic resonance imaging–based study. *Arthroscopy, Sports Medicine, and Rehabilitation*, *3*(2), pp.381-390.

Siebelt, M., Groen, H.C., Koelewijn, S.J., de Blois, E., Sandker, M., Waarsing, J.H., Müller, C., van Osch, G.J., De Jong, M. and Weinans, H., 2014. Increased physical activity severely induces osteoarthritic changes in knee joints with papain induced sulfate-glycosaminoglycan depleted cartilage. Arthritis research & therapy, 16, pp. 1-12.

Sophia Fox, A.J., Bedi, A. and Rodeo, S.A., 2009. The basic science of articular cartilage: structure, composition, and function, Sports health, 1(6), pp. 461-468.

Steinmetz, J.D., Culbreth, G.T., Haile, L.M., Rafferty, Q., Lo, J., Fukutaki, K.G., Cruz, J.A., Smith, A.E., Vollset, S.E., Brooks, P.M., Cross, M., Woolf, A.D., Hagins, H., Abbasi-Kangevari, M., Abedi, A., Ackerman, I.N., Amu, H., Antony, B., Arabloo, J., Aravkin, A.Y., Argaw, A.M., Artamonov, A.A., Ashraf, T., Barrow, A., Bearne, L.M., Bensenor, I.M., Berhie, A.Y., Bhardwaj, N., Bhardwaj, P., Bhojaraja, V.S., Bijani, A., Briant, P.S., Briggs, A.M., Butt, N.S., Charan, J., Chattu, V.K., Cicuttini, F.M., Coberly, K., Dadras, O., Dai, X., Dandona, L., Dandona, R., Luca, K. de, Denova-Gutiérrez, E., Dharmaratne, S.D., Dhimal, M., Dianatinasab, M., Dreinhoefer, K.E., Elhadi, M., Farooque, U., Farpour, H.R., Filip, I., Fischer, F., Freitas, M., Ganesan, B., Gemeda, B.N.B., Getachew, T., Ghamari, S.-H., Ghashghaee, A., Gill, T.K., Golechha, M., Golinelli, D., Gupta, B., Gupta, V.B., Gupta, V.K., Haddadi, R., Hafezi-Nejad, N., Halwani, R., Hamidi, S., Hanif, A., Harlianto, N.I., Haro, J.M., Hartvigsen, J., Hay, S.I., Hebert, J.J., Heidari, G., Hosseini, M.-S., Hosseinzadeh, M., Hsiao, A.K., Ilic, I.M., Ilic, M.D., Jacob, L., Jayawardena, R., Jha, R.P., Jonas, J.B., Joseph, N., Kandel, H., Karaye, I.M., Khan, M.J., Kim, Y.J., Kolahi, A.-A., Korzh, O., Koteeswaran, R., Krishnamoorthy, V., Kumar, G.A., Kumar, N., Lee, S., Lim, S.S., Lobo, S.W., Lucchetti, G., Malekpour, M.-R., Malik, A.A., Mandarano-Filho, L.G.G., Martini, S., Mentis, A.-F.A., Mesregah, M.K., Mestrovic, T., Mirrakhimov, E.M.,

Misganaw, A., Mohammadpourhodki, R., Mokdad, A.H., Momtazmanesh, S., Morrison, S.D., Murray, C.J.L., Nassereldine, H., Netsere, H.B., Neupane Kandel, S., Owolabi, M.O., Panda-Jonas, S., Pandey, A., Pawar, S., Pedersini, P., Pereira, J., Radfar, A., Rashidi, M.-M., Rawaf, D.L., Rawaf, S., Rawassizadeh, R., Rayegani, S.-M., Ribeiro, D., Roever, L., Saddik, B., Sahebkar, A., Salehi, S., Sanchez Riera, L., Sanmarchi, F., Santric-Milicevic, M.M., Shahabi, S., Shaikh, M.A., Shaker, E., Shannawaz, M., Sharma, R., Sharma, S., Shetty, J.K., Shiri, R., Shobeiri, P., Silva, D.A.S., Singh, A., Singh, J.A., Singh, S., Skou, S.T., Slater, H., Soltani-Zangbar, M.S., Starodubova, A. V, Tehrani-Banihashemi, A., Valadan Tahbaz, S., Valdez, P.R., Vo, B., Vu, L.G., Wang, Y.-P., Yahyazadeh Jabbari, S.H., Yonemoto, N., Yunusa, I., March, L.M., Ong, K.L., Vos, T. & Kopec, J.A., 2023, 'Global, regional, and national burden of osteoarthritis, 1990–2020 and projections to 2050: a systematic analysis for the Global Burden of Disease Study 2021', The Lancet Rheumatology, 5(9), pp. 508–522

Stoop, R., Buma, P., Van Der Kraan, P. M., Hollander, A.P., Billinghurst, R.C., Meijers, T.H.M., Poole, A.R. and Van Den Berg, W.B., 2001. Type II collagen degradation in articular cartilage fibrillation after anterior cruciate ligament transection in rats, Osteoarthritis and cartilage, 9(4), pp. 308-315.

Szarek, P., Lilledahl, M.B., Emery, N.C., Lewis, C.G. and Pierce, D.M., 2020. The zonal evolution of collagen-network morphology quantified in early osteoarthritic grades of human cartilage. Osteoarthritis and Cartilage Open, 2(4), p. 100086.

Taffetani, M., Griebel, M., Gastaldi, D., Klisch, S. M. and Vena, P., 2014. Poroviscoelastic Finite Element Model Including Continuous Fiber Distribution for the Simulation of Nanoindentation Tests on Articular Cartilage, Journal of the Mechanical Behavior of Biomedical Materials, 32, pp. 17–30.

Takada, E. and Mizuno, S., 2018. Reproduction of characteristics of extracellular matrices in specific longitudinal depth zone cartilage within spherical organoids in response to changes in osmotic pressure, International Journal of Molecular Sciences, 19(5), p. 1507.

Takahata, Y., Murakami, T., Hata, K. and Nishimura, R., 2021. Molecular mechanisms involved in the progression and protection of osteoarthritis, Current Molecular Pharmacology, 14(2), pp. 165-169.

Taylor, S. D., Tsiridis, E., Ingham, E., Jin, Z., Fisher, J. and Williams, S., 2011. Comparison of Human and Animal Femoral Head Chondral Properties and Geometries, Journal of Engineering in Medicine, 226(1), pp. 55–62.

Teeple, E., Karamchedu, N.P., Larson, K.M., Zhang, L., Badger, G.J., Fleming, B.C. and Jay, G.D., 2016. Arthroscopic irrigation of the bovine stifle joint increases cartilage surface friction and decreases superficial zone lubricin, Journal of biomechanics, 49(13), pp. 3106-3110.

Temp, J., Labuz, D., Negrete, R., Sunkara, V. and Machelska, H., 2020. Pain and knee damage in male and female mice in the medial meniscal transection-induced osteoarthritis. Osteoarthritis and cartilage, 28(4), pp. 475-485.

Temple, D.K., Cederlund, A.A., Lawless, B.M., Aspden, R.M. and Espino, D.M., 2016. Viscoelastic properties of human and bovine articular cartilage: a comparison of frequency-dependent trends, BMC musculoskeletal disorders, 17, pp. 1-8.

Ter Heegde, F., Luiz, A.P., Santana-Varela, S., Chessell, I.P., Welsh, F., Wood, J.N. and Chenu, C., 2019. Noninvasive mechanical joint loading as an alternative model for osteoarthritic pain, Arthritis & Rheumatology, 71(7), pp. 1078-1088.

Usgu, G. and Usgu, S., 2023. The bone and joint structure. In Functional Exercise Anatomy and Physiology for Physiotherapists pp. 53-75. Cham: Springer International Publishing.

Van Zadelhoff, C., Schwarz, T., Smith, S., Engerand, A. and Taylor, S., 2020. Identification of naturally occurring cartilage damage in the equine distal interphalangeal joint using low-field magnetic resonance imaging and magnetic resonance arthrography. Frontiers in Veterinary Science, 6, p. 508.

Waldstein, W., Perino, G., Gilbert, S.L., Maher, S.A., Windhager, R. and Boettner, F., 2016. OARSI osteoarthritis cartilage histopathology assessment system: a biomechanical evaluation in the human knee. *Journal of Orthopaedic Research*, *34*(1), pp. 135-140.

Wan, L., Cheng, X., Searleman, A.C., Ma, Y.J., Wong, J.H., Meyer, R.S., Du, J., Tang, G. and Chang, E.Y., 2022. Evaluation of enzymatic proteoglycan loss and collagen degradation in human articular cartilage using ultrashort echo time-based biomarkers: A feasibility study, NMR in Biomedicine, 35(5), p. 4664.

Wang, C., Brisson, B.K., Terajima, M., Li, Q., Han, B., Goldberg, A.M., Liu, X.S., Marcolongo, M.S., Enomoto-Iwamoto, M., Yamauchi, M. and Volk, S.W., 2020. Type III collagen is a key regulator of the collagen fibrillar structure and biomechanics of articular cartilage and meniscus, Matrix Biology, 85, pp. 47-67.

Wang, L.J., Zeng, N., Yan, Z.P., Li, J.T. and Ni, G.X., 2020. Post-traumatic osteoarthritis following ACL injury. *Arthritis research & therapy*, *22*, pp. 1-8.

Wansin, Y., Latif, M.J.A., Saad, N.M., Alhabshi, S.M.I. and Kadir, M.R.A., 2017. Characterization of articular cartilage using low-field magnetic resonance imaging image, Journal of Medical Imaging and Health Informatics, 7(6), pp. 1149-1152.

Weizel, A., Distler, T., Schneidereit, D., Friedrich, O., Bräuer, L., Paulsen, F., Detsch, R., Boccaccini, A.R., Budday, S. and Seitz, H.J.A.B., 2020. Complex mechanical behavior of human articular cartilage and hydrogels for cartilage repair. Acta biomaterialia, 118, pp. 113-128.

Welsch, G.H., Apprich, S., Zbyn, S., Mamisch, T.C., Mlynarik, V., Scheffler, K., Bieri, O. and Trattnig, S., 2011. Biochemical (T2, T2* and magnetisation transfer ratio) MRI of knee cartilage: feasibility at ultra-high field (7T) compared with high field (3T) strength. European radiology, 21, pp. 1136-1143.

White, C.L., Chauvin, N.A., Waryasz, G.R., March, B.T. and Francavilla, M.L., 2017. MRI of native knee cartilage delamination injuries. American Journal of Roentgenology, 209(5), pp. 317-321.

Winalski, C. S. and Rajiah, P., 2011. The Evolution of Articular Cartilage Imaging and Its Impact on Clinical Practice, Skeletal Radiology, 40(9), pp. 1197–1222.

Wong, M. and Carter, D.R., 2003. Articular cartilage functional histomorphology and mechanobiology: a research perspective, Bone, 33(1), pp. 1-13.

Wright, G.J., Brockbank, K.G., Rahn, E., Halwani, D.O., Chen, Z. and Yao, H., 2014. Impact of storage solution formulation during refrigerated storage upon chondrocyte viability and cartilage matrix, Cells Tissues Organs, 199(1), pp. 51-58.

Wu, P. J., Masouleh, M.I., Dini, D., Paterson, C., Török, P., Overby, D.R. and Kabakova, I.V., 2019. Detection of proteoglycan loss from articular cartilage using Brillouin microscopy, with applications to osteoarthritis, Biomedical optics express, 10(5), pp. 2457-2466.

Wu, X., Zhao, K., Fang, X., Lu, F., Cheng, P., Song, X., Zhang, W., Yao, C., Zhu, J. and Chen, H., 2022. Saikosaponin D inhibited IL-1β induced ATDC 5 chondrocytes apoptosis in vitro and delayed articular cartilage degeneration in OA model mice in vivo. Frontiers in Pharmacology, 13, p. 845959

Xia, Y., 2000. Heterogeneity of cartilage laminae in MR imaging, Journal of Magnetic Resonance Imaging: An Official Journal of the International Society for Magnetic Resonance in Medicine, 11(6), pp. 686-693.

Yan, Y., Fu, R., Liu, C., Yang, J., Li, Q. and Huang, R.L., 2021. Sequential enzymatic digestion of different cartilage tissues: a rapid and high-efficiency protocol for chondrocyte isolation, and its application in cartilage tissue engineering, Cartilage, 13(2_suppl), pp. 1064-1076.

Yang, Y., Li, P., Zhu, S. and Bi, R., 2020. Comparison of early-stage changes of osteoarthritis in cartilage and subchondral bone between two different rat models. *PeerJ*, *8*, p.8934.

Yao, N., Chen, G.C., Lu, Y.Y., Xu, X.M., Zhao, C.X., Huang, X.J., Liu, W.G., Peng, S. and Wu, H., 2021. Bushen Qiangjin capsule inhibits the Wnt/α-catenin pathway to ameliorate papain-induced knee osteoarthritis in rat, Journal of Traditional Chinese Medicine= Chung i tsa Chih Ying wen pan, 41(6), pp. 935-942.

Youssef, D., Hassab-Elnaby, S. and El-Ghandoor, H., 2021. Nanoscale quantitative surface roughness measurement of articular cartilage using second-order statistical-based biospeckle, Plos one, 16(1), p. 0246395.

Zevenbergen, L., Gsell, W., Chan, D.D., Vander Sloten, J., Himmelreich, U., Neu, C.P. and Jonkers, I., 2018. Functional assessment of strains around a full-thickness and critical sized articular cartilage defect under compressive loading using MRI. Osteoarthritis and Cartilage, 26(12), pp.1710-1721.

Zhang, J., Spincemaille, P., Zhang, H., Nguyen, T.D., Li, C., Li, J., Kovanlikaya, I., Sabuncu, M.R. and Wang, Y., 2023. LARO: Learned acquisition and reconstruction optimization to accelerate quantitative susceptibility mapping, NeuroImage, 268, p. 119886.

Zhu, B., Cui, G., Zhang, Q., Cheng, X. and Tang, S., 2019. Desumoylation of aggrecan and collagen II facilitates degradation via aggrecanases in IL-1β-mediated osteoarthritis, Journal of Pain Research, pp. 2145-2153.

Zhou, K., Yuan, M., Sun, J., Zhang, F., Li, X., Xiao, X. and Wu, X., 2025. Co-delivery of IL-1Ra and SOX9 via AAV inhibits inflammation and promotes cartilage repair in surgically induced osteoarthritis animal models. Gene Therapy, 32(3), pp.211-222.

Zhou, X., Tao, Y., Chen, E., Wang, J., Fang, W., Zhao, T., Liang, C., Li, F. and Chen, Q., 2018. Genipin-cross-linked type II collagen scaffold promotes the differentiation of adipose-derived stem cells into nucleus pulposus-like cells, Journal of biomedical materials research Part A, 106(5), pp. 1258-1268.

Zibetti, M.V., Menon, R.G., de Moura, H.L., Zhang, X., Kijowski, R. and Regatte, R.R., 2023. Updates on compositional MRI mapping of the cartilage: emerging techniques and applications. Journal of Magnetic Resonance Imaging, 58(1), pp.44-60.

APPENDICES

Appendix A

MATLAB script

```
img = imread(''C:\MICROSCOPE\Filename'');
img = rgb2gray(img);
img = imrotate(img,-360);
img_raw = img;
threshold = 0.80;
img = imbinarize(img, threshold);
figure, imshowpair(img_raw,img,'montage')
img_thresh = img;

SE = strel('disk',10);
img = imclose(img,SE);
SE = strel('disk',30);
img = imopen(img,SE);

figure, imshowpair(img_thresh, img,'montage')

% Display the image
imshow(img);
title('Select a region of interest using coordinates');

% Define coordinates of the region
x = [0, 1280, 1280, 0, 0];% x-coordinates of the vertices
y = [0, 0, 800, 800, 0];% y-coordinates of the vertices

% Plot the region on the image
hold on;
plot(x, y, 'r', 'LineWidth', 2);

% Create a binary mask from the coordinates
roi_mask = poly2mask(x, y, size(img, 1), size(img, 2));

% Perform further processing or analysis on the selected region

% Calculate Statistics (Percent Coverage)
 % px Values: White =1, black=0
black_px = sum(sum(img == 0));
white_px = sum(sum(img == 1));
total_px = size(img,1)*size(img,2);

per_land = black_px / total_px * 100;

% Read the binary image (assuming it's already processed and available)
binary_img = img;

% Calculate the number of black pixels inside the ROI
black_px_inside_roi = sum(binary_img(roi_mask) == 0);

% Calculate the total number of pixels inside the ROI
total_px_inside_roi = sum(roi_mask(:));

% Calculate the percentage coverage of black pixels inside the ROI
per_land_roi = (black_px_inside_roi / total_px_inside_roi) * 100;
```

```
fprintf('Percentage coverage of black pixels inside the ROI:%.2f%%\n',
per_land_roi);
```

APPENDICES

Appendix B

MATLAB script

```
1.    x=dicomread('C:\MRI\Filename');
2.    info=dicominfo('C:\MRI\Filename');
3.    y=dicomread(info);
4.    figure,imshow(y);
5.    imcontrast;


6.    X2=imcrop(x,maps,[xmin ymin 32 32]);
7. subplot (1,2,1);
8.    imshow(x, maps);
9.    title ('Original Image');
10.   subplot (1,2,2);
11.   11.imshow(X2,maps);
12.   title ('Cropped Image');
13.   whos;
```